



HAL
open science

The encoding of olfactory memory traces in the mouse piriform cortex

Claire Meissner-Bernard

► **To cite this version:**

Claire Meissner-Bernard. The encoding of olfactory memory traces in the mouse piriform cortex. Neurons and Cognition [q-bio.NC]. Université Pierre et Marie Curie - Paris VI, 2017. English. NNT : 2017PA066450 . tel-02293791v1

HAL Id: tel-02293791

<https://theses.hal.science/tel-02293791v1>

Submitted on 22 Sep 2019 (v1), last revised 22 Sep 2019 (v2)

HAL is a multi-disciplinary open access archive for the deposit and dissemination of scientific research documents, whether they are published or not. The documents may come from teaching and research institutions in France or abroad, or from public or private research centers.

L'archive ouverte pluridisciplinaire **HAL**, est destinée au dépôt et à la diffusion de documents scientifiques de niveau recherche, publiés ou non, émanant des établissements d'enseignement et de recherche français ou étrangers, des laboratoires publics ou privés.

Université Pierre et Marie Curie

Ecole doctorale n°158, Cerveaux Cognition et Comportement

Centre Interdisciplinaire de Recherche en Biologie

Equipe "Circuits neuronaux et comportement"

**La formation de traces mnésiques olfactives
dans le cortex piriforme de la souris**

Par **Claire MEISSNER-BERNARD**

Thèse de doctorat de Neurosciences

Dirigée par Alexander FLEISCHMANN

Présentée et soutenue publiquement le 20 Septembre 2017

Devant un jury composé de :

Dr Jason KERR	Rapporteur
Dr Luisa VASCONCELOS	Rapporteur
Dr Boris BARBOUR	Examineur
Pr Anne DIDIER	Examineur
Pr Alain TREMBLEAU	Examineur
Dr Pierre YGER	Examineur
Dr Alexander FLEISCHMANN	Directeur de thèse



Acknowledgments

Merci à Alexander Fleischmann pour m'avoir accueilli dans son équipe et pour la confiance et la liberté qu'il m'a accordée.

Merci à Jason Kerr et Luisa Vasconcelos d'avoir accepté d'être rapporteurs de cette thèse, ainsi qu'à Boris Barbour, Anne Didier, Alain Trembleau et Pierre Yger de faire partie des membres du jury. Merci à Brice Bathellier, Karim Benchenane et Yanniv Ziv d'avoir fait partie de mon comité de mi-thèse.

Merci aux personnes qui m'ont initiée ou formée à diverses techniques, en particulier Assunta Diodato, Pascal Ezan, Marion Ruinart de Brimont, Gérard Parésys, Marie-Annick Thomas, Jérémie Teillon et Jonathan Zapata.

Merci à nos collaborateurs Laurent Venance et Yulia Dembitskaya pour avoir contribué à la partie électrophysiologie de mon projet et à Yves Dupraz pour avoir conçu nos boîtes de comportement.

Merci à Pierre Yger pour les discussions approfondies sur mon travail et l'invitation à donner un séminaire à l'EITN. Merci également à Benjamin Kaupp pour m'avoir invitée à Bonn.

Merci aux membres de l'équipe Fleischmann, en particulier Assunta, Benjamin, Line et Mehdi, pour leur aide, conseils ou soutien. Merci à Agatha pour son dévouement et son écoute pour faire avancer mon projet.

Cela a été un plaisir de travailler à l'étage -1. Merci à vous tous.

Cette thèse a été jalonnée d'embuches. Merci à tous ceux qui ont illuminé cette thèse, en particulier Céline, Isma et Julien. Julien, tes "Miss Claire" résonneront à jamais à mes oreilles.

Merci à tous ceux qui m'ont dépannée quand il me manquait un appareil ou un produit, ainsi que ceux qui ont eu à coeur que mes expériences ne soient pas impactées par les divers travaux et coupures de courant.

Merci à Wulfram Gerstner de m'avoir permis de découvrir les neurosciences théoriques en m'accueillant dans son laboratoire et de m'avoir redonnée foi en la science. Merci à Laureline de m'avoir encadrée pendant la première partie de ma visite. Merci aux autres membres du labo d'avoir si bien accueilli l'extraterrestre scientifique que j'étais à leurs yeux: Alex, Bernd, Chiara, Florian, Friedemann, Johanni, Samuele, Vassiliki.

Merci à l'équipe du Palais de la Découverte pour la formation plus que bénéfique en vulgarisation scientifique mais également confiance en soi. Merci également à la dream team du 3V627 pilotée par Anne Woisard qui a rendu ma mission d'enseignement extrêmement plaisante.

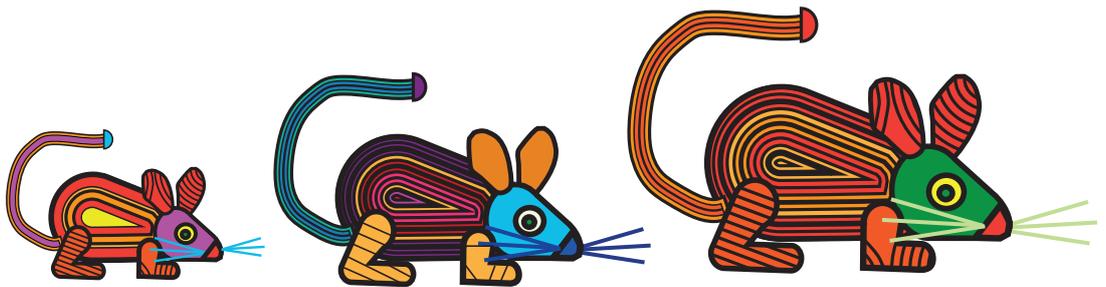
Merci encore à Jean-Marc Edeline et Boris Gourévitch pour le stage de licence qui m'a donné goût mais surtout donné un solide bagage en programmation.

Cette thèse n'aurait pas été possible sans toutes ces souris sacrifiées au nom de la science. Merci à elles ainsi qu'aux animaliers qui s'en sont occupé.

Merci à mon grand-père d'avoir créé des souris spécialement pour moi.

Enfin, le plus grand merci va à mes parents. Mon père pour avoir toujours cru en moi et avoir relu mon manuscrit de thèse. Ma mère pour m'avoir toujours soutenu dans les moments difficiles, pour nos discussions du soir sur mes données, et l'aide plus que précieuse pendant la rédaction du manuscrit. Maman, ton point de vue de physicienne a apporté de la rigueur dans l'interprétation de mes données.

A mes parents et grands-parents



Abstract

Olfaction is an evolutionarily old sensory modality that plays key roles in the survival of many species and is densely interwoven with memory and emotions. However, how odor memories are formed and stored in the brain remains largely unknown. To address these questions, we studied the olfactory (piriform) cortex of mice, which is a good candidate for encoding olfactory memory traces. We used *c-fos* as a marker of neural activity and the *cfos-tTA* transgenic mouse line (and the *fosCreER^{T2}* mouse line to a lesser extent) to selectively express chemogenetic receptors (DREADDs) in piriform neurons that are active during an olfactory fear conditioning task. We found that chemogenetically reactivating these ensembles artificially retrieves the memory while chemogenetically silencing them impairs memory retrieval. Piriform neurons active during olfactory learning thus play a key role in memory retrieval. These results opens new horizons in understanding memory trace formation. We decided to explore in a preliminary way how learning shapes piriform network properties. In parallel, using a theoretical framework, we investigated if a model based on dendritic voltage could predict synaptic plasticity. Taken together, these experiments will provide important insights into the mechanisms of odor coding and memory.

Résumé

Comment les souvenirs sont-ils stockés dans notre cerveau? Leurs mémorisations résultent de changements moléculaires et cellulaires dans le cerveau, créant un motif spécifique d'activité neuronale ou trace mnésique. Dans l'histoire de l'évolution, l'olfaction est considérée comme le sens le plus ancien et joue un rôle important chez de nombreuses espèces animales. En outre, les odeurs ont une capacité unique de déclencher des souvenirs et des émotions. Pourtant, la mémoire olfactive a été très peu utilisée comme modèle d'étude pour décrypter le code neural des souvenirs.

Plusieurs études suggèrent que le cortex olfactif (piriforme) jouerait un rôle important dans la mémoire olfactive. J'ai donc voulu déterminer si cette région du cerveau est impliquée dans le rappel d'un souvenir olfactif. Pour cela, j'ai manipulé l'activité des neurones du cortex piriforme ayant été actifs pendant une tâche olfactive d'apprentissage aversif (association d'une odeur à une petite décharge électrique), en utilisant *cfos* comme marqueur d'activation neuronale. Plus précisément, j'ai choisi de travailler avec la lignée de souris transgénique *cfos-tTA* (ainsi que de manière moins développée avec la lignée *fosCreER^{T2}* mise au point plus récemment) et d'utiliser les récepteurs "DREADDs" pour manipuler l'activité neuronale. J'ai montré que lors du test de mémoire, l'inactivation des neurones du cortex piriforme actifs pendant l'apprentissage olfactif rend la souris amnésique. De manière réciproque, la réactivation artificielle de ces neurones récupère le souvenir de l'association odeur-stimulus aversif. Ainsi, une trace mnésique se forme au niveau du cortex piriforme, et plus précisément au niveau des neurones actifs lors de l'apprentissage.

Ce résultat fascinant ouvre la voie à de nombreux champs d'investigations pour mieux comprendre les mécanismes de la mémoire. J'ai choisi d'explorer de manière préliminaire l'effet de l'apprentissage sur la représentation des odeurs au niveau du cortex piriforme. En parallèle, en utilisant une approche théorique, j'ai étudié si un modèle basé sur les variations de potentiel de membrane dendritique pouvait prédire l'occurrence d'un type de plasticité à une synapse corticale.

L'ensemble de ces travaux ont permis d'accroître nos connaissances sur le fonctionnement du système olfactif ainsi que la formation et le stockage de nos souvenirs, et pourraient également à terme permettre de mieux comprendre les déficits olfactifs observés au stade initial de la maladie d'Alzheimer.

List of abbreviations

4-OHT: 4-hydroxytamoxifen

ACh: acetylcholine

APs: action potentials

Beta-cit: beta-citronellol

BLA: basolateral amygdala

CNO: clozapine-N-oxide

CoA: cortical amygdala

CS: conditioned stimulus

DG: dentate gyrus

d.f.: degree of freedom

Etac: ethyl-acetate

Eug.: eugenol

IEG: immediate-early-gene

i.p.: intraperitoneally

LTD: long-term depression

LTP: long-term potentiation

OB: olfactory bulb

PC: piriform cortex pPC: posterior piriform cortex aPC: anterior piriform cortex

SD: standard deviation

STDP: Spike-Timing Dependent Plasticity

US: unconditioned stimulus

Contents

List of Figures	15
List of Tables	17
I Introduction	18
1 What we know -or not- about memory traces	20
1.1 In search of memory traces	20
1.1.1 A historical overview: where and how are memories encoded in the brain?	20
1.1.2 Memory traces: from encoding to retrieval	21
1.2 Synaptic plasticity and memory trace formation	22
1.2.1 Frequency and timing-dependent plasticity.	22
1.2.2 Neuromodulation, modulating synaptic plasticity	23
1.2.3 A causal link between synaptic plasticity and memory?	23
1.3 Fear memories	24
1.3.1 Fear conditioning	24
1.3.2 The fear circuit: a distributed circuit	25
1.4 Technical breakthroughs in the study of memory traces	27
1.4.1 The immediate early-gene c-fos: a marker of neural activity implicated in learning and memory	27
1.4.2 Labeling neurons active at a given time point (TetTag and TRAP)	28
1.4.3 Artificially activating or silencing neuronal activity	30
1.5 Has the memory trace been found?	31
2 Olfactory memories	33
2.1 Ethological considerations: why study olfactory memories	33
2.2 The organization of the olfactory system	34
2.3 The piriform cortex is a good candidate for encoding memory traces	34
2.3.1 Manipulating piriform activity	34
2.3.2 Piriform cortex circuits and odor representations	36
2.3.3 Experience-shaped odor representations	37
2.3.4 "Memory" computations performed by the PC	37

2.3.5	Neuromodulation of piriform activity and learning	38
2.3.6	Connectivity of the piriform cortex	39
2.3.7	Summary and glimpse into human findings	40
2.4	Hypothesis: The piriform cortex encodes olfactory memory traces	40
II	Materials and Methods	42
3	Toolbox to study olfactory memory	43
3.1	cfos-promoter transgenic mouse lines	43
3.1.1	cFos transgenic mouse lines: housing and genotyping	43
3.1.2	Injecting adeno-associated virus in the piriform cortex to express DREAADs in Fos-positive neurons	44
3.1.3	Immunohistochemistry, Microscopy, Cell counting	45
3.2	Olfactory fear conditioning	48
3.2.1	Behavioral apparatus	48
3.2.2	Behavioral procedures	49
3.2.3	Automated tracking of the mouse	50
3.2.4	Quantification of escape behavior	53
3.3	Statistics	55
III	Results	56
4	Manipulating piriform neurons active during learning	57
4.1	Tet-Tagging piriform neurons	57
4.1.1	Endogenous Fos expression in PC	57
4.1.2	cfos-tTA/tetO-DREADDs	58
4.2	Manipulating the activity of piriform neurons	60
4.2.1	Methods	60
4.2.2	Results	61
4.3	Silencing piriform neurons active during learning impairs odor memory retrieval	65
4.3.1	Experimental design	65
4.3.2	Results	66
4.4	Memory deficits are odor-specific	72
4.4.1	Experimental design	72
4.4.2	Results	73
4.5	Preliminary results: Memory deficits are experience- dependent	75
4.5.1	Experimental design	75
4.5.2	Preliminary results	75
4.6	Artificially re-activating piriform neurons active during learning	75
4.6.1	Experimental procedure	77

4.6.2	Results	77
4.7	Reactivation of fos-tagged ensembles during memory retrieval	80
4.7.1	Experimental design	80
4.7.2	Results	82
4.8	Discussion	83
5	Mechanisms of memory trace formation.	88
5.1	Hypothesis	88
5.2	Role of Acetylcholine in olfactory learning	89
5.2.1	Experimental procedure	89
5.2.2	Preliminary results	90
5.3	Stabilization of odor representation after learning?	91
5.3.1	Experimental design	91
5.3.2	Preliminary results	92
6	TRAPing piriform neurons	94
6.1	TRAPing odor-responsive neurons	94
6.2	Inactivating neurons TRAPed during fear conditioning	97
6.2.1	Experimental design	98
6.2.2	Results	98
6.3	Discussion	100
IV	Modeling project	103
7	Predict synaptic plasticity using dendritic recordings	104
7.1	Introduction	104
7.2	Methods	105
7.2.1	Voltage-based model of synaptic plasticity	105
7.2.2	Postsynaptic voltage traces	106
7.2.3	Parameters	107
7.3	Results	107
7.3.1	Validation of the model	107
7.3.2	Dendritic voltage shapes synaptic plasticity in the neocortex	108
7.3.3	Dendritic voltage shapes synaptic plasticity in the allocortex	108
7.3.4	Dendritic plateau potentials play an important role in the generation of plasticity	111
7.4	Conclusion	111

V Conclusion	113
VI Appendices	116
VII Bibliography	127

List of Figures

1.1	Spike-timing dependent plasticity and neuromodulation.	24
1.2	Classical fear conditioning.	26
1.3	Inducible transgene expression dependent of the fos promoter.	29
1.4	Optogenetics and chemogenetics.	30
2.1	The organization of the olfactory system.	35
2.2	Pattern completion.	39
3.1	Fear conditioning setup.	47
3.2	Chemical structure of the odors used.	48
3.3	Automated tracking of the mouse: mains steps.	51
3.4	Automated tracking of the mouse: graphical output files.	52
3.5	Behaviour of the mouse during odor-shock pairing.	54
4.1	Histological characterization of fos-tagged piriform ensembles.	59
4.2	Native fluorescence in DREADDs-expressing cells.	60
4.3	Immunohistochemical analysis of GABA expression in hM3Dq-positive neurons.	62
4.4	Verification of morphological and membrane properties of DREADDs-expressing and non-expressing cells.	63
4.5	Excitability of DREADDs-expressing cells after CNO application.	64
4.6	Membrane properties of DREADDs-expressing and non-expressing cells after CNO application.	65
4.7	Silencing fos-tagged ensembles during memory retrieval.	67
4.8	Indirect histological confirmation of hM4Di expression in the PC.	68
4.9	(a) Position as a function of time after CS+ (top) or CS- (bottom) presentation for each mouse and each trial.	70
4.9	(b) continuation of the previous figure.	71
4.10	Odor specificity of fos-tagging and inactivation.	74
4.11	Experience-dependence of fos-tagging and inactivation.	76
4.12	Artificial reactivation of fos-tagged ensembles: experimental design and histology	78
4.13	Artificial reactivation of fos-tagged ensembles: behavior	81
4.14	Reactivation of piriform neurons during memory retrieval.	84

5.1	Hypothesis.	90
5.2	Blocking acetylcholine neuromodulation in the PC during olfactory fear conditioning.	91
5.3	Stability of odor representations after learning.	93
6.1	Histological characterization of fos-TRAPed piriform ensembles.	95
6.2	Morphology of TRAPed cells.	96
6.3	TRAPing in the piriform cortex after odor stimulation.	97
6.4	Histological confirmation of hM4Di expression in the PC.	99
6.5	Inactivation of fos-TRAPed ensembles during memory retrieval.	101
7.1	Scheme of the model.	106
7.2	Plasticity experiments with pairings of presynaptic and postsynaptic spikes.	108
7.3	Distance-dependent STDP at synapses between layer 2/3 and layer 5 pyramidal neurons in somatosensory cortex.	109
7.4	Plasticity in the hippocampus.	110
7.5	Necessity of dendritic spikes for the induction of LTP using different experimental protocols.	112

List of Tables

3.1	List of primary antibodies used	45
3.2	Interval between sections and position of the first section relative to bregma along the anterior-posterior axis.	46
3.3	Filter parameters.	46
3.4	CS+ and CS- used.	50
3.5	Mean \pm SD values of different parameters describing the mouse behavior during olfactory fear conditioning. Values in brackets represent the minimum and maximum value.	55
7.1	Values of the parameters of the model obtained in the fit	107

Part I

Introduction

Introduction

”And suddenly the memory revealed itself. The taste was that of the little piece of madeleine which... my aunt Léonie used to give me, dipping it first in her own cup of tea or tisane.” Who has not vividly recalled long-forgotten memories from his childhood after smelling a particular odor, as the character from Marcel Proust’s novel ”A la recherche du temps perdu ” (a.k.a the Proust phenomenon)? Indeed, olfaction has a unique ability to trigger emotional memories, and this ability has been exploited in areas as diverse as olfactory marketing and olfactotherapy. Since the Antiquity, we humans have questioned the nature of memory (our current knowledge about memories is presented in Chapter 1). Curiously however, how odor memories are formed and stored in the brain remains largely unknown. In the past decades, memory studies have mainly focused on episodic memories or memories involving visual or auditory stimuli.

I propose to investigate where and how olfactory memories are encoded in the brain. I focus on the piriform cortex, a subdivision of the olfactory system which seems a good candidate for forming and retrieving olfactory memories. This region is described in detail in Chapter 2. I take advantage of recent tools to label and manipulate ”memory cells”: engineered receptors to manipulate neural activity (chemogenetics or optogenetics) and transgenic mouse lines based on inducible activity-dependent promoters (TetTag and TRAP system). These tools are described in Chapter 1 and more specifically characterized in the piriform cortex in Chapter 4 and 6. In Chapter 4, I identify a piriform neuronal subpopulation necessary and sufficient for olfactory memory retrieval. Synaptic connections between neurons can be modified: by changing the way information flows in the brain, synaptic plasticity has been proposed as the key mechanism for learning and memory formation. I investigate in Chapter 5 how learning shapes piriform odor representations at a network level. Finally, in Chapter 7, I explore synaptic plasticity at a cellular level in a theoretical framework.

Chapter 1

What we know -or not- about memory traces

1.1 In search of memory traces

Let us start the search for an olfactory memory trace with an ethological observation. When a rat locates a novel food source, it seldom eats everything at once. Instead, it will eat a little bit of it, go away for several hours, and then return to eat everything. However, the rat will not return to finish the food, if it is poisoned and made the rat sick (Barnett, 2009). Learning enables animals to acquire knowledge about the external world and adapt their behavior. Memory is the storage of that knowledge in the brain.

1.1.1 A historical overview: where and how are memories encoded in the brain?

”The enduring though primarily latent modification in the irritable substance produced by a stimulus”. This is how in 1921, Richard Semon defined a memory trace (Semon, 1921). But would this ”modification” be located in a specific brain region? In the same way that we define sensory and motor systems, is there a memory system? The first attempt to identify the brain region where memories are encoded goes back to 1950. Karl Lashley trained some rats to learn where food was hidden in a maze and then lesioned different brain regions. What correlated with the severity of the memory impairment was not the location but the extent of the lesion. Lashley thus concluded that memory is a function distributed throughout the brain (Lashley, 1929). Further work with experimental animals and amnesic patients hinted towards the existence of not one but multiple memory systems (Squire, 2004): in human research, the distinction between explicit and implicit -or declarative and non-declarative- memories emerged, depending on whether the recall is conscious or not. More specifically, some brain regions would be more important than others for each

type of memory. Two famous examples illustrate this idea.

The pioneer in the study of episodic memories (memory of autobiographical events that can be explicitly stated) was Brenda Milner in 1957 who studied the case of H.M. H.M. underwent surgery to treat his drug-resistant epilepsy: his temporal lobes (i.e hippocampus, amygdala and entorhinal cortices) were removed. H.M. was unable to form new episodic memories as well as to recall memories of events which had happened the year before his surgery. Nevertheless, H.M.'s other types of memory, such as learned motor skills were largely unaffected (reviewed in Squire, 2009). Since then, the hippocampus has been a key brain region in the study of spatial learning and episodic memories.

Sixty years earlier, Ivan Pavlov was laying down the foundations of classical conditioning. He studied this learning process in detail on dogs (Pavlov, 1927). Classical conditioning is now widely used in animal research to understand the neural basis of learning and memory and will be described in more detail in section 1.3. Lesions studies in rodents identified the amygdala, a subcortical region, as playing a key role in classical conditioning leading to the formation of fear memories (LeDoux, 2002).

How are memories encoded in the brain? While some researchers were searching for the location of memory traces, others were trying to understand the mechanisms leading to the formation of memory traces. In the 1950s, Donald Hebb brought together earlier ideas and findings in a tremendously influential postulate (Hebb, 1949): "When an axon of cell A is near enough to excite B and repeatedly or persistently takes part in firing it, some growth process or metabolic change takes place in one or both cells such that A's efficiency, as one of the cells firing B, is increased.". At the network level, the strengthened connections of coactive neurons lead to the emergence of a "cell assembly". Hebb's theoretical work about synaptic plasticity was experimentally validated twenty years later by the discovery of long-term potentiation (LTP). Bliss and Lømo (1973) showed that the response of hippocampal neurons after a single stimulation of their afferent fibres was enhanced after high-frequency stimulation of these same afferent fibres. As repeated high-frequency stimulation of presynaptic fibers most likely drove activity in postsynaptic hippocampal cells, Hebb's rule was followed. In parallel, Kandel et al. (1964) were unraveling the biochemical mechanisms of learning and memory using the invertebrate *Aplysia*, a model organism with "only" 20 000 nerve cells. Kandel's work was also the first to strongly link synaptic plasticity and memory storage.

1.1.2 Memory traces: from encoding to retrieval

Until recently, the toolkit for the study of memory in non-humans animals consisted of lesion studies and electrophysiological recordings combined to behavioral assays. In the last decades however, molecular-genetics tools allowing to selectively and persistently tag and manipulate neurons that are active at a given time were developed, and this has led to a development in the search for memory traces. But what is the lifetime and characteristics of a memory trace (for reviews see

Josselyn et al. 2015; Ben-Yakov et al, 2015; Tonegawa et al., 2015)?

Memory encoding induces a set of biophysical, biochemical and/or structural changes which can be probed at different levels of the brain - molecular, cellular or circuit level. These persistent changes form a physical trace of the memory or memory trace. They outlast the learning experience and enable to store information about the learning experience.

Current views suggest that the memory trace is likely to be sparse and anatomically distributed, involving the coordinated interplay of multiple storage sites. Memory traces are strengthened and reorganized across brain areas over time (Bergstrom, 2016; Dudai et al., 2015), a process termed memory consolidation. One of the first experimental evidence of memory consolidation came from the observation that hippocampal lesions result in temporally-graded amnesia¹, both in humans (patient H.M. for example, see above), as well as in other species (Zola-Morgan & Squire, 1990; Kim and Fanselow, 1992). This could allow to adapt memory representations to a constantly changing environment. Memory consolidation is thought to rely on the replay of memories, among others during sleep.

During memory retrieval, the memory trace which had entered a dormant state, is reactivated. The content of the memory trace should produce the appropriate behavior in the presence of retrieval cues. The prevailing theory is that memory traces are formed by strengthening of pre-existing synaptic connections between a population of neurons that are active during learning. As a consequence, at least a part of this population should be reactivated during memory retrieval.

During retrieval, the memory trace enters a labile state, and is reconsolidated.

1.2 Synaptic plasticity and memory trace formation

As already mentioned, a prevailing view since Hebb's postulate is that memory traces are formed by strengthening of pre-existing synaptic connections between neurons active during learning.

1.2.1 Frequency and timing-dependent plasticity.

We have already mentioned in the historical overview the discovery of long-term potentiation, which is an increase in the synaptic efficacy between two neurons. The converse of LTP, i.e. a decrease in the synaptic efficacy, or long-term depression (LTD) was discovered after applying low frequency trains of stimulation to hippocampal afferents (Dudek & Bear, 1992).

Nevertheless, the tetanic stimulations used in the early LTP studies were not realistic firing patterns. Controlling timing between pre- and post-synaptic spikes in a more strict way lead to the emergence of Spike-Timing Dependent Plasticity (STDP), (Markram et al., 1997). During STDP plasticity protocols, single pre- and postsynaptic action potentials (APs) are paired several times with varying time intervals. Fig.1.1 shows an example of STDP learning window: the change of

¹memories acquired close to the amnesia-inducing event are lost, while more remote ones are spared

the synaptic weight is plotted as a function of the relative timing of pre- and postsynaptic APs. In typical STDP windows, if the postsynaptic AP follows the presynaptic AP, then the synapse is potentiated, following Hebbian's rule ("causal" activity, Markram et al., 2011). If the postsynaptic AP precedes the presynaptic AP (and thus the latter does not cause the former to spike), then the synapse is depressed.

A great diversity of firing patterns have been observed in vivo, including burst firing, single spikes and irregular low-frequency firing patterns. As a consequence, the relative importance of spike timing and burst firing in eliciting synaptic plasticity remains largely unknown (Sjostrom et al., 2008).

1.2.2 Neuromodulation, modulating synaptic plasticity

Neurons exhibit spontaneous spiking activity and respond to "not-to-be-remembered" sensory stimulations, generating some unwanted pairs of pre-post APs. How can the brain select the synapses to be strengthened, both in time and space? Neuromodulation has been proposed to resolve this problem (see Pawlak et al., 2010 for a review).

Neuromodulatory systems are activated in vivo and salient behavioral events increase the activity of neuromodulatory nuclei. Nevertheless, the typical timing window of STDP does not exceed 100 ms, while neuromodulation occurs over a slower time course (on the order of seconds). One possible mechanism is that a Hebbian coactivation of two neurons would create a time-decaying "eligibility trace" at the synapse. The interaction between this "trace" and neuromodulators would lead to synaptic weight change.

Several effects of neuromodulation on STDP have been demonstrated (reviewed in Pawlak et al., 2010; Pedrosa & Clopath, 2017), including a shift of the plasticity induction threshold and requirement of neuromodulation for STDP to occur (see Fig.1.1). At the behavioral level, blocking neuromodulation has been shown to severely impair learning and memory (Puig et al., 2014; Anagnostaras et al., 1999). As an example, systemic blockade of acetylcholine receptors disrupts acquisition of auditory fear conditioning (Anagnostaras et al., 1999). But is there some evidence demonstrating more than a correlative link between synaptic plasticity and memory formation?

1.2.3 A causal link between synaptic plasticity and memory?

Activity-dependent synaptic plasticity has been suggested to be both necessary and sufficient for the formation of memory traces. This is also referred as the "Synaptic Plasticity and Memory" hypothesis (Martin et al., 2000; Takeuchi et al., 2013). Changes in synaptic efficacy have been shown to occur after learning. Furthermore, comparison studies find that some of the molecular mechanisms required for the induction of LTP are also required for associative learning and memory formation (Maren, 2005; Rodrigues et al., 2004). The development of electrophysiological recordings in awake behaving animals allows to record changes in synaptic efficacy while measuring behavioral performance with or without manipulation of synaptic plasticity induction,

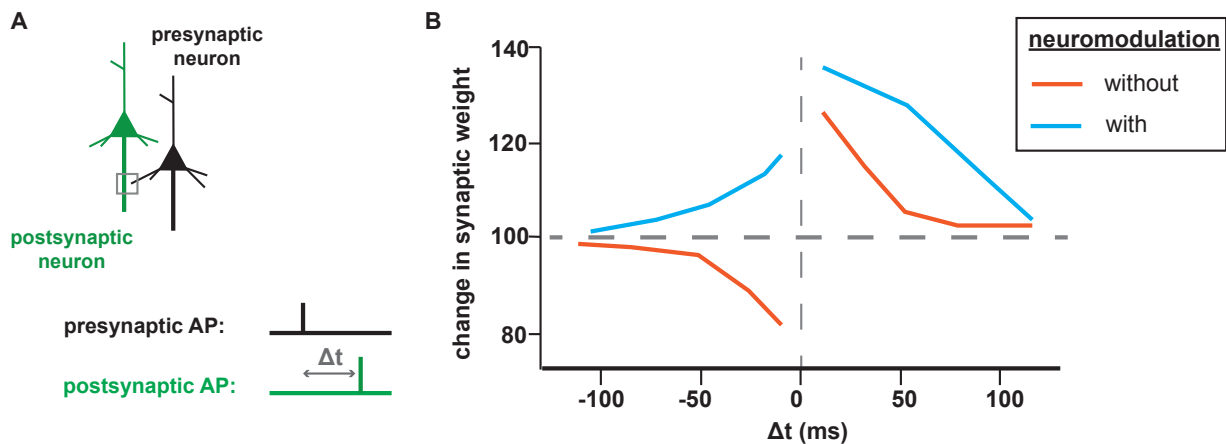


Figure 1.1: **Spike-timing dependent plasticity and neuromodulation.** (A) STDP protocol: presynaptic and postsynaptic spikes are paired several times (usually 50-100 times) with a fixed time interval Δt and at a fixed frequency. The synaptic weight is measured as the amplitude of the postsynaptic potential after a presynaptic stimulation. (B) STDP window: the strengthening of the synaptic connection as a function of the relative timing of pre- and postsynaptic spikes depends on the presence of neuromodulators. Adapted from Pawlak et al., 2010.

thus providing a stronger evidence in support of the necessity of synaptic plasticity in memory formation (Pastalkova et al., 2006; Nabavi et al., 2014).

1.3 Fear memories

As mentioned in the historical overview, different types of memory exist and they are likely to involve different brain regions. Of particular interest is the study of emotional memories. As pinpointed by Charles Darwin in 1872 in his book "The Expression of the Emotions in Man and Animals", a key characteristic of emotions is their phylogenetic continuity. Fear occurs in a majority of animal species -at least in the ones where it has been studied. A scared dog will hide its tail between its hind legs, while a cat will arch its back probably to look bigger and scare an eventual intruder (Darwin, 1872). Several behavioral fear responses have been described, ranging from vocalizations to warn others to escape or freezing. Switch from escape to freezing is thought to depend on the distance from the predator (Adolphs, 2013). Freezing animals could avoid being detected if an escape is not possible (no space and/or time). Fear is only one example of emotion, but it has several advantages in the study of learning and memory over other emotions (Le Doux, 2002).

1.3.1 Fear conditioning

Fear can be innate or learned, and fear conditioning, a learning procedure based on the work of Ivan Pavlov, is a valuable behavioral paradigm for studying the neural basis of memory. Fear conditioning relies on the association of a conditioned stimulus (CS) and an unconditioned stim-

ulus (US), Fig.1.2. The CS is a neutral stimulus which has no behavioral effect, whereas the US is a stimulus which elicits an innate, strong and consistent behavioral response, or unconditioned response (UR). In the case of fear conditioning, the US is an aversive stimulus which produces a fear response (mild electric foot shock in most of the cases). After pairing the CS with the US, reexposure to the CS alone elicits the same physiological changes than the US, in our case a fear response (or conditioned response). This can be interpreted as an anticipatory response to threat and danger. If the CS is then repeatedly presented without the US, the probability and/or intensity of the fear response decreases, a process termed extinction. There are two main types of fear conditioning: cued fear conditioning, which pairs a single sensory cue to an aversive stimulus and is thus modality-specific, and contextual fear conditioning, which combines complex polymodal information and represents memories for fearful locations. To disentangle between the two, memory retrieval should be tested in a different or the same conditioning box, respectively (see Fig.1.2).

Fear conditioning is a very effective learning procedure -a single or few CS-US pairings are often sufficient- and happens as quickly in rats than in humans. Furthermore, stimuli used in fear conditioning in animal model systems like rodents are usually novel and irrelevant for them, which enable observation of learning and memory *stricto sensu*. At last, many human mental disorders (anxiety disorders, post-traumatic shock disorders) are due to the brain's inability to control fear (LeDoux, 2002). Thus, a better understanding of the processing of fear and related memories might lead to new treatments of fear disorders.

1.3.2 The fear circuit: a distributed circuit

The amygdala is an almond-shape structure of the brain which seems to be highly conserved across species, ranging from primates, rodents to reptiles (Phelps et al., 2005). It is now well established that this brain region is involved in the formation and storage of both contextual and cued fear memories (LeDoux, 2002). The amygdala is organized in several subregions, three of them being the basolateral amygdala (BLA), the central nucleus (CE), and the cortical amygdala (CoA). In a simplified way, the basolateral amygdala (BLA) receives convergent sensory inputs from the CS and US, processes information and relays it to the central nucleus (CE), which is the output structure of the amygdala. The CE connects among others with areas of the midbrain and brain stem involved in the physiological expression of fear (Krettek et al., 1978). The amygdala is a permanent storage site of fear memories; its integrity for memory retrieval is needed months after learning (Gale et al., 2004; Maren et al, 1996).

In contrast to the amygdala, some brain regions are differently involved in cued and contextual fear conditioning. Lesions of the hippocampus have been shown to interfere only with contextual fear conditioning (Phillips et al., 1992). Neurons in the hippocampus encode spatial information: some neurons -or place cells- spike selectively when the animal is located in a specific part of the environment or 'place field'. The hippocampus is subdivided in four major subregions, the dentate gyrus (DG), CA1, CA2 and CA3. The DG receives its main input from the entorhinal cortex, which projections convey polymodal sensory information. The DG projects to CA3,

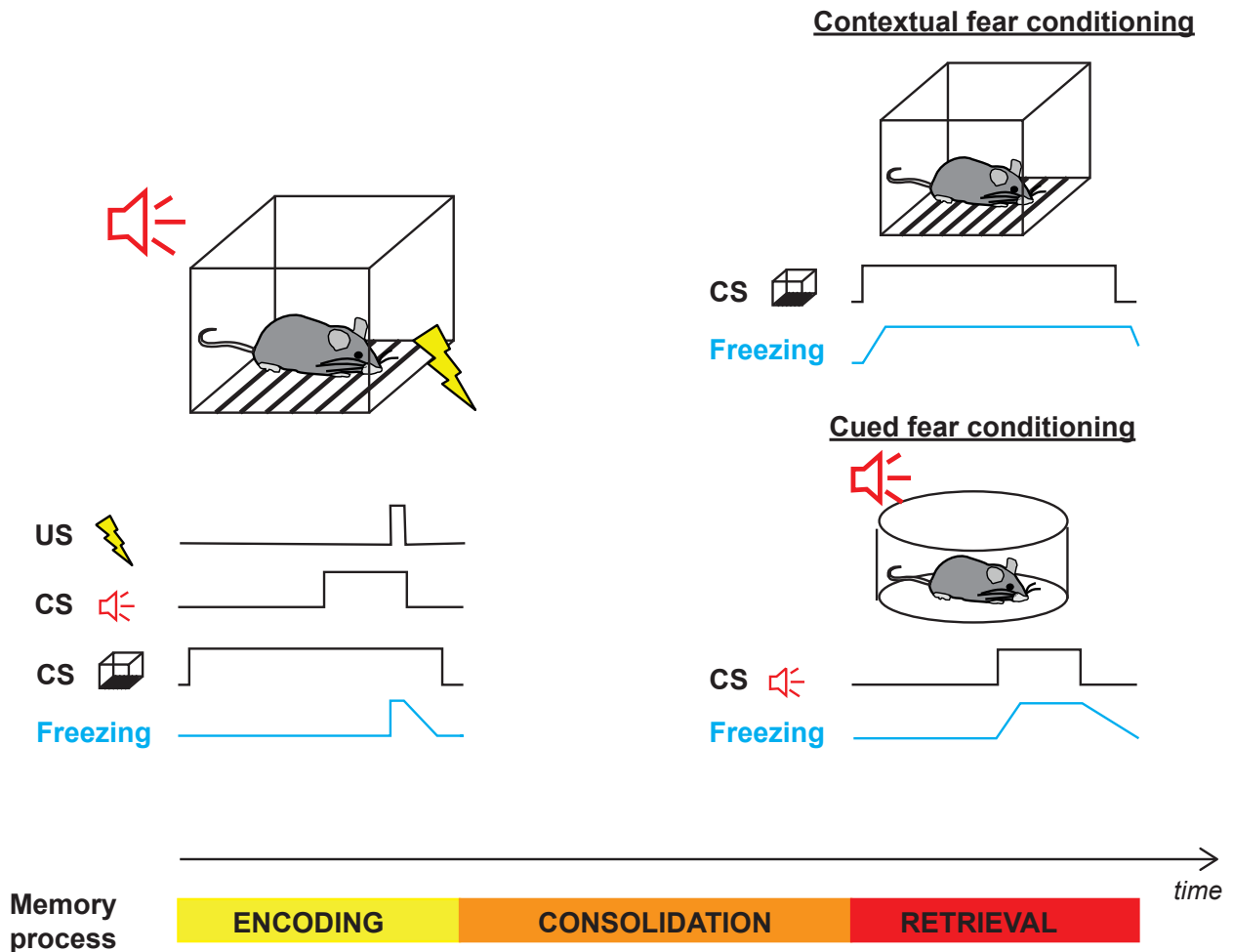


Figure 1.2: **Classical fear conditioning.** Mice are placed in a conditioning box (context), in which a sensory cue (here a tone) is paired with an unconditioned stimulus (US, here foot shock). The tone and the context are the conditioned stimuli (CS). Following memory encoding and consolidation, the presentation of either CS will elicit a fear response (freezing), even when no US is present. To test for contextual memory retrieval, mice are returned to the conditioning box. To test for cued memory retrieval, mice are placed in a novel box.

where cells are densely interconnected (associative network), and CA3, in turn, projects to CA1. Hippocampal-processed information is then sent to the BLA. While the hippocampus is required for memory retrieval few days after fear conditioning, other regions can compensate at later times (Bergstrom, 2016; Goshen et al., 2011; Eichenbaum et al., 2000). Indeed, during memory consolidation, information encoded in the hippocampus is thought to be transferred in the neocortex. The extent and speed of this transfer is, however, still a matter of debate (see Kitamura et al., 2017).

During auditory and visual fear conditioning, sensory information is sent to the BLA directly from the thalamus, or indirectly from the thalamus to BLA via sensory cortices. Longstanding evidence suggests that the BLA is a critical storage site of CS-US association (Blair et al., 2001; Gore et al., 2015; Grewe et al., 2017): incoming auditory synaptic inputs to BLA neurons are strengthened when consecutive US inputs on these same neurons lead to strong postsynaptic activity. However, recent advances also point towards a more distributed storage of fear memories (Herry et al., 2014; Letzkus et al., 2011), with specific information about fearful experiences being stored in sensory cortices. Indeed, changes in neuronal response properties occur in sensory cortices after modality-related fear conditioning (Weinberger et al., 2004; Gdalyahu et al., 2012). In the auditory cortex, the observed plasticity was highly specific to the CS frequency and was retained for several weeks. However, if this simply reflects a more efficient sensory processing of behaviorally relevant sensory cues, or if the sensory cortices are storing an important piece of information needed to reconstruct the whole memory needs further investigations. Interestingly, plasticity in sensory cortices has been suggested to depend on the integrity of the amygdala among others through its connections with the cholinergic system (Weinberger, 1995). Lesion studies have also suggested a role of sensory cortices in fear memories depending on time of retrieval (Sacco et al., 2010) or complexity of the sensory stimuli used as a CS (Romanski et al., 1992; Letzkus et al., 2011).

1.4 Technical breakthroughs in the study of memory traces

Before discussing the latest scientific breakthroughs which have been made in the past few years in the study of memory traces, we want to introduce the recent technical advances which have allowed them.

1.4.1 The immediate early-gene c-fos: a marker of neural activity implicated in learning and memory

In a pioneering work, Reijmers et al. (2007) created a "TetTag" transgenic mouse enabling the expression of any protein of interest at a given time in c-fos-positive neurons. c-Fos is an immediate early gene (IEG), highly conserved across species (Curran et al., 1984). IEGs, including Arc and Zif268, are activated rapidly by a plethora of physiological and pathological stimuli, and do not require de novo protein synthesis (Sheng et al., 1990). At a molecular level, c-fos expression is induced by two main second messengers: calcium (Ca^{2+}) and cAMP. These second

messengers activate multiple intracellular signaling cascades which lead to the activation of c-fos (Platenik et al., 2000). On average, c-fos mRNA synthesis peaks around 30 min, while protein synthesis peaks between 1 and 1h30, and both mRNA and protein have a short half-life². c-fos is part of a class of IEG encoding transcription factors: it forms an heterodimer with Jun to form the transcription factor AP1 which regulates the expression of a variety of target genes (Herdegen et al., 1998). Nevertheless, not much detail is available on the exact identity of these target genes (Kovacs, 1998). Several studies have shown a low basal level of c-fos expression and a significant increase upon a broad range of external stimuli and brain states (Harris et al. 1998; Herrera et al., 1996). Furthermore, some correlations between glucose uptake, an indirect measure of neuronal activity (Attwell et al., 2010), and c-fos expression have been observed (Sharp et al., 1989). As a consequence, c-fos has been used in brain mapping studies as a marker of neural activity (Dragunow et al., 1989; Guzowski et al., 2005). Nevertheless, the precise patterns of neuronal activity which lead to c-fos induction remain largely unknown. Studies from brain cultures indicate that bursts of APs correlate with c-fos expression in excitatory neurons (Schoenenberger et al., 2009; Fields et al., 1997; but see also Luckmann et al., 1994). c-fos mRNA levels decreased significantly after injection of an antagonist of NMDA receptors, a class of Ca²⁺ channels known to play a key role in the induction of synaptic plasticity (Tayler et al., 2011). Indeed, several studies have shown an increase in Fos expression after associative learning (Milanovic et al., 1998; Radulovic et al., 1998; Holahan et al.). Several studies hint towards a key role of IEG in memory formation -likely through gene regulation (Tischmeyer et al., 1999; Minatohara et al., 2016; Cole et al., 1989; Guzowsky et al., 2002). Long-term memory and synaptic plasticity were impaired in mice lacking c-fos in the central nervous system (Fleischmann et al., 2003). Interfering with c-fos production in the perirhinal cortex led to impaired recognition memory (Seoane et al., 2012).

1.4.2 Labeling neurons active at a given time point (TetTag and TRAP)

The TetTag system combines the c-fos promoter with the TetOff system (Reijmers et al., 2007), see Fig.1.3. The Tet-Off system is a binary transgenic system in which expression of the target transgene is dependent on the activity of an inducible transcriptional activator (the tetracycline-controlled transactivator protein or tTA). In the TetTag mouse, the tTA is under the control of the c-fos promoter. In c-fos-positive neurons, tTA expression will be induced. In other words, neurons that are sufficiently active to drive c-fos will express tTA. tTA will then bind to the tetracycline-responsive promoter element (TRE). The TRE is a fusion of a Tet operator (tetO) sequence concatemers fused to a minimal promoter and controls expression of a downstream target gene. However, expression of the target gene is regulated by doxycycline (Dox) administered to mice via food, water or injection. In the presence of doxycycline, tTA cannot bind to TRE, preventing expression of the target gene. Thus, neurons active at a specific time point in response to a specific stimuli will be "tagged" and genetically modified.

A more recent transgenic mouse line - the TRAP mouse- combines the c-fos promoter with the

²Half-lives can vary depending on brain region and inducing stimuli

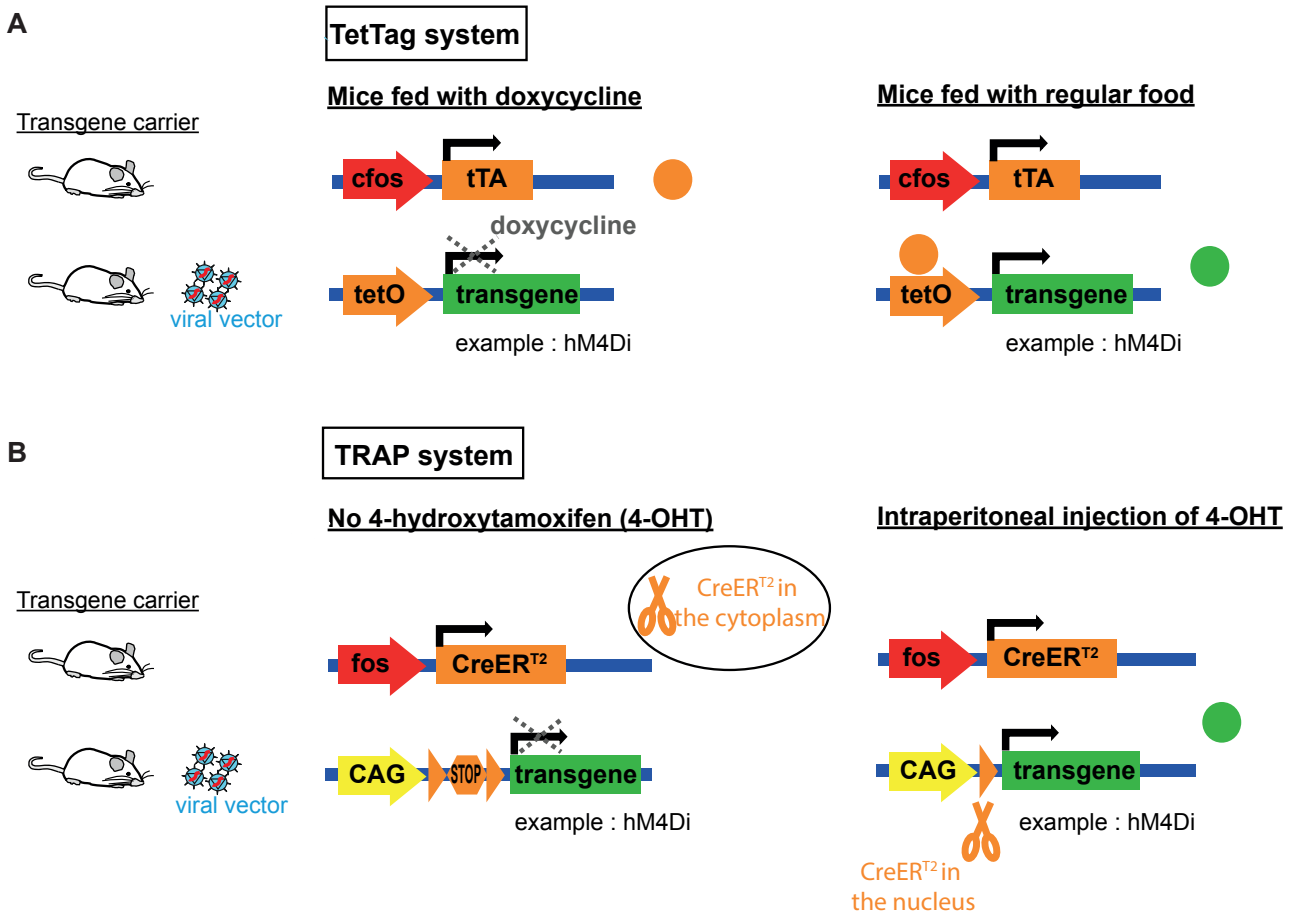


Figure 1.3: **Inducible transgene expression dependent of the fos promoter.** (A) The TetTag system: The activity-dependent c-fos promoter drives the expression of the tetracycline-controlled transactivator (tTA) gene. The transgene of interest is under control of the tet operator (tetO). In the presence of doxycycline, tTA cannot bind to tetO: activation of the latter is blocked. In the absence of doxycycline, the transgene of interest is expressed in active neurons. (B) The TRAP system: The CreER^{T2} recombinase is under the control of the activity-dependent c-fos promoter. The transgene of interest is expressed in a Cre-dependent manner. In the absence of 4-OHT, active neurons express CreER^{T2} which is retained in the cytoplasm. In the presence of 4-OHT, CreER^{T2} translocates in the nucleus of active neurons. For both systems, the transgenes are carried either by a transgenic mouse, either by a viral vector. To obtain expression, transgenic mice have to be crossed, or the virus stereotactically injected.

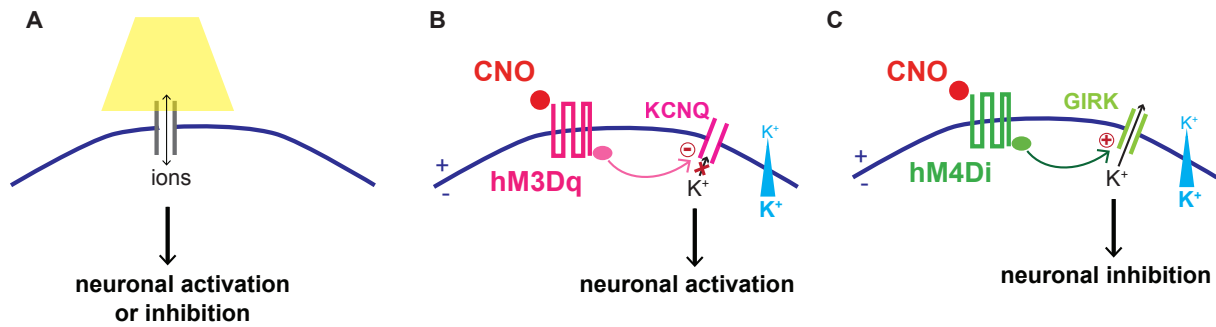


Figure 1.4: **Optogenetics and chemogenetics.** (A) Photostimulation of ion channels leads to neuronal activation (e.g. ChR2) or inhibition, depending on the nature of the ion channel. (B-C) Binding of the inert ligand clozapine N-oxide (CNO) to hM3Dq (B) or hM4Di (C) activates a second messengers cascade associated with Gq or Gi signaling, therefore inducing neuronal activation (B) or silencing (C).

tamoxifen-dependent Cre recombinase $CreER^{T2}$ (Guenther et al., 2013), see Fig.1.3. A second transgene expresses a target gene in a recombination-manner (loxP-flanked transcriptional stop signal for example). Expression of the target protein is restricted to fos-positive neurons and inducible: the $CreER^{T2}$ recombinase translocates into the nucleus of the cell only in the presence of tamoxifen or 4-hydroxytamoxifen (4-OHT) (and excise the loxP stop signal). This allows neurons active at a specific time point to be "TRAPed". This strategy has also been combined with the IEG arc (Denny et al., 2014).

1.4.3 Artificially activating or silencing neuronal activity

Another breakthrough was the development in the last fifteen years of tools that allowed neuroscientists to establish causal relationships between the activity of specific groups of neurons and circuits, and animal behavior. The two commonly and widely used tools to manipulate neuronal activity are optogenetics (Deisseroth, 2011) and chemogenetics (Alexander et al., 2009). Optogenetics relies on photoactivable receptors, while chemogenetics relies on ligand-gated receptors (see Fig.1.4). While neuronal activity can be manipulated on a millisecond timescale with optogenetics, the temporal resolution of chemogenetics is on a timescale of hours. However, chemogenetics allows the manipulation of neuronal activity in spatially distributed regions with minimal invasiveness, an advantage over optogenetic approaches. For reasons which will be highlighted later, chemogenetics will be used in our study, and will thus be described now in more details.

DREADDs³ are engineered G-coupled receptors generated from human muscarinic receptors, which are only activated by the ligand clozapine-N-oxide (CNO). CNO is a pharmacologically inert, non-endogenous and selective ligand which can cross the blood brain barrier. Via a Gq-coupled signaling pathway, activation of hM3Dq induces closure of voltage-gated potassium channels (KCNQ), which will lead to increased neuronal excitability and at last to neuronal activation. Via a Gi-coupled signaling pathways, hM4Di activates G-coupled inward rectifier potassium

³Designer Receptors Exclusively Activated by Designer Drugs

channels (GIRK), which will lead to decreased neuronal excitability and membrane hyperpolarization, thus inhibiting neuronal activity, see Figs.1.4B, C (Dong et al., 2010; Rogan et al., 2011, Wulff et al. 2012, Armbruster et al., 2007 ; Ferguson et al., 2011 ; Krashes et al., 2011 ; Sasaki et al., 2011, Shapiro et al. 2012). Among others, electrophysiological recordings in slices demonstrate the hyperpolarization and reduced firing of neurons expressing hM4Di when CNO is applied (Krashes et al., 2011).

Combining optogenetics or chemogenetics with transgenic mouse lines based on activity-dependent promoters leads to new sets of tools which we will define as the "label and manipulate" approach.

1.5 Has the memory trace been found?

The "label and manipulate" approach described in the previous section provides unprecedented opportunities to study memory traces. It allows to target a subpopulation of neurons that may be functionally related to each others (for review see Huang et al., 2013). As such, it overcomes the limitation of lesion and pharmacological manipulations by "damaging" less and more precise neuronal ensembles. However, to validate the use of this approach for studying memory traces, it has to be proven that the labeled subpopulation is part of a specific memory trace.

The majority of the studies using the "label and manipulate" approach have used contextual fear conditioning as a learning procedure. Neurons active during fear conditioning are "labeled" with fluorescent markers, photoactivable receptors or ligand-gated receptors and subsequently manipulated or characterized. These studies are based on the "Hebbian" premise that at least some neurons active during memory encoding will become part of the memory trace. Experimental evidence suggests that this premise is likely to be true (Denny et al., 2014; Reijmers et al., 2007; Tayler et al., 2013). The number of neurons activated both during contextual fear conditioning and during memory retrieval was significantly greater than chance level in the BLA, hippocampus and some regions of the cortex. Chance level is defined as the probability to have neurons activated during both memory processes knowing the percentage of neurons activated during each independent process. Chance level also corresponded to the proportion of reactivated neurons when mice were fear-conditioned in one context, but memory retrieval tested in another context (Tayler et al., 2013; Reijmers et al., 2007). Furthermore, the strength of the memory is correlated with the amount of reactivated neurons (Reijmers et al., 2007). However, the observed neuronal reactivation may be unrelated to memory retrieval. It could be that re-exposure to the same context re-activates neurons which were active on the first exposure. Thus, direct manipulation of the "labeled" ensemble will give strong support for the "memory" function of these neurons.

As mentioned in section 1.1, artificial activation of a memory trace must lead to memory retrieval in the absence of the natural retrieval cue⁴ ("sufficiency"). Conversely, its inactivation in presence of the retrieval cue must impair memory retrieval ("necessity"). Several study report the "sufficiency" and "necessity" of hippocampal ensembles "labeled" during fear conditioning

⁴original stimuli (or part of it) delivered during learning

(see Minatohara et al., 2016 or Tonegawa et al., 2015 for a review). As an example, Denny et al., 2014 showed that photo-inhibition of DG and CA3 TRAPed neurons abolished freezing behavior in the conditioned context (see also Tanaka et al., 2014 for "labeling" in CA1). Conversely, Liu et al., 2012 showed that photo-activation of DG-tagged neurons lead to freezing behavior (see also Cowansage et al., 2014 for "tagging" in the retrosplenial cortex). Interestingly, optical reactivation of a "tagged" neocortical ensemble and reactivation with contextual cues lead to activation of a similar population of neurons in the amygdala (Cowansage et al., 2014). In a similar manner, silencing a "tagged" hippocampal ensemble prevents reactivation of neocortical neurons (Tanaka et al., 2014). This indicates that even partial artificial manipulation is sufficient to perturb the reconstruction of the entire memory trace and that "artificial" retrieval mimics "natural" retrieval. These studies also support the view that memory traces are stored in a distributed network. But most importantly, these studies confirm that a population of neurons active during learning are incorporated in the memory trace and that the "label and manipulate" approach is an efficient technique to capture these neurons.

To qualify as a memory trace, an ensemble of cells must also demonstrate that changes in cellular or network properties occur following learning. Ryan et al., 2015 have characterized some molecular and electrophysiological alterations within ensembles "labeled" during learning that presumably mediate memory trace formation: DG "labeled" neurons showed an increase of synaptic strength and dendritic spine density and an increased connectivity with CA3 "labeled" neurons. This and upcoming studies will provide valuable information about the nature of the learning-induced changes in Fos-expressing neurons as well as more specific information about their characteristics after fear conditioning.

While contextual, auditory and visual fear conditioning have been extensively studied, much less is known about olfactory fear conditioning. Yet, many species rely heavily on their sense of smell.

Chapter 2

Olfactory memories

2.1 Ethological considerations: why study olfactory memories

Why should we study olfactory memory?

First, the nature of odor stimuli suggests an important role of experience and memory in shaping our sense of smell. The odor of chocolate contains over 600 different types of volatile molecules (Counet et al., 2002), yet we do not perceive each of the 600 molecules as a single odor, but we rather group them as a perceptual "whole". Each of these molecules can be characterized by several chemical structures (chain length, functional group...) as well as their concentration in air, but when they are combined together, feature description becomes tedious (Auffarth, 2013). It seems unlikely that all the possible combinations of molecules which might convey meaningful information are hardwired in the brain and lead to innate behavioral responses.

Second, olfaction is one of the oldest evolutionary senses. Yet, there is a striking similarity in the structure and function of the olfactory system between different classes of organisms, including fish, insects and mammals (Kaupp, 2010; Davis, 2004). For many species, sampling and memorizing odors is vital because it regulates many behaviors that are crucial for survival and reproductive success (foraging, mating, identification of conspecifics and predators, maternal bonding... DeBose et al., 2008; Hansson & Stensmyr, 2011). It is thus not surprising that many animals exhibit an acute sense of smell and a great capacity for olfactory learning (Slotnick, 2001). As an example, Gambian pouched rats can be trained to detect landmines or the presence of tuberculosis in human's sputum using their sense of smell (NGO Apopo). In Norwegian rats, olfactory fear memories extinguish more slowly than auditory or visual fear memories (Richardson et al., 2002). Olfaction also has a unique ability to trigger memories and emotions in humans (Chu et al., 2000). Who has not vividly recalled long-forgotten memories from his childhood after smelling a particular odor, as the character from Marcel Proust's novel "A la recherche du temps perdu" (a.k.a the Proust phenomenon)? Larsson et al., 2008 have shown that olfactory cues tend to recall memories from earlier in life than verbal and visual cues. Olfactory cues can also precipitate the recollection of traumatic memories in post-traumatic shock disorders (Vermetten et al., 2003).

Thus, the unique features of olfactory learning and memory, as well as the similarities between species will enable to generate more easily general principles about olfactory memories.

2.2 The organization of the olfactory system

How does the brain know which volatile chemical compounds are in the air? Olfactory processing begins with the odorant binding to G-protein-coupled receptors expressed at the surface of sensory neurons in the olfactory epithelium. Each neuron expresses only one of the 1300 receptor genes in the mouse genome. The axons of all the sensory neurons expressing the same receptor converge to a spatially invariant structure in the olfactory bulb (OB) called a glomerulus (Mombaerts et al., 1996). Each odorant activates a subset of olfactory receptors, resulting in a spatial sensory map in the olfactory bulb (Mori et al, 2006). Bulb-processed information is then sent to higher-order brain regions including the anterior olfactory nucleus, the amygdala, the entorhinal cortex, and the piriform cortex via the output cells of the OB, the mitral/tufted cell which innervate a given glomerulus (see Figs.2.1A,B). The piriform cortex (PC) is the largest olfactory cortex and is located on the ventrolateral surface of the brain. We will focus on this brain region and demonstrate why it is a good candidate for encoding memory traces in mice.

2.3 The piriform cortex is a good candidate for encoding memory traces

Several features make the piriform cortex a good candidate for encoding memory traces and we are going to describe them in detail now. We will focus on studies using rodents as a model system and whenever possible, on studies relating to fear conditioning.

2.3.1 Manipulating piriform activity

Manipulating piriform activity is the most evident way to test for the functional relevance of this brain region in olfactory learning and memory. To our knowledge, there are only two studies disrupting piriform activity after an associative olfactory learning task (Staubli et al., 1987; Sacco et al., 2010). Both studies demonstrated the need of an intact PC during olfactory learning and memory retrieval. More precisely, Sacco et al., 2010 showed that excitotoxic lesions of the posterior part of the PC (pPC) impair remote but not recent fear memories in rats. If the pPC was lesioned one month after fear conditioning, rats did not freeze upon presentation of the conditioned odor, but did freeze if the pPC was lesioned one day after conditioning. This time-dependent effect, as well as the preserved ability to discriminate between a novel and familiar odor in lesioned animals, excluded the possibility of pure perceptual impairments. Furthermore, unconditioned fear in the presence of a predator odor was preserved. At last, memory impairment was related

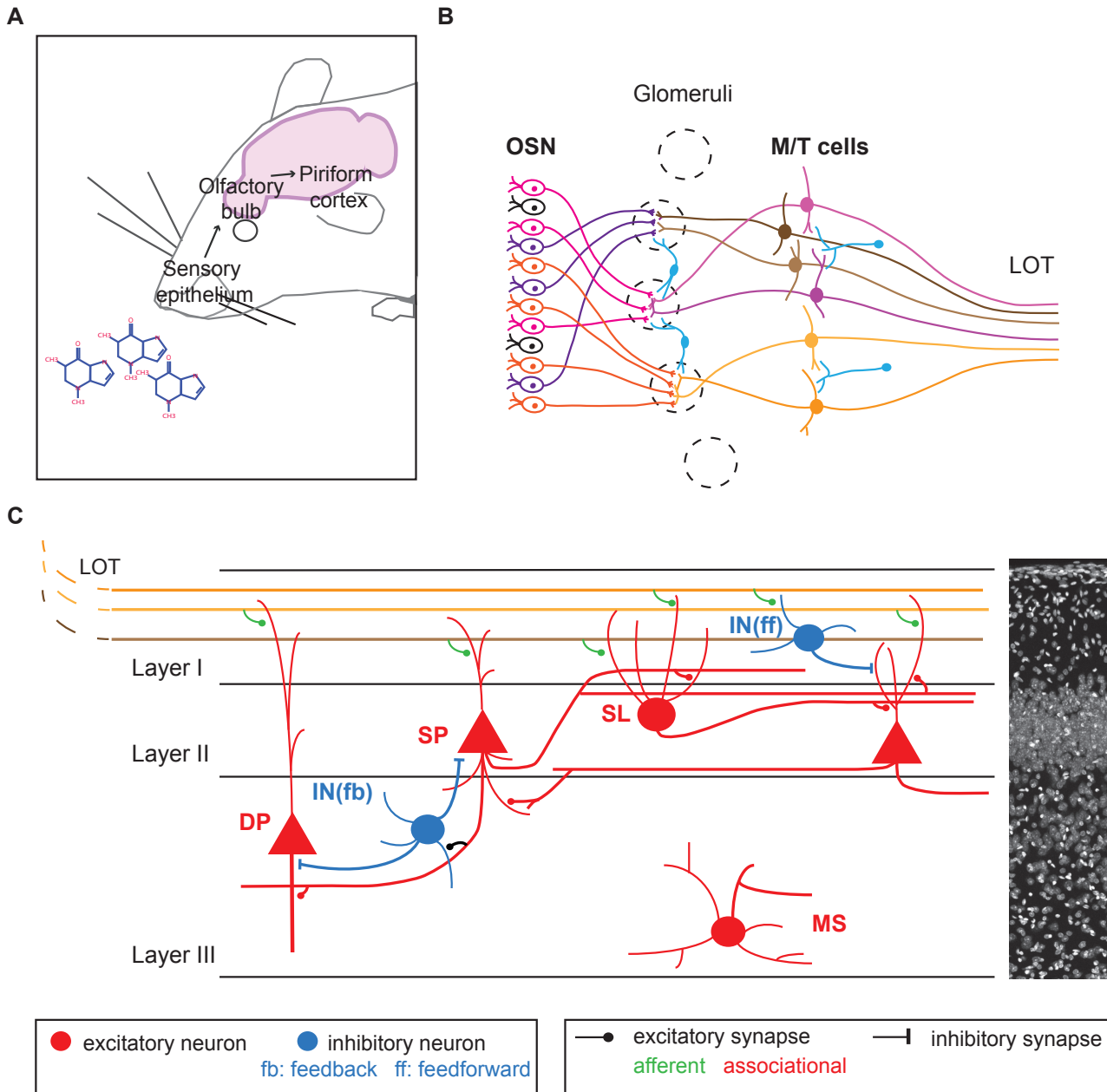


Figure 2.1: The organization of the olfactory system. (A) Odors are detected at the level of the sensory epithelium. Information is transmitted to the olfactory bulb and then to the piriform cortex. (B) Each olfactory sensory neuron (OSN) in the olfactory epithelium expresses only one of 1000 odorant receptor genes. Axons from all OSNs expressing the same receptor converge onto the same glomerulus (dashed circles) in the olfactory bulb (OB). A glomerulus is a structure defined by the OSNs synapsing with the dendrites of the OB output cells, the mitral and tufted cells (M/T). The axons of the M/T cells fasciculate to form the lateral olfactory tract (LOT), which projects to the olfactory cortex. The OB also contains several types of interneurons (light blue), including periglomerular and granule cells. (C) Circuit organization of the piriform cortex (PC): excitatory neurons are colored in red, inhibitory neurons in blue. Semilunar (SL) and superficial pyramidal (SP) cells have their somata in layer II. Deep pyramidal (DP) and multipolar spiny (MS) cells are found at lower density in layer III. Inhibitory interneurons (INs) are distributed uniformly across all layers. Excitatory cells receive afferent inputs from the OB and intracortical associational inputs from other piriform excitatory cells. Interneurons in layer I receive afferent inputs from the OB and provide feedforward inhibition to SP/SL cells. Interneurons in layer II and III are activated by piriform excitatory cells and provide strong feedback inhibition. Light shapes (NeuroTrace counterstain) on the right represent the relative density of neuronal somata in the different layers.

specifically to the olfactory modality, as lesion of the PC did not disrupt visual or auditory fear conditioning. Thus, this study suggests a key role of the PC in storing the emotional value of encountered stimuli.

Furthermore, optogenetic experiments have revealed that the activity of piriform neurons is sufficient to drive behaviors dependent on learning and experience (Choi et al., 2011). Choi et al., 2011 photostimulated random ensembles of channelrhodopsin (ChR2)-expressing piriform neurons and paired photostimulation (conditioned stimulus) with foot shock or water reward (unconditioned stimulus). After training, photostimulation alone elicited escape behavior or licking, respectively. This shows that the PC can encode "artificial" memories.

2.3.2 Piriform cortex circuits and odor representations

The PC is a three-layered structure. It contains four main types of excitatory neurons which all extend their dendrites in layer I, but differ in their morphologies, connectivity and soma location: superficial pyramidal (SP) and semilunar cells (SL) whose somata are located in layer II, and deep pyramidal (DP) and multipolar spiny (MS) cells, located in layer III. Inhibitory interneurons are scattered more uniformly across all layers and can also be classified in several subtypes (see Fig.2.1C), (Suzuki and Bekkers, 2010; for reviews see Giessel et al., 2014 and Bekkers et al., 2013)).

Genetic tracing techniques have shown that piriform neurons receive random convergent inputs from the olfactory bulb, and that mitral/tufted cells project diffusively to layer I of the PC, without any apparent topography (Miyamichi et al., 2011; Ghosh et al., 2011; Sosulski et al., 2011). Cooperative mitral and tufted cells inputs drive activity of excitatory cells (Apicella et al. 2010). Besides receiving afferent input from the OB, excitatory cells -especially SP and SL- are densely interconnected across the PC, forming a large recurrent -or associational- circuit. The probability of a given excitatory neuron to synapse with another one does not depend on their respective location (Franks et al., 2011). Inhibitory neurons located in layer I receive input from the OB and mediate local feedforward inhibition. Inhibitory neurons in other layers are activated by piriform excitatory cells and mediate feedback synaptic inhibition (Poo et al., 2011; Suzuki et al., 2012), Fig.2.1C.

The distinction is often made between the anterior and posterior PC (aPC and pPC, respectively). Anatomically, the aPC ends and pPC begins where the lateral bundle of afferent fibers -or lateral olfactory tract- ends. The aPC receives more afferent inputs and fewer associational inputs relative to the pPC (Hagiwara et al., 2012).

Consistent with this network organization, each odor activates a unique ensemble of neurons distributed across the PC, without any spatial preference. There are no spatial clusters of cells responding to similar stimulus features (Stettler et al., 2009; Rennaker et al., 2007; Illig et al., 2003; Miura et al, 2012; Roland et al., 2017). Furthermore, a neuron within an ensemble responds to multiple dissimilar odors and piriform neuronal activity in response to a mixture is not the sum of the activity to the individual components (Stettler et al., 2009 ; Poo et al., 2009). This indicates

that the PC performs synthetic processing (Wilson et al., 2003), further supporting that each odor will be processed as a single perceptual "whole".

The apparent random connectivity from the OB to the PC and the loss of OB topographical organization suggests that information contained in piriform odor representations and decoded by downstream regions should be shaped by experience.

2.3.3 Experience-shaped odor representations

Several line of evidence suggest that the PC is a highly plastic structure. It has been shown by slice electrophysiology that both afferent and recurrent synapses can be potentiated by high-frequency stimulation of their respective fibers, with a greater magnitude at recurrent synapses (Kanter & Haberly, 1990). An associative form of long-term potentiation can be induced by coactivation of afferent and recurrent fibers (Kanter & Haberly, 1993; Johenning et al., 2009). Plasticity was also evident in recordings from awake rats after fear learning: Sevelinges et al. (2004) showed a transient increase in OB stimulation-induced field potentials after CS presentation, 1 day after conditioning. These effects appeared in pPC but not in aPC. Changes in piriform response properties were also observed after other forms of associative learning (Roman et al., 1993; Litaudon et al., 1997), with some changes restricted to pPC (Mouly et al., 2001; Roesch et al., 2006). Due to their different connectivity (see above) and differential plasticity, the nature of information encoded in aPC and pPC is likely to differ.

At a network level, fear conditioning in rats sparsened piriform odor representation, when one odor was paired with shock (conditioned stimulus plus, CS+), while a second one was not (conditioned stimulus minus, CS-). Freezing was specific to the CS+. However, when a simple odor-shock association was made, fear responses were generalized to odors similar to the CS+ and a broadening of aPC odor representations was observed (Chen et al., 2011). Interestingly, sparsening was also observed in the PC after odor discrimination learning (Shakhawat et al., 2014), as well as in somatosensory cortex after tactile fear conditioning (Gdalayhu et al., 2012). Many studies now indicate that memory traces are likely to be quite sparse and embedded in a dense population of neurons (Reijmers et al., 2007 & 2009), and that sparsification may emerge as associations are learned. Theoretical studies emphasize that sparseness optimizes storage capacity (Marr, 1971).

At last, it should be noted that fear learning also enhances responses to the CS+ and induces structural plasticity earlier in the olfactory system, at the level of the sensory epithelium and OB (Jones et al., 2008; Kass et al., 2013, Fletcher, 2012). Furthermore, simple odor experience led to sparsening of OB odor representations for at least 1 week (Kato et al., 2012).

2.3.4 "Memory" computations performed by the PC

One feature of the external world is that not all odor stimuli are relevant. Electrophysiological data suggests that the PC performs figure-ground segregation, i.e. filters out background odors by

rapid sensory habituation (reviewed in Wilson et al. 2003).

Another key feature of the olfactory world is its inconstancy. A recent study from our lab has shown that despite changes in odor concentration, the identity of a monomolecular odor could be decoded by a subpopulation of concentration-invariant piriform neurons (Roland et al., 2017). However, odors are usually composed of several molecules whose proportion can vary depending on temperature, humidity, speed and direction of the wind to cite a few. If an odor stimulus is degraded, sensory input from the OB will be partial. However, even though a subset of pyramidal neurons is activated at first, recurrent connections can bypass missing afferent OB input and reactivate some of the neurons which would have been activated by the missing external information. Thus, the circuit organization of the PC is well suited to perform pattern completion (Wilson, 2009; Wilson et al., 2003; Gottfried, 2010). Using virtual ensembles of single neuron responses, Chapuis et al., 2011 showed that aPC ensemble activity to a mix of 10 odorant components "10c" and ensemble activity when removing one of the 10 components "10c-1" were significantly more correlated in the aPC than in the OB. At a behavioral level, this translated in rats having difficulty in discriminating between "10c" and "10c-1". Furthermore, we have shown in the previous section that learning potentiates recurrent synapses in an Hebbian way. Therefore, learning enhances pattern completion, which promotes perceptual stability (Wilson et al., 2003). Partially degraded odors or similar odors will be accurately decoded by downstream regions to lead to appropriate behavior (see Fig.2.2). The PC has been modeled as a 'content-addressable memory' system, where the entire memory is searched to determine whether a specific input pattern can be matched against previously experienced input patterns and if it is the case, retrieve previously stored memories (Haberly, 2001 & 1985). Nevertheless, some situations require pattern completion to shift towards pattern separation: odors sharing a high percentage of their physicochemical components can have acquired opposite ethological relevance by experience (for example if a piece of food is rotten or not). If the mouse had to learn to discriminate between two mixtures varying either in the components ratio (mix of two odors) or in the presence of a 10th component, piriform odor representations changed and became less correlated. This effect was observed both in CatFISH¹ experiments (Shakhawat et al., 2014) and using virtual ensembles of single-neuron responses (Chapuis et al., 2011). Furthermore, this effect was not seen in the OB, arguing for a piriform-specific form of plasticity. Nevertheless, the aforementioned "network-level" studies were done in aPC, and it remains thus unknown if similar network changes occur in the pPC.

2.3.5 Neuromodulation of piriform activity and learning

As mentioned in Chapter 1, behaviorally salient events are thought to activate neuromodulatory systems. The PC receives among others cholinergic input from the Horizontal Lateral Diagonal Band and several studies have demonstrated a role of acetylcholine (ACh) in modulating both olfactory learning and PC synaptic plasticity. Intraperitoneal injection of an acetylcholine antago-

¹The cellular compartment analysis of temporal activity by fluorescence in situ hybridization (catFISH) takes advantage of the time-dependent localization of the IEG Arc RNA after neuronal activation: nuclear Arc RNA signal a few min after neuronal activation for up to 15 min, and cytoplasmic Arc RNA signal 20–45 min after activation.

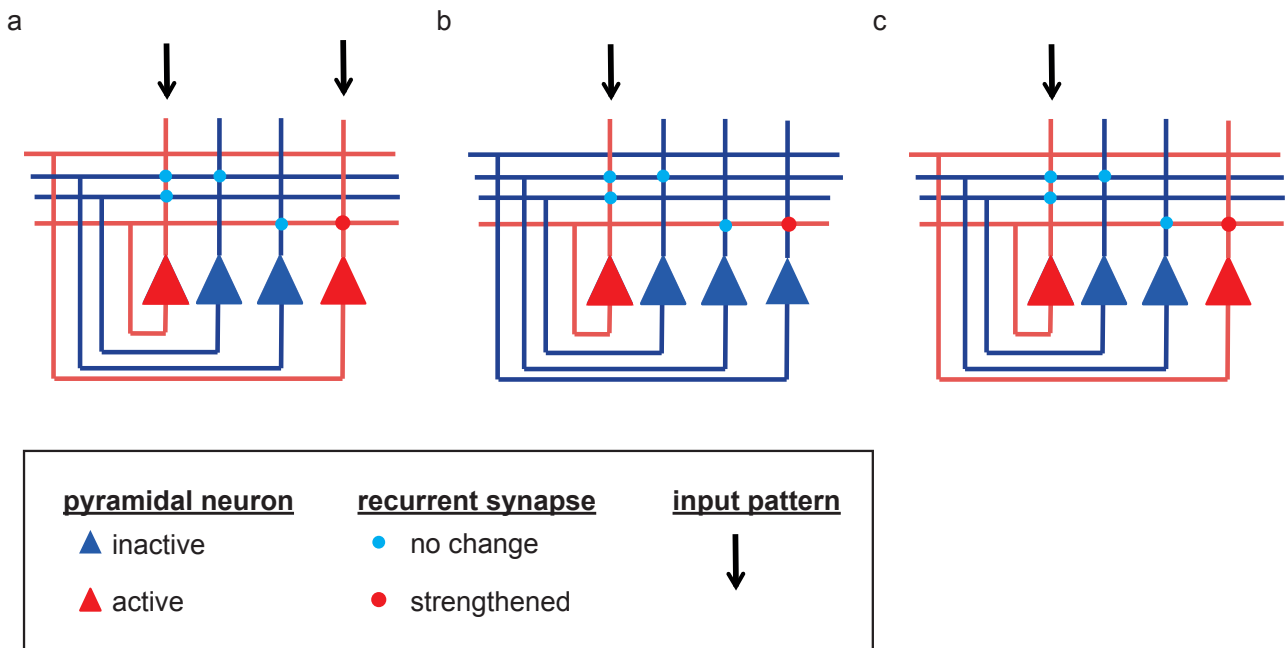


Figure 2.2: **Pattern completion.** An ensemble of piriform pyramidal neurons is activated (red) by a particular olfactory experience (the arrows symbolize the input pattern). During learning, recurrent connections between these neurons are strengthened (a). If the olfactory stimuli is presented again, but with some missing components, the input pattern will be partial (b). However, even though a subset of the ensemble representing the stimuli is activated at first, strengthened recurrent connections will activate the missing neurons (c).

nist before olfactory fear conditioning reduced fear levels on the following days when mice were presented with the conditioned odor (Pavesi et al., 2013). At a cellular level, ACh facilitates the induction of LTP at recurrent synapses by suppressing inhibitory transmission (Kanter & Haberly, 1993; Patil et al., 1998; Hasselmo et al., 1995). Therefore, ACh could act as a contextual signal enabling the formation and storage of memory traces. Computational, behavioral and electrophysiological studies have also suggested a role of ACh in increasing pattern separation (De Rosa & Hasselmo 2000; Chapuis et al., 2013a). Acetylcholine antagonists decreased synaptic transmission between recurrent connections, thus preventing the spread of activity and the incorporation of previously modified synapses in the newly formed memory. This would reduce interference between similar stored odor memories.

2.3.6 Connectivity of the piriform cortex

The PC has reciprocal and direct connections with many limbic areas (Witter et al., 1989), which reinforces the idea that it could be part of a broader network involved in mnemonic processes. We have mentioned in Chapter 1 the important role of the amygdala in fear memories. At a behavioral level, excitotoxic lesions of the BLA prior to olfactory fear conditioning lead to impaired memory formation and retrieval (Otto et al., 2000). At a cellular level, fear conditioning resulted in enhanced odor-evoked responses in the BLA in anesthetized rats (Rosenkranz and Grace, 2002).

More recently, a study (Gore et al., 2015) suggested that after olfactory fear conditioning, foot shock (US)-responsive neurons in the BLA carry important information about the learned CS-US association. The PC has reciprocal connections with the CoA and BLA (Luna et al. 2012; Johnson et al, 2000; Majak et al., 2004). However, in contrast to the dense projections from the PC to CoA, projections to the BLA are very sparse, and it has been proposed that olfactory information could transit to the BLA via the perirhinal cortex. Interestingly, projections from the BLA modulate odor-evoked activity in the pPC of anesthetized mice (Sadrian et al. 2015). Thus, there could be a coordinated interplay between the BLA and the PC during memory formation.

Other regions being connected to the PC and having been shown to be involved in learning and memory include the perirhinal cortex (Otto et al., 2000), orbitofrontal cortex (Alvarez et al., 2002; Schoenbaum et al., 2003) and lateral entorhinal cortex (Chapuis et al., 2013b).

In contrast to the lack of input topography, some studies suggest that projection neurons are topographically organized within the PC (layer-specificity, Diodato et al., 2016; along the rostro-caudal axis, Chen et al., 2014), even though this is controversial (Johnson et al., 2000).

2.3.7 Summary and glimpse into human findings

To summarize, several features of the PC make this brain region well suited for encoding olfactory fear memory traces:

- storage of information is made possible by the plasticity of connections, and is modulated by neuromodulatory inputs.
- recurrent connectivity and plasticity allows pattern completion, and thus retrieval of the appropriate fear response even if olfactory inputs signaling danger are degraded.
- the PC is interacting with regions known to play a key role in associative learning.
- one lesion study has shown impaired memory retrieval if the PC was damaged after olfactory fear conditioning.

Note that we have only cited experiments done in rodents, as it is the model organism we are going to use in this study, with fear conditioning as a learning procedure whenever possible. However, we want to mention that a spatial reorganization of sensory coding in the pPC was also observed in humans after aversive olfactory conditioning using fMRI (Li et al., 2008). Discrimination between two initially indistinguishable enantiomers was enhanced both perceptually and in PC neural activity patterns after one of them was paired with electric shock.

2.4 Hypothesis: The piriform cortex encodes olfactory memory traces

In the previous sections, we have highlighted several features of the PC which make this brain region a good candidate for being involved in olfactory learning and memories. As a consequence, we propose the following working hypothesis:

The piriform cortex encodes olfactory memory traces.

We propose to test this hypothesis by combining the TetTag system described in Chapter 1 with olfactory fear conditioning. In the first two chapters, we have pointed out the advantages of studying fear memories and given evidence that neuronal ensembles expressing cfos are part of memory traces. Furthermore, cfos expression has been shown to increase significantly after olfactory fear conditioning in the PC (Ressler et al., 2002).

Therefore, we can make the following prediction:

Manipulating piriform neurons that were active during olfactory fear conditioning affects memory retrieval.

We will describe in the next Chapter the methods used to evaluate this prediction. Specific experimental procedures will then be detailed in each Results section.

Part II

Materials and Methods

Chapter 3

Toolbox to study olfactory memory

3.1 cfos-promoter transgenic mouse lines

The three main transgenic mouse lines used were cfos-tTA (Reijmers et al., 2007, provided by M. Mayford), FosCreER^{T2} (Guenthner et al., 2013, Jackson Laboratory, stock number 021882) and Cre-dependent tdTomato (Madisen et al., 2010, Jackson Laboratory, stock number 007908).

3.1.1 cFos transgenic mouse lines: housing and genotyping

Mice

Mice were housed at 22°C–24°C with a 12-hour light/12-hour dark cycle with standard food and water provided ad libitum. Mice were group-housed with littermates until the beginning of the surgery and then single-housed in ventilated cages throughout the duration of the experiment. The ages of experimental animals ranged from 10 to 15 weeks. WT control animals were siblings that did not carry the transgene. Experiments were carried out according to European and French National institutional animal care guidelines (protocol number 2016012909576100).

cfos-tTA mice had been raised on a diet containing 1g doxycycline per kg (SNIFF and SafeDiets for "tag beta-citronellol" experiment, chapter 4.4) for a minimum of 4 days before surgery.

Genotyping

The REDExtract-N-AmpTM Tissue PCR Kit (Sigma Aldrich, XNAT) was used to extract DNA and amplify targets of interest by PCR (the protocol can be found on SIGMA's website). Primers were as follows: 5'-ACCGAGAAGCAGTACGAGA-3' and 5'-ACTCGCACTTCAGCTGCTT-3' for cfos-tTA mice, 5'-CATACTGGAAAATGCTTCTGTCC-3' and 5'-GCAATTTCCGGCTATACGTAACAGG-3' for fos-CreER^{T2} mice and 5'-CCGAAAATCTGTGGGAAGTC-3' and 5'-AAGGGAGCTGCAGTGGAGTA-3' for tdTomato mice (10μM). Amplification of DNA was carried out using the following parameters: 94°C for 3 min and then 35 cycles of 94°C for 40s, followed

by 60°C for 40s and 72°C for 1min 30s and to finish, after the cycles, 72°C for 10 min.

3.1.2 Injecting adeno-associated virus in the piriform cortex to express DREADs in Fos-positive neurons

Constructs and viruses

- tetO hM4Di virus : cloning and virus packaging

The hSynapsin promoter of a pAAV-hSyn-HA-hM4Di-IRES-mCitrine (kindly provided by B. Roth, University of North Carolina at Chapel Hill) was excised using the restriction enzyme XbaI (New England Biolabs) and replaced by the Tetracycline Response Element¹ of a pAAV-TRE-EYFP (excised with XbaI et NheI, plasmid kindly provided by S. Tonegawa, MIT, Boston). Before ligation, vector arms were dephosphorylated by alkaline phosphatase (CIP, New England Biolabs). After sequencing, the pAAV-tetO-HA-hM4Di-IRES-mCitrine (see Appendix A) was sent to the University of Pennsylvania Vector Core to generate an Adeno-associated virus (AAV), serotype 8 (10¹³ genome copies/mL, 1:2 dilution with sterile PBS on the day of injection).

- tetO-hM3Dq

The pAAV-PTRE-tight-hM3Dq-mCherry (Zhang et al., 2015) was purchased from Addgene (#66795) and sent to the University of Pennsylvania for the production of the AAV8 (10¹³ genome copies/mL, 1:2 dilution with sterile PBS on the day of injection).

- other viruses

Conditional AAV8-hM4Di-based vector (double-floxed inverted open reading frame (DIO) AAV-hSyn-DIO-hM4Di-mCherry) was purchased from University of North Carolina Vector Core. AAV1-GCaMP-based viral vector (AAV-GCaMP5) was purchased from Penn Vector Core, University of Pennsylvania.

Stereotaxic Injection into the Mouse Brain

Mice were anaesthetized with ketamine/xylazine. AAV-based vectors were injected stereotaxically into the PC (coordinates from bregma: anterior-posterior, -0.6 mm; dorsal-ventral, -4.05 mm; lateral, 4.05 mm and -4.05 mm for bilateral injections). Using a micromanipulator and injection assembly kit (Narishige; WPI), a pulled glass micropipette (Dutscher, 075054) was slowly lowered into the brain and left for 10-30 seconds in place before infusion of the virus at an injection rate of 0.2-0.3 μ L per min. 0.8-1 μ L of virus was sufficient to label a large area of PC. The micropipette was left in place for an additional 3-4 min and then slowly withdrawn to minimize diffusion up the injector tract. Skin was glued back with Vetbond tissue adhesive. To obtain maximal expression of the virus, experiments started around 10 days after viral injection.

¹tetO sequence concatemers fused to a minimal promoter

3.1.3 Immunohistochemistry, Microscopy, Cell counting

Tissue Slice Preparation and Immunohistochemistry

At the end of the experiment, mice anesthetized with pentobarbital were perfused transcardially with phosphate-buffered saline (PBS) followed by 4% paraformaldehyde. Brains were post-fixed 4h or overnight in 4% paraformaldehyde (overnight for post-hoc histological analysis of injections after behavioral experiments). 100 or 200 μm coronal sections were vibratome-cut for immunohistochemistry (200 μm for post-hoc histological analysis of injections). Sections were permeabilized in 0.1% Triton-X100/PBS (PBST) for 1 h, then blocked in 2% heat-inactivated horse serum (HIHS)-PBST for 1 h. Sections were incubated in 2% HIHS-PBST containing polyclonal primary antibodies (see Table 3.1) with gentle agitation at 4° C overnight. Next, sections were rinsed 3 times in PBST for 20 min, blocked in 2% HIHS-PBST, and incubated in NeuroTrace 640/660² (N21483, Invitrogen) and species-appropriate Alexa Fluor 488 (green) and/or Alexa Fluor 568 (red)-conjugated³ secondary antibodies (1:1000, Invitrogen) at 4°C overnight. Sections were then washed 2 times in PBST and 1 time in PBS, mounted on slides and cover-slipped with Vectashield mounting medium (Vectorlabs). Z-stacks (70 to 140 μm in total thickness, step between 7 and 10 μm) were acquired with a Leica SP5 confocal microscope or Zeiss Axio Zoom microscope and processed in Fiji.

Antibody	Dilution	Company	Species
α -GFP	1:1000	Abcam/Invitrogen	Chicken/rabbit
α -dsRed	1:200	Clontech	Rabbit
α -cFos	1:500	Santa Cruz	Goat
α -HA	1:200	Cell signaling	Rabbit
α -GABA	1:500	Sigma	Rabbit

Table 3.1: List of primary antibodies used

Automated cell counting

Z-stacks (step either 7 or 10 μm) were acquired with a Leica SP5 confocal microscope with a 20X objective and a resolution of 512x512 or 1024x1024 pixels (1 pixel: 0.72 μm). First, the PC was delineated on a maximum projection⁴ of each stack using a custom-written ImageJ macro. Cells were then counted using a custom-written ImageJ plugin, except for HA staining which was counted by hand. For each mouse, at least 4 sections were analyzed. The interval between sections and the position of the first section relative to bregma along the antero-posterior axis are indicated in Table 3.2. Care was always taken to have the same parameters (z-step/resolution/interval between section) within and between groups of mice belonging to the same experiment. For protein expressed through viral injections, sections with less than 10 positive neurons were excluded.

²except sections from the TRAP system, incubated in TO-PRO3 (T3605, Life Technologies).

³except anti-rabbit Cy3 (Santa Cruz Biotechnology).

⁴projection type: maximum intensity

	Chapter	Y-coordinate of first section	Interval (μm)
tomato	6	-0.4 mm	500
tetO-DREADDs, endogenous fos	4, 5	0 mm	600

Table 3.2: Interval between sections and position of the first section relative to bregma along the anterior-posterior axis.

Automated cell detection can be prone to error. Thus, the detection efficiency was checked on a few pictures by two people blind to the experimental conditions.

The main steps of the automated cell counting are (see Appendix B):

1) **image pre-processing**: background intensity is decreased (Subtract background, radius 20 pixels⁵) and outlier pixels are removed (Remove Outliers, radius 1 pixels⁵, threshold 70 bright). Depending on the cellular localization of the protein of interest, different types of filters are then applied. The staining is restricted to the nucleus or soma (fos/hM3Dq/GFP) or extends to dendritic and axonal fibers (tomato). Table 3.3 reports the filters⁵ used and their radius value depending on the type of staining.

	<u>Protein localization</u>	
	<u>Nuclear/cytosolic</u>	<u>Soma+ Fibers</u>
<u>Filter</u>	-Median filter, radius 1.5	-Minimum filter, radius 2 -Maximum filter, radius 2

Table 3.3: Filter parameters.

2) **thresholding and object identification**: the pre-processed z-stack is thresholded using the RenyiEntropy algorithm (Kapur et al., 1995). On each slice⁶, objects with an area smaller than $30\mu m^2$ for nuclear staining, $40\mu m^2$ for cytosolic or cytosolic+fibers are removed using the Analyze Particle command in ImageJ. A mask of each slice from the stack is created containing the filled outline of the measured particles. The number of cells is the number of 3D objects detected in the stack.

In the case of multiple stainings, co-labeled neurons are detected by overlapping the 3D objects population of each staining. If there is more than 5% overlap, then the neuron is defined as double-positive.

To count the total number of neurons counterstained with NeuroTrace, a separate method was used, because layer II piriform neurons are densely packed and staining is not homogeneous inside the cells. Background and outlier pixels are removed and a minimum filter of 2 pixels⁵ is applied. The number of neurons corresponds to the local maxima determined using the Find Maxima command in ImageJ (Noise Tolerance of 8).

⁵The radius for the filters are indicated for 512x512 images. The plugin automatically detects the resolution of the image and multiplies the values by 2 if the resolution is 1024x1024.

⁶images that make up a stack

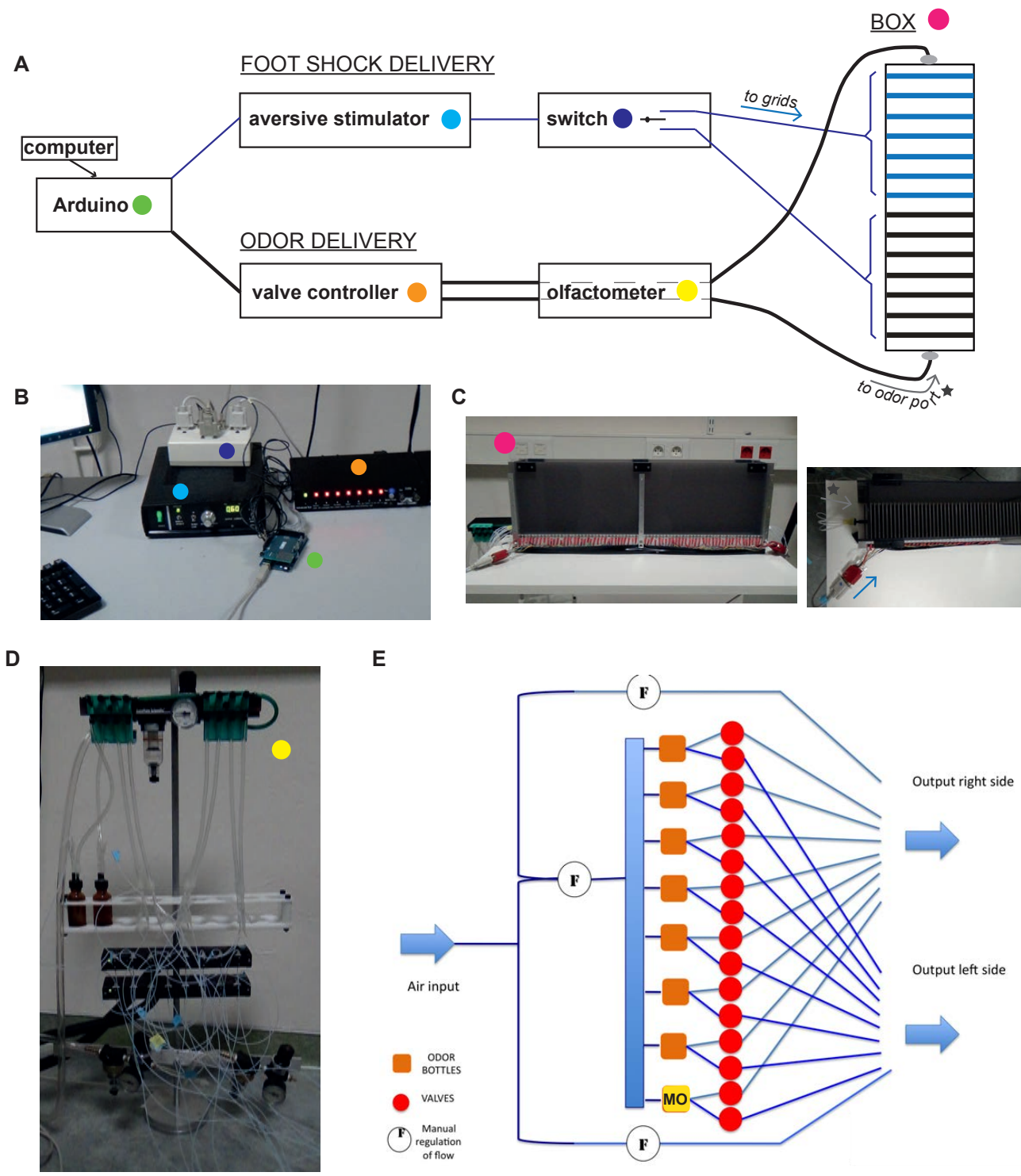


Figure 3.1: Fear conditioning setup. (A) Scheme of the behavioral setup. An Arduino board controls foot shock and odor delivery. The shock and odor can be delivered independently to each side of the box. The colored round labels refer to the corresponding picture of the apparatus. (B) Picture of the Arduino card, aversive stimulator, switch and valve controller. (C) Picture of the training box used for fear conditioning: front view (left), upper view (right). (D) Picture of the olfactometer. (E) Scheme of the olfactometer. An air flow is divided into three streams. Two of them deliver constant air flow to the box (one per side), the third one is connected to the olfactometer. For each odor, two electronic valves control delivery either to the right or the left side. When no odors are presented, air flows through a mineral oil bottle (MO).

3.2 Olfactory fear conditioning

3.2.1 Behavioral apparatus

* Apparatus

The *conditioning chamber* or *training box* (after Choi et al. 2011, custom-made) (Fig.3.1 C) was used to train mice to escape an odor. The chamber is rectangular (L 57 cm, W 17 cm, H 64 cm), with a grid floor made of 72 stainless-steel rods (diameter 6mm, space between rods of 2 mm). Walls are made of gray Altuglas Visio. Current is delivered by an aversive stimulator (MedAssociates, 115V, 60 Hz). A custom-made switcher allows a mild electric foot-shock to be applied independently to either half-side of the chamber, and is controlled with an Arduino Mega (Arduino CC), Fig.3.1 A-C.

The *testing box* was used to test memory retrieval or to present odors. Its dimensions are similar to the conditioning chamber. Materials for the walls (black expanded PVC) and floor (white Altuglas) are different from the conditioning chamber to create a different context.

* Odor delivery and odors used

Odors were delivered using an 8 channels olfactometer (Automate Scientific) (Fig.3.1 A, D, E). Clean air flowed constantly through 3 pressure regulators (pressure 3 u.i). 2 of them delivered constant air flow to each side of the boxes and the last one was directed to 8 individual air lines each connected to a 10 mL bottle containing mineral oil in which odors were diluted. The bottles themselves were connected via Tygon tubing to solenoid valves (Valvelink, Automate Scientific), whose opening was controlled by a computer (Arduino, see section above). The constant air line and the 8-controlled air lines reached each extremity of the boxes via a custom-made adapter, which was plugged in an odor port (see Fig. 3.1 A, C). To avoid pressure changes, one of the 8 air lines was connected to a bottle containing only mineral oil, and when an odor was presented, the valve was closed while the valve connected to an "odorized" bottle opened.

The following odors (Sigma), diluted in 1 mL of mineral oil (Sigma Aldrich) were used: ethyl-acetate 1%, beta-citronellol 1%, eugenol 1% and limonene 1% (see Fig.3.2).

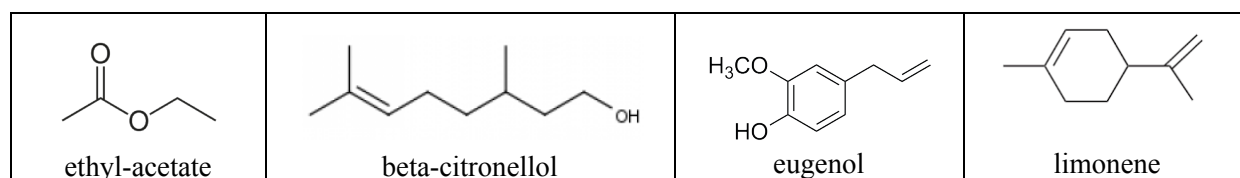


Figure 3.2: Chemical structure of the odors used.

3.2.2 Behavioral procedures

General rules

Behavioral experiments were carried out during the light phase (daytime). After stereotaxic injections, all animals were single-housed in a ventilated rack and recovered for at least 1 week from the surgery. Mice were then habituated to the room and boxes. For the *cfos-tTA* system, habituation occurred five days before odor presentation or fear conditioning. Doxycycline was removed the day after. For the *FosCreER^{T2}* system, habituation occurred one or two days before odor presentation or fear conditioning. 4-OHT was injected 20 mn before odor presentation or fear conditioning, or just after odor presentation.

The behavioral paradigm is adapted from Choi et al. (2011). During fear conditioning (training), three odors are presented: one is associated with foot-shock (Conditioned stimulus + (CS+)) and the two others are not (Conditioned stimulus - (CS-)). Odors can be presented at each extremity of the training box, and in the case of the CS+, the corresponding half-side of the box is electrified for 0.6 s (0.6 mA), Fig. 3.1 A. Before each mouse's training session, the current in each side of the box is measured using the ENV software (MedAssociates) to ensure that each mouse receives the same amount of current. Choice between CS+ and CS- as well as side of presentation was pseudo-randomized. After leaving mice undisturbed for 2 min in the box, training always starts with one presentation of each CS- followed by the first pairing of the CS+ with the US, and then again a CS-. A CS- following a CS+ is always presented on the side opposite to where the CS+ was presented. The foot-shock is delivered 4 seconds after CS+ presentation, and the CS+ lasts for 2 more seconds after shock delivery. The two CS- odors are presented during 7 seconds, 3 times each, with a total presentation of 3 on the right side and 3 on the left side. The total number of CS-US pairings -4 in this case- resulting in a consistent aversive response to odor alone was determined in a pilot experiment. A majority of mice ran away before foot-shock delivery at the fourth presentation, indicating that they had learned the association between the CS+ and the US. Furthermore, more pairings often resulted in mice becoming too stressed and staying in the middle of the box or starting to be scared by the extremities of the box.

During testing, the CS+ is presented 4 times (2 times each side), and each CS- once on each side (7s presentation). As for the training session, order and side of odor presentations was pseudo-randomized: testing always started with one presentation of each CS- followed by one CS+ presentation.

Table 3.4 lists the CS+ and CS- used. Odors were always presented when mice were close to the odor ports.

Training and testing sessions were video-recorded using a Sony camera.

Drugs

Clozapine-N-oxide (C0832, Sigma-Aldrich) was dissolved in dimethylsulfoxide (DMSO, D24-38, Sigma, final concentration of 1%) and further diluted in 0.9% sterile saline solution (0.2 mg/mL). Aliquots were stored for up to two months at -20°C and were taken out one hour be-

	Chapter	CS +	CS-
cfos-tTA experiments	4,5	ethyl-acetate	eugenol, beta-citronellol
fosCreER experiments	6	beta-citronellol	ethyl-acetate, eugenol

Table 3.4: CS+ and CS- used.

fore use to equilibrate to room temperature. The solution was then administered intraperitoneally (i.p.) (3 mg/kg). After injection, mice were left undisturbed for 25 minutes in their home cage before the start of the experiment (Sections 4.3, 4.4, 4.5 & 6.2).

4-hydroxytamoxifen (H6278 Sigma-Aldrich) was first dissolved in 100% ethanol (20 mg/mL) during 2 min in a water bath 37° C and then for an additional 18 min in a shaker at 37°C. Corn oil (Sigma Aldrich) was added to obtain a final concentration of 10 mg/mL and the ethanol was evaporated by vacuum under centrifugation. Aliquots of 4-OHT dissolved in ethanol were stored at -20°C for a maximum of 1 week and shaken at 37° C during 15 min before use. 4-OHT was i.p. injected, either 20 min before the start of the experiment or just after the end of the experiment.

Scopolamine hydrobromide (Tocris Bioscience, #1414) was dissolved in 0.9% sterile saline solution (40 mg/mL). Stock solutions were kept for one month maximum at -20°C. Mice were anaesthetized with isoflurane before the solution was infused in the brain.

3.2.3 Automated tracking of the mouse

Mouse behavior is analyzed with Matlab. I have written a program to automatically extract the position of the mouse in a region of interest, and determine when an odor stimulus is presented (see Appendix C).

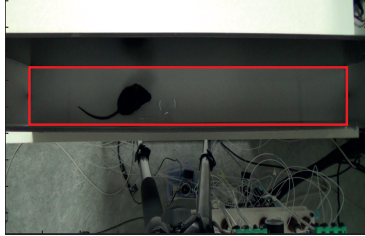
The code is divided in three main steps (see Fig.3.3):

1) The first step requires input from the user. The user first has to define the region of interest. In our case, we draw a rectangle around the inside of the box. Since the size of the boxes are known, this allows the program to convert pixels in mm. Then, in case of odor stimuli, the user has to indicate the number of stimuli. The spectrogram of the audio file is displayed, as valve opening and closing have a characteristic "signature". The user then clicks on each stimulus onset.

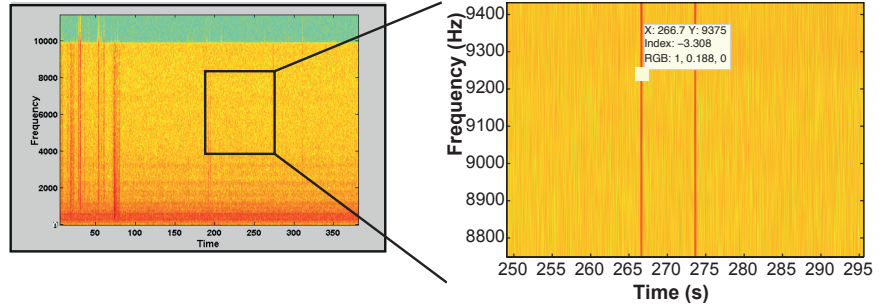
2) The second step, semi-automated, allows to detect the mouse and to determine some parameters as for example the average velocity of the mouse. First, the program calculates the background image by taking for each pixel the median value over the first 3 minutes, considering 1 frame every 2 seconds (default mode). This works well in the majority of the cases because mice are exploring the box, and seldom stay still in one part of the box. In the rare case where the mouse has a side preference, the time over which the background is calculated can be adjusted. Another way of defining the background could be to start recording the video before the mouse is in the box. After the background is defined, the background is subtracted from each frame of the video. A color threshold is set (40 for black mice and 20 for white mice where the numbers corre-

A STEP 1 :

1.1) Video data: ROI definition



1.2) Audio data: Stimuli onset definition



B STEP 2 : automated detection of the mouse

2.1) Compute background



2.2) Background subtraction



C 2.3) Thresholding and centroid estimation



● centroid of the detected object

D Example of multiple objects

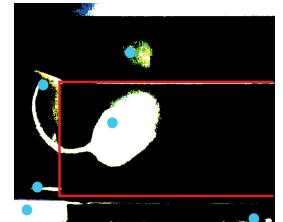
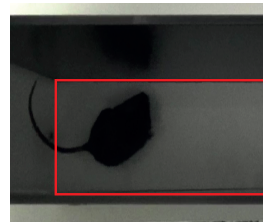


Figure 3.3: **Automated tracking of the mouse: main steps.** (A) The region of interest (ROI, red rectangle) is defined on the first frame of the video (1.1). In case of odor stimuli, the spectrogram of the audio data is displayed, as the opening and closing of the valves controlling odor delivery have a characteristic "signature". The user then clicks on each valve opening "signature" to define the time of stimuli onset (1.2). (B) The background image is computed and then subtracted to each frame. (C) The resulting image is then thresholded and the centroid of the detected object estimated. (D) Whenever more than one object is detected, some constraints are set in order to select the appropriate one as being the mouse (see text for more details).

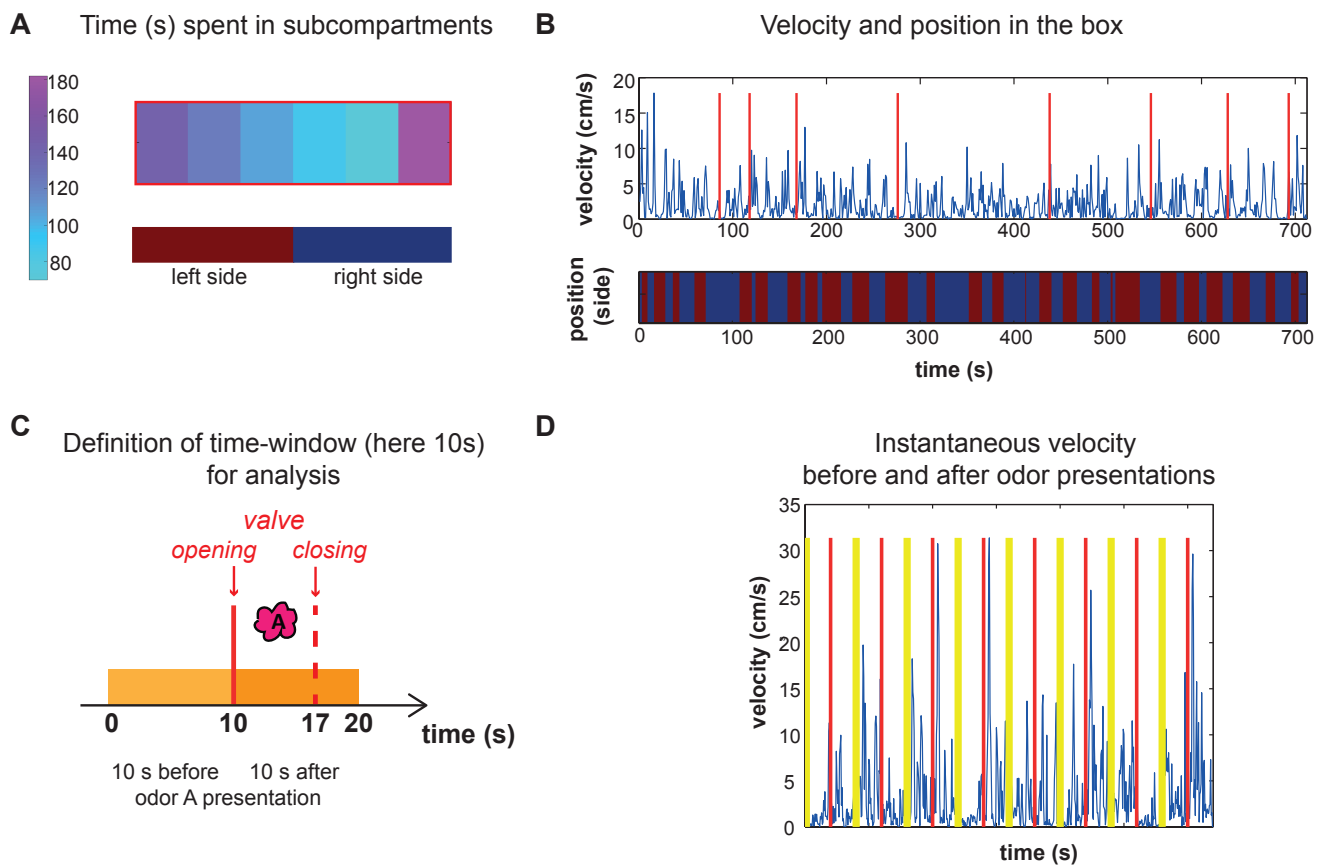


Figure 3.4: **Automated tracking of the mouse: graphical output files.** (A) The ROI is divided into 6 subcompartments and the time spent in each during the testing session is computed. (B) Instantaneous velocity and position of the mouse during the testing session. The red lines indicate odor presentations. (C) In case of odor stimuli, a time window surrounding the odor stimulus is defined. (D) Instantaneous velocity starting from 10 s before odor presentation (yellow line) until 10 s after.

spond to the RGB color code) and a binary image is obtained. This allows to only detect moving objects in each frame. Finally, the centroid of the mouse is determined using the regionprops Matlab function. The regionprops extracts different sets of properties of the white connected pixels or objects in a binary image. This allows to set some conditions on the size, length and location of the object characterized as being the mouse. Indeed, in some cases, the thresholding fragments the tail which is lighter than the rest of the body, creating multiple objects. As well, some little movements can occur in some frames, creating new small objects. More specifically:

- the object should have a number of pixels higher than 5000. This corresponds to a lower limit approximation of pixel area of the mouse in our different setups. The number was determined empirically, as it is dependent on the resolution of the camera as well as the distance between the camera and the mouse.
- the object should have a length inferior to 1000. This corresponds to a high limit approximation of the length of a mouse in pixel in our different setups.

In rare cases, no object satisfies the above-mentioned conditions. In these cases, the frame

is displayed and the user has to manually click on the mouse. Once the (x,y) coordinates of the mouse's centroid are known for each frame, several parameters can easily be calculated, such as the velocity of the mouse, the time spent in subcompartments of the region of interest..., see Fig.3.4 for some examples.

3) Finally, in case of odor stimuli, step 2 is repeated⁷ but with a higher temporal resolution (5 frames per second, default). For the sake of speed, a user-defined time window before and after stimulus presentation (10 s by default) is analyzed (Fig.3.4).

The properties of the video were as follows: 1920 x 1080 pixel resolution, 25 frames per second. The mean duration of a video was 25 min. On a MacBookPro 2,5 GHz, 16 Go, processing of one video takes approximately 40 min (10 min for the first stage, 30 min for the second stage).

3.2.4 Quantification of escape behavior

Now that mice can be automatically tracked in different boxes, it is important to define some criteria to assess if a mouse escaped during testing, thus remembering the odor. During testing, mice should have a similar reaction to the CS+ as during the training session. As already mentioned, during the latter, the odor is presented at the extremity of the box where the mouse stands, 4 s before a 0.6 s foot shock is delivered. Only half of the box is electrified allowing the mice to escape safely and avoid the shock by running towards the other extremity of the box.

The training sessions of 2 WT and 4 cfos-tTA mice from the experiment described in chapter 4, section 4 were randomly chosen. 3 out of 6 mice escaped already at the fourth CS+ presentation.

The training and testing boxes are such that the mouse can barely move along the y-axis (width) except for turning around. Thus, only the position of the mouse along the x-axis (length) is plotted as a function of time, during the 10 s following odor presentation. As the CS+ is presented twice on each side of the box to avoid contextual learning, the length of the box is scaled to 100, with 0 corresponding to the extremity of the box where the odor is presented. As we can see on Fig.3.5A&C and Table 3.5, all mice were close to the odor port when the CS+ was delivered. This was also the case 4 s after CS+ presentation, when the foot shock was delivered. The mean position 6 s after the foot-shock was 71.25 ± 23.99 , indicating that mice moved away from the CS+.

An escape behavior is most of the time linked to an increase of velocity. Thus, I plotted the maximum velocity before and after CS+ presentation, within a 10 s time window (Fig.3.5B). The average maximum velocity of mice before the odor-shock pairing was 16.33 ± 7.42 , and was almost quadrupled after odor-shock presentation (59.12 ± 32.41) (cf Table 3.5).

The above-mentioned parameters seem to describe well how the mouse reacts to the US. As the shock elicits a strong reaction, they should describe to a lesser extent the behavior of mice in response to the CS+ alone during testing. Thus, mice having learned the task and escaping from the CS+ should have crossed the midline of the testing box (corresponding to a position of 50) at the end of the CS+ presentation, and have at least a 1.5-fold increase of their maximum velocity a

⁷except for the background image calculation

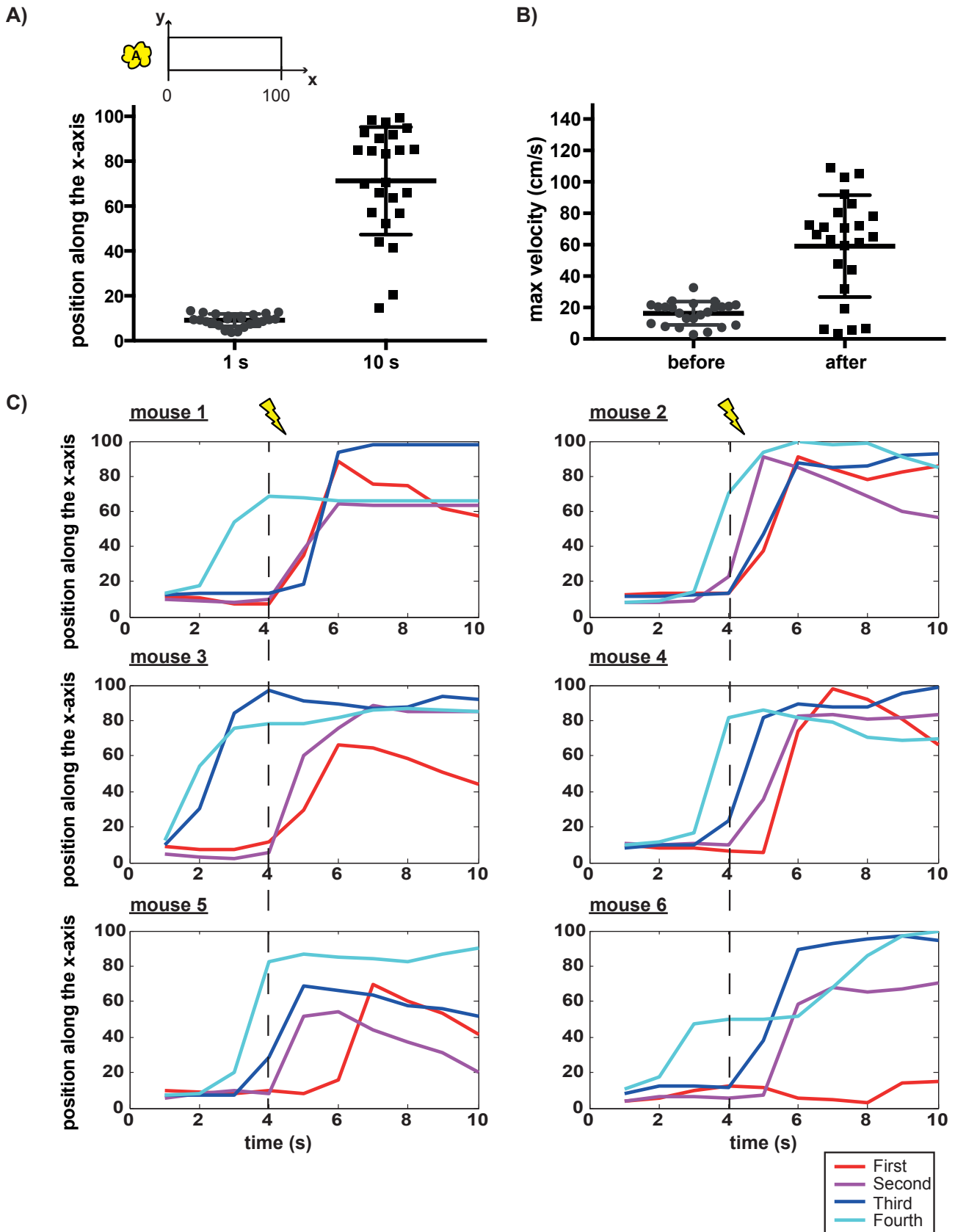


Figure 3.5: **Behaviour of the mouse during odor-shock pairing.** (A) The odor is presented randomly on the left or right side of the training box: the length of the box (x-axis) is scaled to 100, with 0 corresponding to the extremity of the box where the odor is presented (inset). Mouse position along the x-axis 1s and 10s after CS+ presentation (n=6). (B) Maximum velocity during the 10s before and after CS+ presentation (n=6). (C) Position of each of the 6 mice as a function of time after odor presentation. Each curve represents one presentation, and the color code the order of presentation. The dotted line represents the time of shock delivery for the first two trials.

Parameters	Values
Position when CS+ presented (t=0)	9, 157 ± 2, 75 (3,682; 13,32)
Position 10 s after CS+ presentation (t=10)	71, 25 ± 23, 99 (14,54; 99,46)
Maximum velocity 10 s before CS+ presentation	16, 33 ± 7, 42 (2,792; 32,68)
Maximum velocity 10 s after CS+ presentation	59, 12 ± 32, 41 (3,243; 109,1)

Table 3.5: Mean ± SD values of different parameters describing the mouse behavior during olfactory fear conditioning. Values in brackets represent the minimum and maximum value.

few seconds after CS+ presentation.

I decided not to look at reaction times, because while odor delivery is well-controlled by the olfactometer, the position of the mouse's snout relative to the odor port is not.

3.3 Statistics

Statistical analysis was performed with Prism (GraphPad). Non-parametric tests were used. Values are represented as means ± standard deviation (SD), unless otherwise stated.

Part III

Results

Chapter 4

Manipulating piriform neurons active during learning

We first determined whether the TetTag system (see Chapter 1.4 for a detailed description) could be used to selectively label neurons in the PC that were active during olfactory fear conditioning.

4.1 Tet-Tagging piriform neurons

4.1.1 Endogenous Fos expression in PC

Previous studies have shown a significant increase in Fos expression in the PC after odor presentation (Ilig & Haberly, 2003; Datiche et al., 2001). We confirmed these results by comparing expression of Fos in two groups of mice: mice in the home cage group (HC) remained in their home cage, while mice in the fear conditioning group (FC) were fear-conditioned to ethyl acetate (for details about the fear conditioning procedure, see Chapter 3.2). One hour after the start of the experiment, mice were perfused, and immunohistochemistry was performed. As previously observed, no or very few Fos-positive neurons were detected in the PC of HC mice (n=2). In FC mice (n=3), Fos-positive cells were widely distributed in all the pPC with no apparent spatial clusters (see Fig.4.1A). This is in line with *in vivo* two-photon Ca^{2+} imaging in anesthetized mice, which shows that odors activate a distributed ensemble of neurons in the PC (Stettler et al., 2009; Roland et al., 2017). Furthermore, there was a continuous variation in the intensity of the stained cells (see Fig.4.1A). Automated cell counting yielded 0% of Fos-positive cells in the HC group and $0.8 \pm 0.4\%$ of Fos-positive cells in the FC group. In the FC group, the repartition of the Fos-positive cells along the rostro-caudal axis was homogeneous (data not shown) in the pPC. Furthermore, there was a similar percentage of Fos-positive cells in the right and left hemisphere of the brain, consistent with Datiche et al., (2001). The percentage of Fos-positive cells in the right hemisphere divided by the percentage of Fos-positive cells in the left hemisphere was 0.9 ± 0.2 .

To our knowledge, there are no studies in mice quantifying the percent of total neurons ex-

pressing Fos after odor presentation.

Endogenous Fos is significantly expressed after olfactory fear conditioning. This validates the use of the *cfos* promoter to drive the expression of any protein of interest in piriform neurons that were active during learning.

4.1.2 *cfos*-tTA/tetO-DREADDs

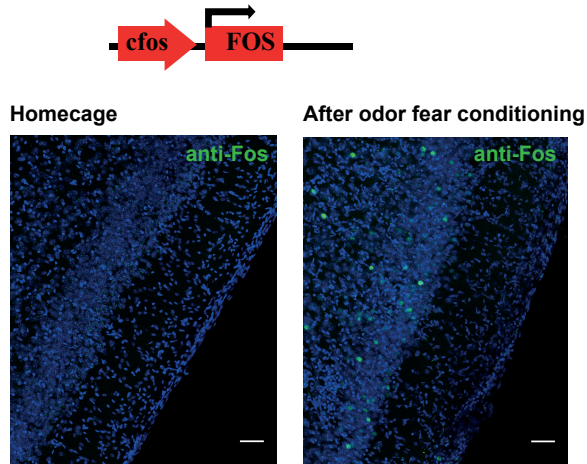
DREADDs were chosen for manipulating the activity of piriform neurons. Indeed, the PC is a large area. With chemogenetics, the targeted region is only delineated by DREADDs expression in the brain, and does not depend on light diffusion as in the case of optogenetics. We thus designed a pAAV-tetO-HA-hM4Di-IRES-mCitrine and purchased the pAAV-tetO-hM3Dq-mCherry (Zhang et al., see Chapter 3) to generate AAVs carrying DREADDs under the control of inducible *cfos* promoters. Stereotaxic injections of these AAVs enabled us to restrict DREADD expression to the PC (see Figs.4.1B, C).

mCherry's red fluorescence directly reflects levels of hM3Dq expression, while immunoreactivity targeting the HA tag directly reflects levels of hM4Di. mCitrine, a green fluorescent protein, only indicates neurons transduced by the AAV vector, which are not necessarily HA-positive (see Fig.4.2A and Pina et al., 2015 for similar results). Since there is a major overlap between mCherry endogenous fluorescence and anti-dSRed staining (see Fig.4.2B), and anti-dSRed staining renders counting more complicated due to amplification of dendritic and axonal hM3Dq expression, fluorescence of mCherry was not amplified by anti-dSRed antibody.

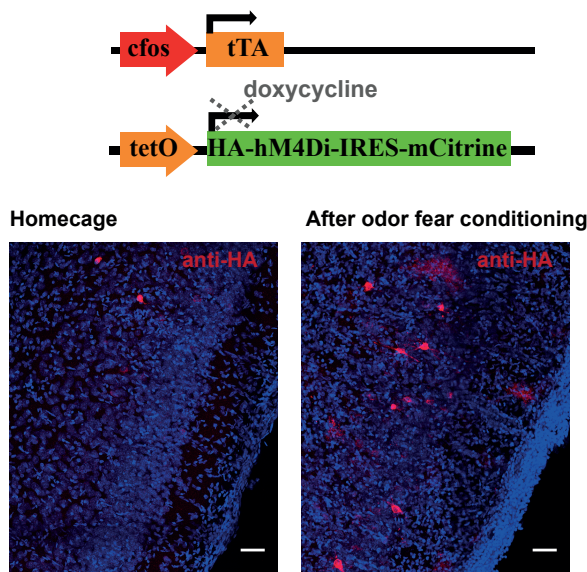
As in the previous section, we compared DREADDs expression in both HC mice and FC mice. HC mice remained on a doxycycline diet, while FC mice were taken off doxycycline five days before fear conditioning. Mice were perfused three days after fear conditioning. Indeed, previous studies have shown that TetTag-dependent expression of opsins one day after fear conditioning is greater than homecage controls (Cowansage et al., 2014; Liu et al., 2012), lasts for at least four days but is gone by thirty days (Liu et al., 2012). TetTag-dependent levels of hM3Dq have not been quantified, but CNO was injected four days after tagging and expression was similar to baseline levels thirty days after tagging (Zhang et al., 2014).

As described in chapter 3, HA-positive cells were counted by hand, while hM3Dq-positive cells and neurons labeled with Neurotracer were counted with the custom-written automatic cell counting plugin. In the HC group, 0.3% of the neurons were HA-hM4Di-positive (n=1), while $0.6 \pm 0.1\%$ were hM3Dq-positive (n=2). Zhang et al. (2015) who created the pAAV-tetO-hM3Dq did also report the presence of basal transgene expression with doxycycline. Fear conditioning lead to a 2-fold increase in the number of HA-hM4Di-positive cells (0.6%, n=1), while it lead to a 1.5-fold increase in the number of hM3Dq-positive cells ($0.9 \pm 0.2\%$, n=18). Nevertheless, the number of mice in 3 out of 4 conditions is momentarily too low to apply statistics to conclude that olfactory fear conditioning significantly increases DREADDs expression levels compared to baseline levels.

A) endogenous expression



B) AAV-tetO-hM4Di in cfos-tTA mouse



C) AAV-tetO-hM3Dq in cfos-tTA mouse

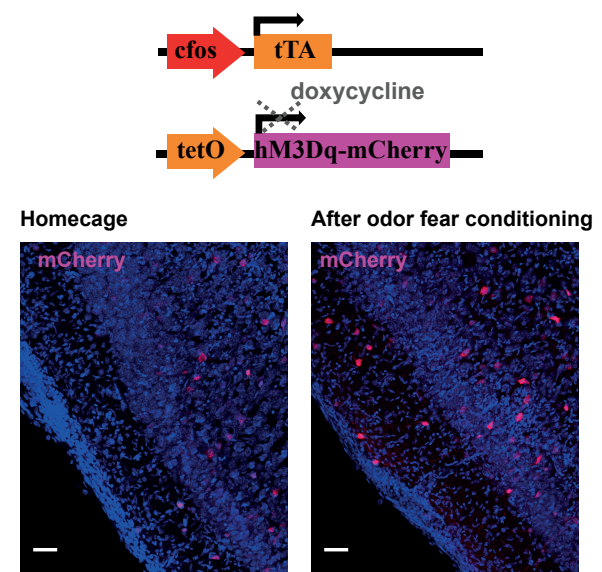


Figure 4.1: **Histological characterization of fos-tagged piriform ensembles.** A) Endogenous Fos expression in mice remaining in their homecage (left) or after odor fear conditioning (right) (see text for details). B) The "silencing" TetTag system: hM4Di is expressed in cfos-expressing piriform neurons upon doxycycline removal. Mice remained in their homecage on doxycycline (left) or were fear conditioned to ethyl-acetate (right). Neurons expressing hM4Di were visualized with HA-tag immunostaining. C) The "activating" TetTag system: hM3Dq is expressed in cfos-expressing piriform neurons upon doxycycline removal. Mice remained in their homecage on doxycycline (left) or were fear conditioned to ethyl-acetate (right). Neurons expressing hM3Dq were visualized with mCherry fluorescence. Neurotrace counterstain in blue. Scale bars, 50 μ m.

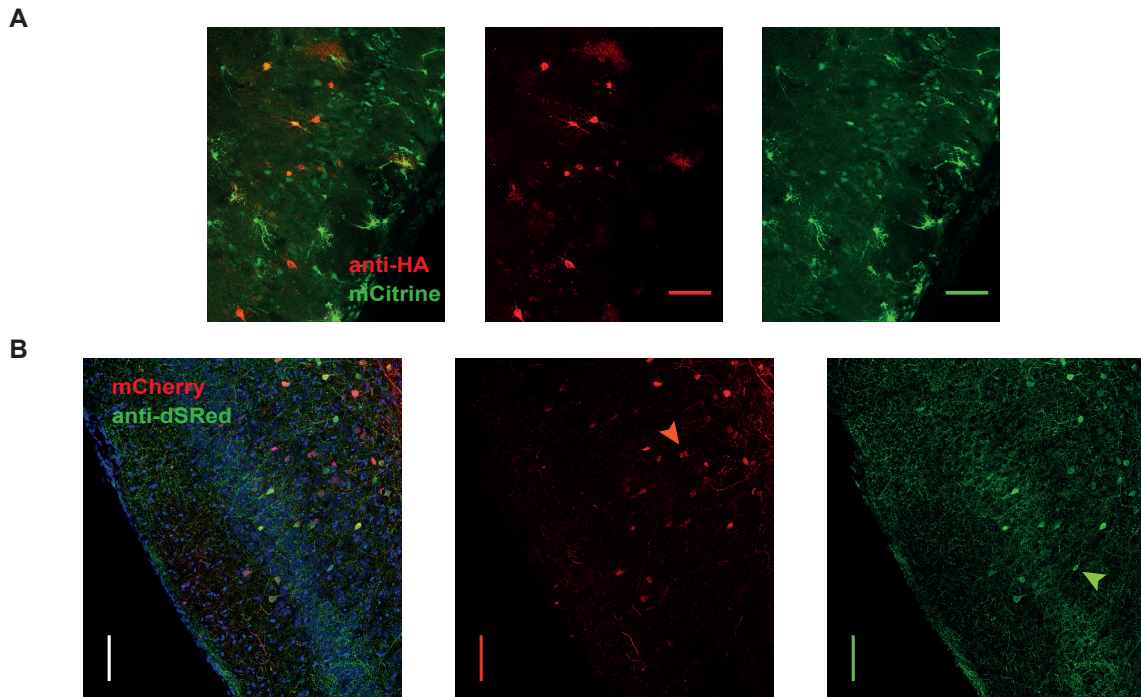


Figure 4.2: **Native fluorescence in DREADDs-expressing cells.** (A) Native mCitrine fluorescence indicates neurons transduced by AAV. HA staining indicates neurons expressing hM4Di. (B) Native mCherry fluorescence colocalizes with anti-dSRed staining. A few neurons are not double-positive (red and green arrows). Scale bars, 100 μm .

4.2 Manipulating the activity of piriform neurons

In collaboration with Yulia Dembitskaya and Laurent Venance from Collège de France, Paris, we then performed slice electrophysiology to ensure that CNO perturbed the activity of Fos-tagged piriform neurons expressing DREADDs.

4.2.1 Methods

Piriform cortex slice preparation

Parasagittal or coronal slices (300 μm thick) of the PC were prepared from 6-8-week-old female cfos-tTA mice injected with AAV-tetO-hM4Di-IRES-mCitrine or AAV-tetO-hM3Dq-mCherry (see Constructs in Chapter 3 for more details) in accordance with the guidelines of the local animal welfare committee (Center for Interdisciplinary Research in Biology Ethics Committee) and the EU (directive 2010/63/EU). Animals were anaesthetized with isoflurane, anesthetized with ketamine and xylazine, perfused with ice-cold ACSF solution (125 mM NaCl, 2.5 mM KCl, 25 mM glucose 25 mM NaHCO₃, 1.25 mM NaH₂PO₄, 2 mM CaCl₂, 1 mM MgCl₂, 1 mM pyruvic acid, bubbled with 95% O₂/5% CO₂ and osmolarity adjusted to 295 ± 5 mOsm) and decapitated. The brain was cooled with ice-cold ACSF solution and then sliced using a 7000SM2 vibrating microtome (Campden Instruments, UK). Slices were incubated in the same solution at 34°C for

one hour and then kept at room temperature. The slices were then transferred to the recording chamber and continuously perfused with ACSF solution at 34° C.

Two-photon imaging and electrophysiology

DREADDs expression was verified with two-photon excitation (830nm, Chameleon MRU-X1, Coherent, UK) under a Scientifica TriM Scope II microscope (LaVision, Germany), with a 60x/1.00 water-immersion objective. The fluorescence of mCitrine (hM4Di) and mCherry (hM3Dq) was collected by photomultipliers within 525/50 and 620/60 nm ranges, respectively. Whole-cell recording pipettes with 5-7 M Ω resistance were filled with the following solution (in mM): 122 K-gluconate, 13 KCl, 10 HEPES, 10 phosphocreatine, 4 Mg-ATP, 0.3 Na-GTP, 0.3 EGTA (adjusted to pH 7.35 with KOH). The recording solution also contained the morphological tracer Alexa Fluor 594 (5 μ M, red channel) for non-expressing and hM4Di-positive cells or the Ca²⁺-sensitive dye Fura-2 (300 μ M, replacing EGTA in the recording solution, green channel) for hM3Dq-positive cells, to enable identification of the patched cell and to visualize its morphology. The excitability of three cell types was measured in current-clamp mode by 500ms steps of current injections from -300 to +500 pA with steps of 20 pA, before and after CNO (5 μ M) application. The series resistance was usually <20 M Ω , and data were discarded if it changed by more than 20% during the recording. Signals were amplified using EPC9-2 amplifiers (HEKA Elektronik, Lambrecht, Germany). All recordings were performed at 34°C, using a temperature control system (Bath-controller V, Luigs & Neumann, Ratingen, Germany) and slices were continuously superfused with ACSF solution, at a rate of 2 mL/min. Voltage-clamp recordings were filtered at 5 kHz and sampled at 10 kHz and current-clamp recordings were filtered at 10 kHz and sampled at 20 kHz, with the Patchmaster v2x32 program (HEKA Elektronik).

Data Analysis

Electrophysiological data were analyzed with custom made software in Python 3.0 and averaged in MS Excel (Microsoft, USA). Statistical analysis was performed with Prism 5.02 software (San Diego, CA, USA). In all cases “n” refers to an experiment on a single cell from a single slice and results are expressed as mean \pm SEM. Statistical significance was assessed using nonparametric tests: Mann Whitney and Wilcoxon signed-rank test, as appropriate, using the indicated significance threshold (p).

4.2.2 Results

First, we identified DREADDs-expressing neurons under a two-photon microscope. Three main cell types were found: pyramidal cells, semilunar cells and inhibitory interneurons (see Fig.2.1). This was confirmed by anti GABA immunohistochemistry (see Fig.4.3).

We patched mice expressing hM4Di with a solution containing the morphological tracer Alexa Fluor 594 (5 μ M). hM4Di-expressing cells showed a fluorescent signal in the red channel (Alexa Fluor 594) and in the green channel (mCitrine), while hM4Di-negative cells showed a fluorescent signal only in the red channel (Fig.4.4 A,B). Similarly, we patched mice expressing hM3Dq with a

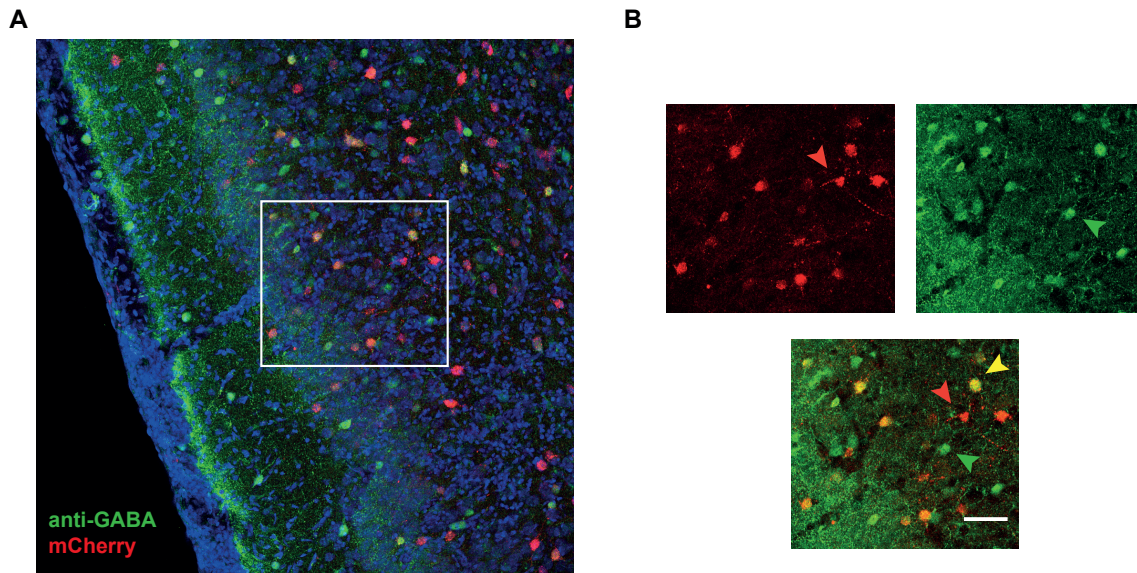


Figure 4.3: **Immunohistochemical analysis of GABA expression in hM3Dq-positive neurons.** (A) hM3Dq is expressed in excitatory and inhibitory neurons. Overlap between GABA-positive and cfos-driven hM3Dq-mCherry positive neurons. NeuroTrace counterstain in blue. (B) High magnification of piriform layer II and III (boxed area in A). The red arrowhead points towards a hM3Dq-positive and GABA-negative neuron, the green arrowhead points towards a hM3Dq-negative but GABA-positive neuron, and the yellow arrowhead towards a double-positive neuron. Scale bar, 50 μm .

solution containing the Ca^{2+} -sensitive dye Fura-2. hM3Dq-expressing cells showed a fluorescent signal in the red channel (mCherry) and in the green channel (Fura-2), while hM3Dq-negative cells showed a fluorescent signal only in the green channel (Fig.4.4A,C). After we could reliably distinguish DREADDs-negative and DREADDs-positive cells, we compared their basic membrane properties. We observed no significant difference in the resting membrane potential of non-expressing cells (-70.47 ± 0.93 mV, $n=24$) compared to hM4Di-expressing cells (-71.89 ± 0.86 mV, $n=14$) ($p = 0.515$) and to hM3Dq-expressing cells (-71.72 ± 0.94 mV, $n=15$) ($p = 0.399$) (Fig.4.4 D). We also observed no significant difference in the input resistance of non-expressing cells (186.55 ± 15.28 M Ω , $n=23$) compared to hM4Di-expressing cells (190.17 ± 34.65 M Ω , $n=12$) ($p = 0.461$) and to hM3Dq-expressing cells (213.17 ± 21.78 M Ω , $n=14$) ($p = 0.356$) (Fig.4.4E). Finally, we observed no significant difference in the threshold for action potentials (AP) generation of non-expressing cells (-30.68 ± 1.23 mV, $n=24$) compared to hM4Di-expressing cells (-31.86 ± 1.39 mV, $n=14$) ($p = 0.911$) and to hM3Dq-expressing cells (-30.26 ± 1.56 mV, $n=15$) ($p = 0.722$) (Fig.4.4 F). Therefore, DREADDs expression does not change basic membrane properties of the neuron.

We then tested how bath application of the DREADDs' agonist CNO would affect the excitability of those cells, by delivering depolarizing current steps. We defined the step when the neuron started spiking as the first one and the step when the number of APs reached a plateau value as the last one (to account for inherent differences in spiking patterns, since we recorded from three different cell types). We first quantified the number of APs resulting from the third current step injection, counting from the first step, before and after CNO application. In non-expressing cells

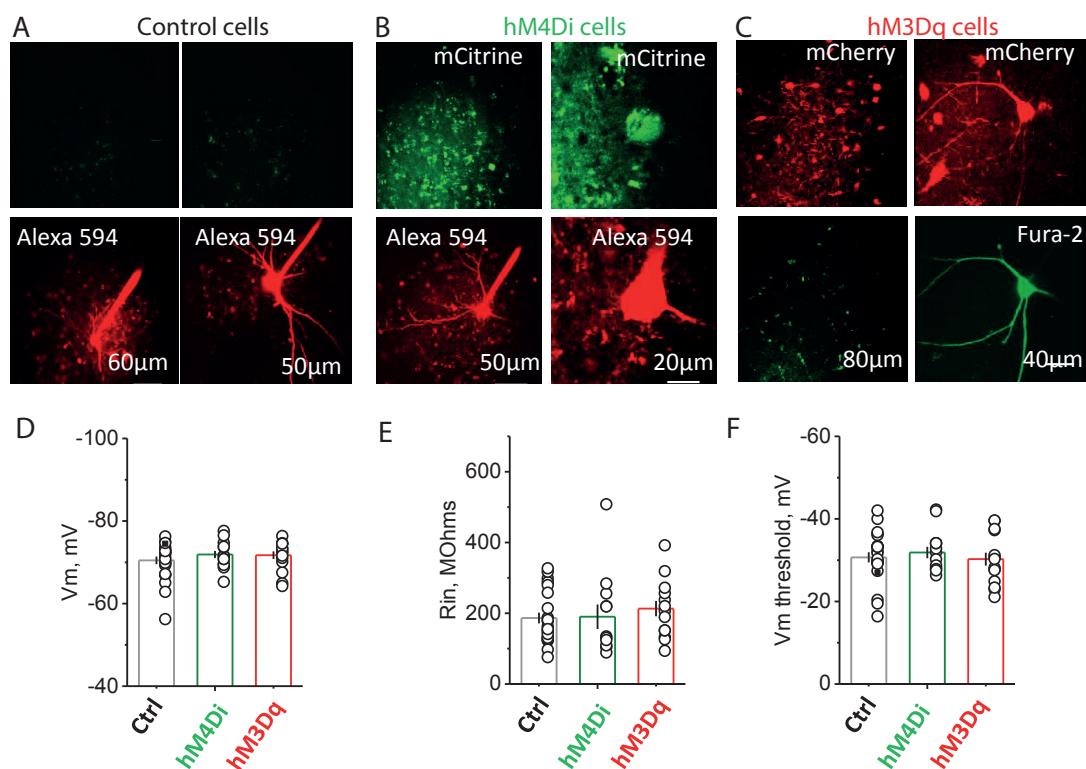


Figure 4.4: **Verification of morphological and membrane properties of DREADDs-expressing and non-expressing cells.** (A) Non-expressing cells (Control, Ctrl) with Alexa Fluor 594 fluorescence. (B) hM4Di-expressing cells showing a fluorescent signal in the red channel (Alexa Fluor 594) and in the green channel (mCitrine). (C) hM3Dq-expressing cells showing a fluorescent signal in the red channel (mCherry) and in the green channel (Fura-2). (D-F) The resting membrane potential (D), the input resistance (E) and the threshold for action potentials generation (F) did not differ between DREADDs-expressing and non-expressing cells.

we did not observe a significant change in the number of APs after CNO application ($n=9$, $p = 0.672$) (Fig.4.5 A). In hM4Di-expressing cells, the number of APs significantly decreased after CNO application ($n=10$, $p = 0.010$), as seen on Fig.4.5 B. In contrast, in hM3Dq-expressing cells, the number of APs significantly increased after CNO application ($n=11$, $p = 0.006$), as seen on Fig.4.5C. Similarly, we compared the number of APs resulting from the third current step counting from the last step, before and after CNO application. In non-expressing cells we did not observe a significant change in the number of APs after CNO application ($n=12$, $p = 0.168$) (Fig.4.5 D). In hM4Di-expressing cells, we observed a significant decrease in the number of APs after CNO application ($n=10$, $p = 0.014$) (Fig.4.5 E). In hM3Dq-expressing cells, we did not observe a significant change in the number of APs after CNO application ($n=9$, $p = 0.703$) (Fig.4.5 F). Thus, CNO does not alter the excitability of non-expressing cells, while it decreases the excitability of hM4Di-expressing cells. CNO increases the excitability of hM3Dq-expressing cells until the applied depolarization reaches saturation level in firing.

Finally, we compared how membrane properties changed after CNO application, by calculating parameters ratio after/before CNO. There was no significant difference in input resistance be-

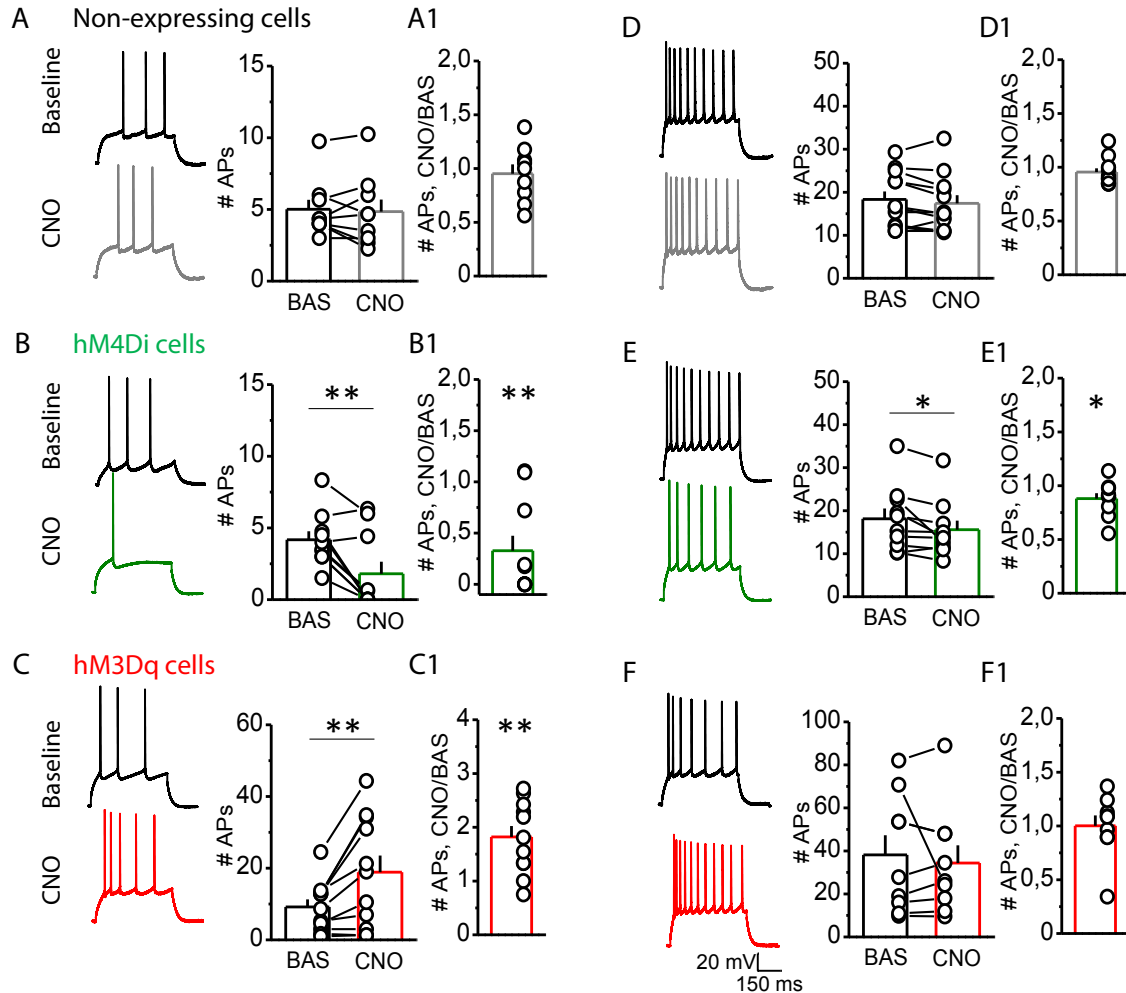


Figure 4.5: **Excitability of DREADDs-expressing cells after CNO application.** (A-C) Number of APs resulting from the third depolarizing current step, counting from the first step (when the neuron starts spiking), before and after CNO application: non-expressing cells (A), hM4Di-expressing (B) and hM3Dq-expressing cells (C). (A1-C1) Number of APs ratio after/before CNO. After CNO application, the number of APs in non-expressing cells does not change (A1), significantly decreases in hM4Di-expressing cells (B1) and significantly increases in hM3Dq-expressing cells (C1). (D-F) Number of APs resulting from the third current step, counting from the last step (when the number of APs saturates) before and after CNO application: non-expressing cells (D), hM4Di-expressing (E) and hM3Dq-expressing cells (F). (D1-F1) Number of APs ratio after/before CNO. After CNO application, the number of APs does not change in non-expressing cells (D1), significantly decreases in hM4Di-expressing cells (E1) and does not change in hM3Dq-expressing cells (F1). BAS=baseline, measured before CNO application. * $p < 0.05$, ** $p < 0.01$

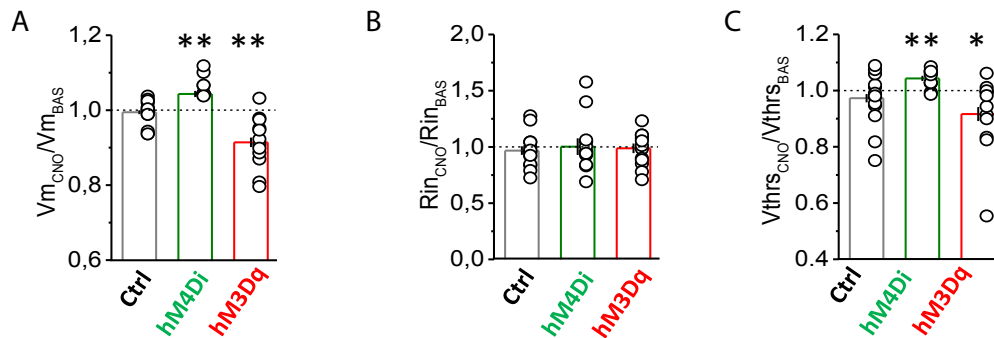


Figure 4.6: **Membrane properties of DREADDS-expressing and non-expressing cells after CNO application.** (A) The resting membrane potential does not change in non-expressing cells (Ctrl), hyperpolarizes in hM4Di-expressing cells and depolarizes in hM3Dq-expressing cells after CNO application. (B) Input resistance does not change in DREADDS-expressing and non-expressing cells after CNO application. (C) The threshold for action potentials generation does not change in non-expressing cells, increases in hM4Di-expressing cells and decreases in hM3Dq-expressing cells after CNO application. BAS=baseline, measured before CNO application. * $p < 0.05$, ** $p < 0.01$

fore and after CNO application in non-expressing cells ($n=15$, $p=0.252$), or in hM4Di-expressing ($n=12$, $p = 0.622$) and hM3Dq-expressing cells ($n=13$, $p = 0.825$) (Fig.4.6A). Nevertheless, after CNO application, the resting membrane potential hyperpolarized in hM4Di-expressing cells ($n=12$, $p=0.007$), depolarized in hM3Dq-expressing cells ($n=13$, $p = 0.001$), while it remained unchanged in non-expressing cells ($n=15$, $p = 0.890$) (Fig.4.6B). Furthermore, the threshold for APs generation after CNO application did not change significantly in non-expressing cells ($n=15$, $p = 0.489$), but increased in hM4Di-expressing cells ($n=12$, $p = 0.002$) and decreased in hM3Dq-expressing cells ($n=13$, $p = 0.013$) (Fig.4.6C). These data suggest that CNO application does not affect membrane properties of non-expressing cells, but changes the resting membrane potential and the threshold for APs generation in DREADDS-expressing cells.

Thus, slice electrophysiology confirmed that the activity of fos-tagged piriform neurons expressing DREADDS could be manipulated with CNO.

4.3 Silencing piriform neurons active during learning impairs odor memory retrieval

A key prediction of our hypothesis which we will now test is that piriform neurons that were active during the encoding of an olfactory fear memory are necessary for memory retrieval.

4.3.1 Experimental design

AAV-tetO-hM4Di was stereotaxically injected in both hemispheres of the PC of cfos-tTA transgenic male mice. Mice were then given ten days to recover, before being habituated on

day 11 to the training and testing boxes (40 and 10 min each). Twenty-four hours after habituation, doxycycline was removed and replaced by a normal food diet. Five days later, mice were trained to associate ethyl-acetate (etac) with foot shock. The odor was presented randomly on one side of the training box, and the corresponding half of the box floor was electrified for less than a second. Mice thus learned to escape to the opposite side when the odor was presented (for more details, see Chapter 3). Training included presentation of two other odors (eugenol and beta-citronellol) which were not paired with foot shock. During training, hM4Di expression was induced in active piriform neurons. Immediately after fear conditioning, mice were put back on a doxycycline diet to avoid further expression of hM4Di. Three days later, memory retrieval was tested in the presence of CNO (see Fig.4.7 A). As a consequence, piriform neurons active during learning were silenced. If these neurons are necessary for memory retrieval, silencing them should impair memory retrieval.

Two controls groups were used: cfos-tTA mice expressing GCaMP instead of hM4Di (injection AAV-hSyn-GCaMP5, n=5) and WT mice injected with the AAV-tetO-hM4Di vector (n=10). The experimental group consisted of cfos-tTA mice injected with tetO-hM4Di (n=16). 3 mice had to be excluded from the analysis as they were too stressed during testing and stayed in the middle of the box. After histological posthoc analysis, only mice who were bilaterally injected with at least all the posterior part of the PC infected were included in the analysis (see Fig.4.8). As a consequence, of the 13 remaining mice in the experimental group, 6 additional mice were excluded from the analysis (among these 6, 3 were unilateral injections).

4.3.2 Results

Impaired memory retrieval

As determined in Chapter 3, we combined two parameters to quantify escape behavior and thus test if the memory was retrieved: the position of the mouse in the box after odor presentation (the length of the box is defined as an x-axis, 0 being the extremity where the odor is presented and 100 the opposite extremity), and the maximum velocity during a 7s¹ time window before and after odor presentation. A mouse escaped during the odor presentation if both conditions were met:

- the mouse crossed the midline (position greater or equal to 50).²
- its maximal velocity after odor presentation is at least 1.5 greater than its maximal velocity before odor presentation (ratio after/before).²

We also plotted the value of the maximum velocity after odor presentation². While it is difficult to determine the value corresponding to an escape response, the comparison of the value between groups can nevertheless be informative.

As expected, the control groups exhibited an escape behavior after CS+ presentation (averaged

¹corresponds to the duration of an odor presentation

²averaged value of four presentations

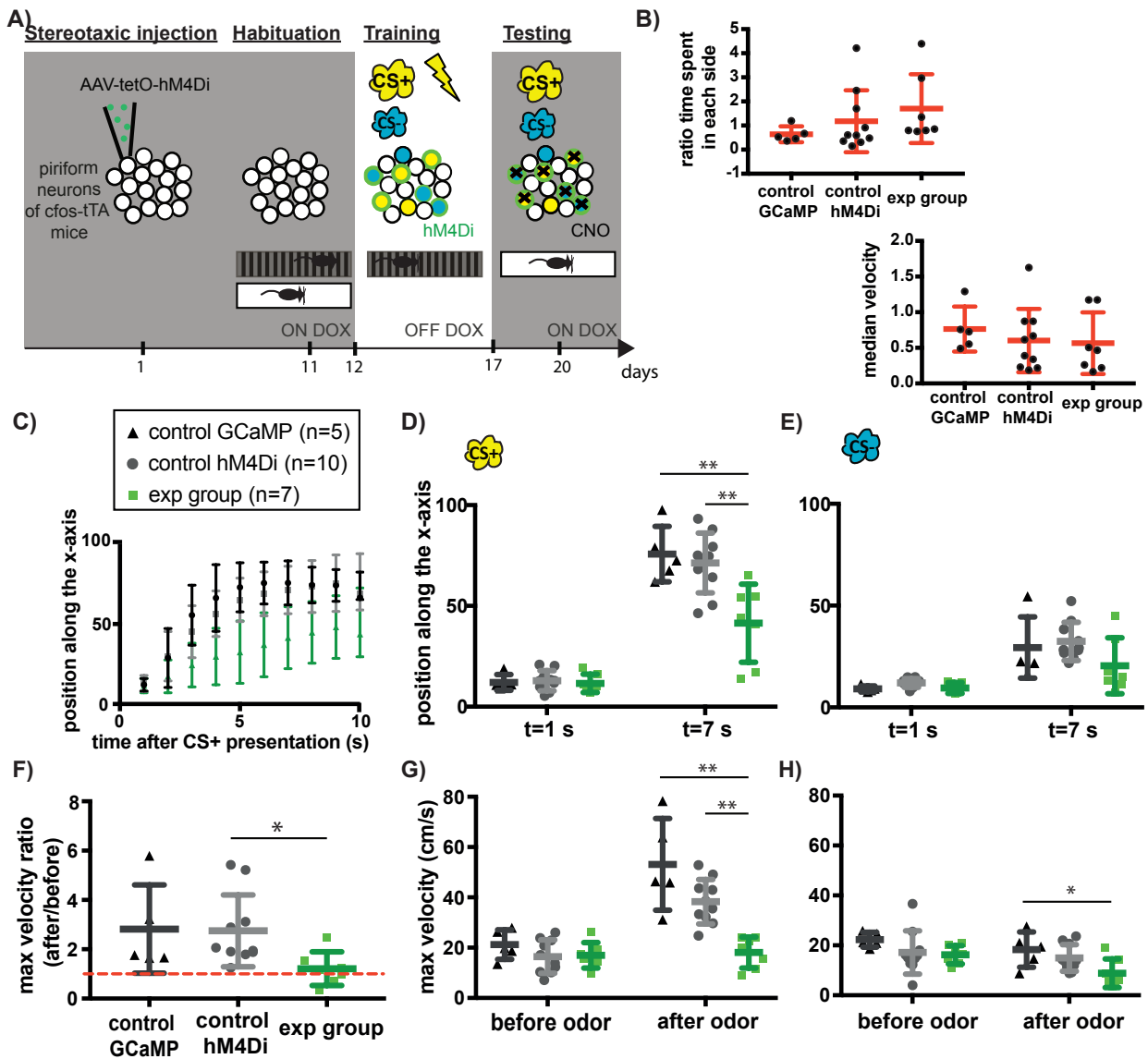


Figure 4.7: **Silencing fos-tagged piriform ensembles during memory retrieval.** (A) Experimental design: cfos-tTA transgenic mice are stereotaxically injected with AAV-tetO-hM4Di (green dots) in both hemispheres of the PC. Mice are then habituated to the training and testing boxes. Upon doxycycline (DOX) removal, mice are trained to associate one odor with a foot shock (CS+ odor, ethyl-acetate). Training includes presentation of two other odors which are not paired with foot shock (CS- odor, eugenol and beta-citronellol). During training, hM4Di expression (neurons surrounded by green) is induced in Fos-positive neurons (neurons filled in blue and yellow). Two days later, memory retrieval is tested in the presence of clozapine-N-oxide (CNO). CNO silences the activity of hM4Di-expressing neurons (black crosses). (B) Median velocity during the testing session (left panel) and time spent in the left side of the testing box divided by the time spent in the right side. There was no significant difference between the 3 groups tested. cfos-tTA mice were injected either with AAV-tetO-hM4Di (exp group, n=7) or with AAV-hSyn-GCaMP (control GCaMP, n=5), or WT mice were injected with AAV-tetO-hM4Di (control hM4Di, n=10). (C to H) Olfactory memory retrieval after CNO injection assessed by position in the testing box and maximum velocity. Memory retrieval was significantly impaired in cfos-tTA mice expressing hM4Di in piriform neurons that were active during learning (exp group, * $p < 0.05$, ** $p < 0.01$). (C-E) The odor is presented randomly on the left or right side of the testing box: the x-axis of the box is scaled to 100, with 0 corresponding to the extremity of the box where the odor is presented (see Fig.3.5). (C) Mouse position along the x-axis as a function of time after CS+ presentation. (D-E) Position along the x-axis 1s or 7s after CS+ (D) or CS- (E) presentation. (F) Maximum velocity ratio after/before CS+ presentation. (G-H) Maximum velocity during the 7s before and after odor presentation. CS+ (G) or CS- (H) odor. Data are shown as mean \pm SD.

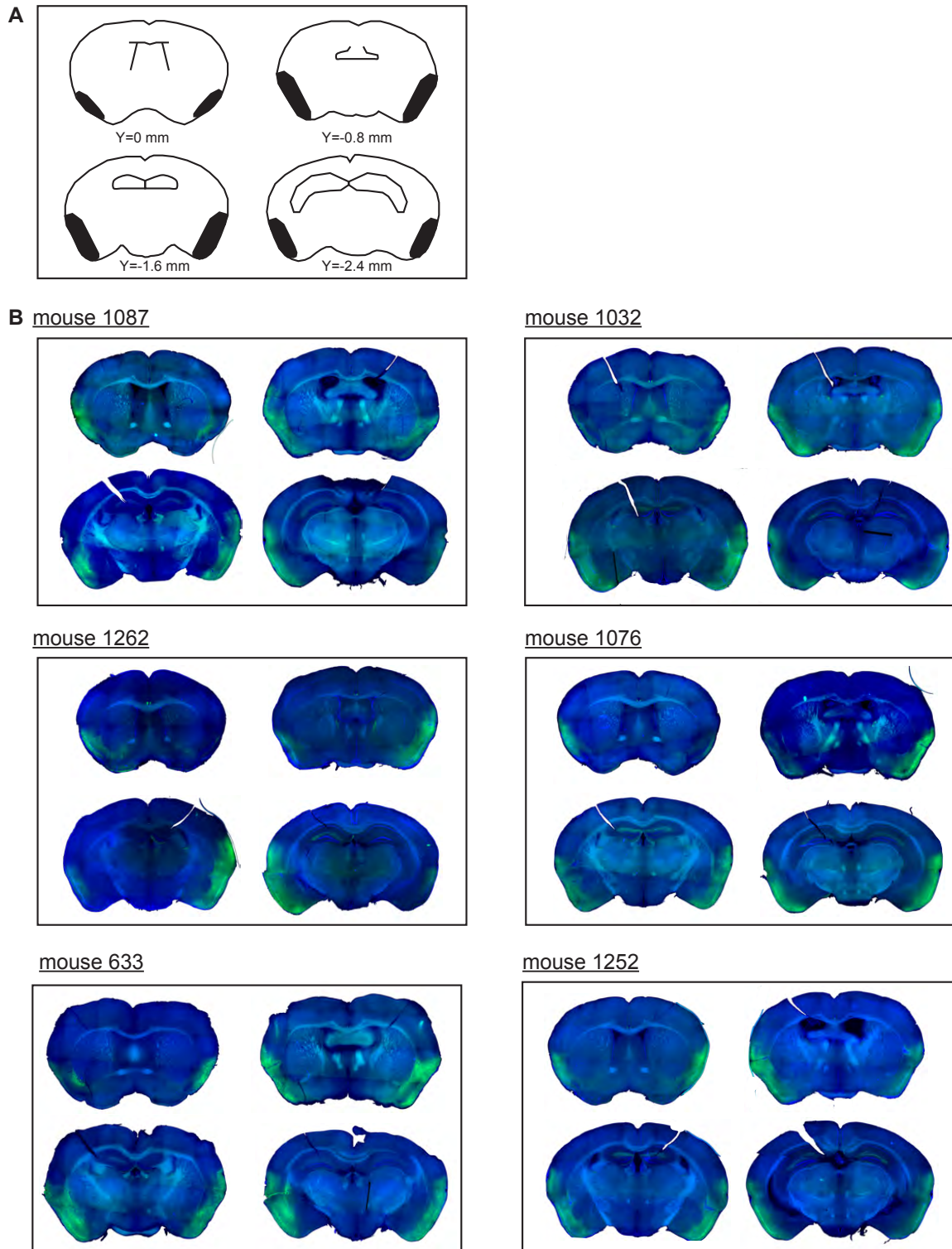


Figure 4.8: Indirect histological confirmation of hM4Di expression in the PC. (A) Four $200\mu\text{m}$ coronal sections spaced $800\mu\text{m}$ apart were taken from each mouse in the experimental group to determine the extent of the viral infection. The PC is highlighted in black, and position of the section relative from bregma along the anterior-posterior axis (Y) is indicated. The anterior PC ends around Y=0 mm. (B) mCitrine expression (anti-GFP, in green) in virally transduced piriform neurons of fear-conditioned *cfos-tTA* mice. All the posterior PC was transfected. The anterior PC was only partly infected. Images were acquired using an Axio Zoom microscope (Zeiss).

position of 72 and 75, 2.7 and 2.8-fold increase of the maximum velocity for WT mice expressing hM4Di and for cfos-tTA mice expressing GCaMP respectively). In contrast, the experimental group failed to escape after CS+ presentation (averaged position of 42, 1.2-fold increase of the maximum velocity). There was a significant difference in the position of the mice 7s after CS+ presentation between control and experimental groups ($H=9.89$, 2 d.f., $p=0.003$), Fig.4.7 D, as well as in the maximum velocity after CS+ presentation ($H=14.9$, 2 d.f., $p < 0.0001$) and the maximum velocity ratio after/before ($H= 9.071$, 2 d.f., $p= 0.006$), Fig.4.7 F, G. The mean rank of the experimental group's position (5.143) was significantly lower compared to control mice: WT mice expressing hM4Di (14.2, $p=0.014$) and cfos-tTA mice expressing GCaMP (15, $p=0.029$). The mean rank of the experimental group's maximum velocity (4) was significantly lower than the one of WT mice expressing hM4Di (13.7, $p=0.007$) and the one of cfos-tTA mice expressing GCaMP (17.6, $p=0.001$). The mean rank of the experimental group's maximum velocity ratio after/before (5.429) was only significantly different from the mean rank of control mice expressing hM4Di (14.7, $p= 0.011$; mean rank of 13.6, $p=0.095$ when compared to control mice expressing GCaMP). There was no difference between the two control groups for the three parameters (position $p > 0.999$, velocity $p=0.819$, velocity ratio $p > 0.999$). Individual positions of the 23 mice during the 10s following CS+ presentation are shown in Figs. 4.9(a) and (b), and the mean \pm SD for each group is plotted in Fig.4.7 C.

All mice were close to the odor port when CS+ odor presentation occurred ($t=1$ s, $H=0.896$, $p=0,656$), and had a similar maximum velocity during the 7 s that preceded odor presentation ($H= 2.157$, $p=0.352$). This excludes any inherent differences between groups due to how the CS+ was presented.

The observed fear behavior was specific to the CS+, as none of the mice escaped from the CS-. As seen on Figs.4.7E and H, mice stayed on the side where the odor was presented and had a similar maximum velocity before and after CS- presentation. There was no significant difference in the mouse position after CS- presentation between the 3 groups ($H= 4.176$, $p=0.1239$). Nevertheless, cfos-tTA mice expressing GCaMP had a higher maximum velocity than cfos-tTA mice expressing hM4Di ($p=0.037$).

Even though mice from the experimental group failed to escape to the CS+, it should be noted that they behaved differently after CS+ and CS- presentation. They were further away from the odor port after CS+ presentation than after CS- presentation (however, this difference did not reach statistical significance, $U=9$, $p=0.053$), and their maximum velocity was significantly higher ($U=5$, $p=0.011$). This could indicate a partial remembrance of the learned association. Several reasons could explain this tendency: incomplete silencing of fos-tagged neurons in the PC, incomplete tagging of CS+-responsive neurons, or the existence of parallel pathways encoding the memory.

We have shown that inactivation of neurons active at the time of memory encoding abolishes memory retrieval, suggesting their necessity in this process. Nevertheless, the amnesia of the experimental group could be secondary to sensory or motor disturbances, and as a consequence not be specifically related to memory impairments.

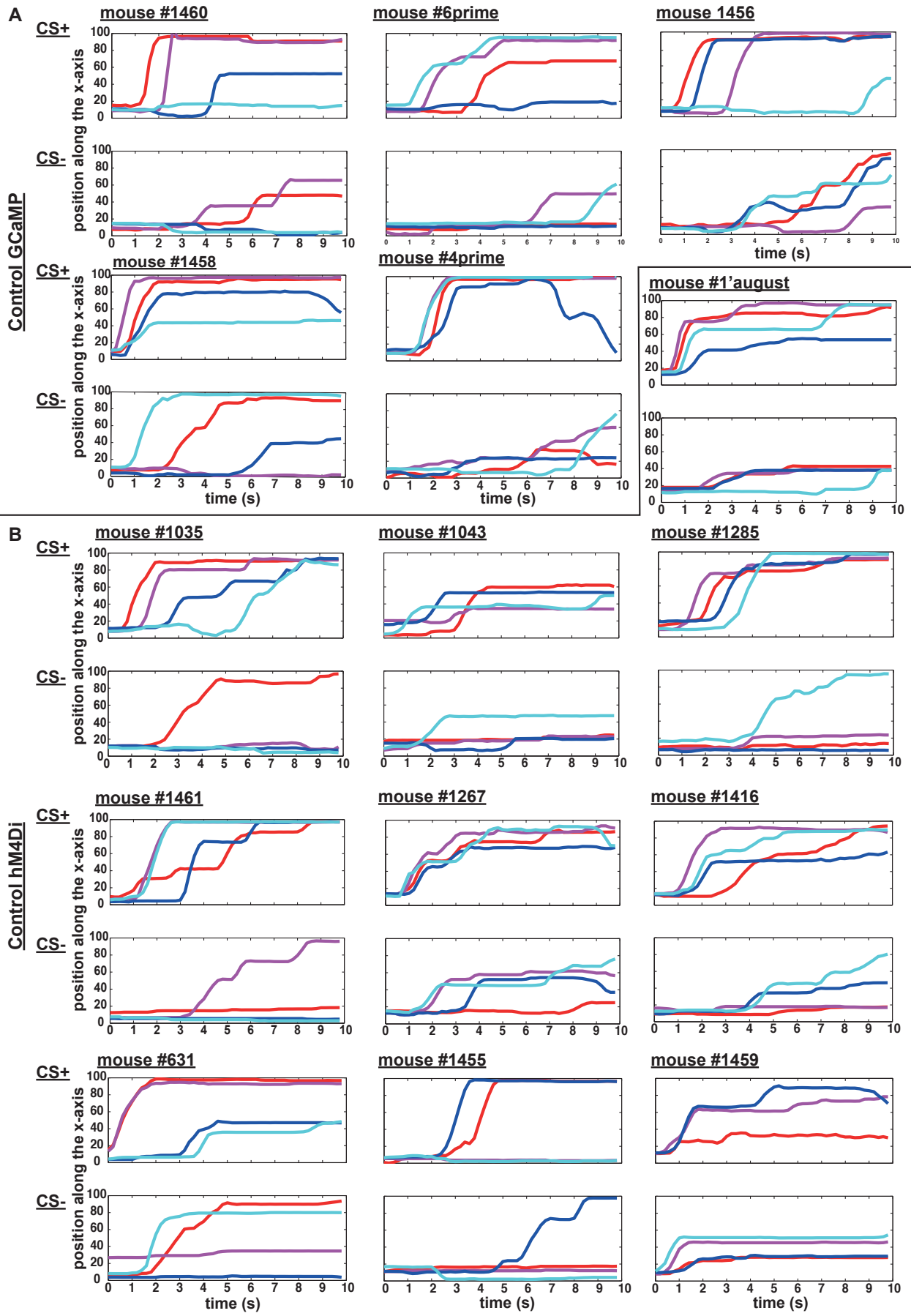


Figure 4.9(a): see caption Fig.4.9(b)

C

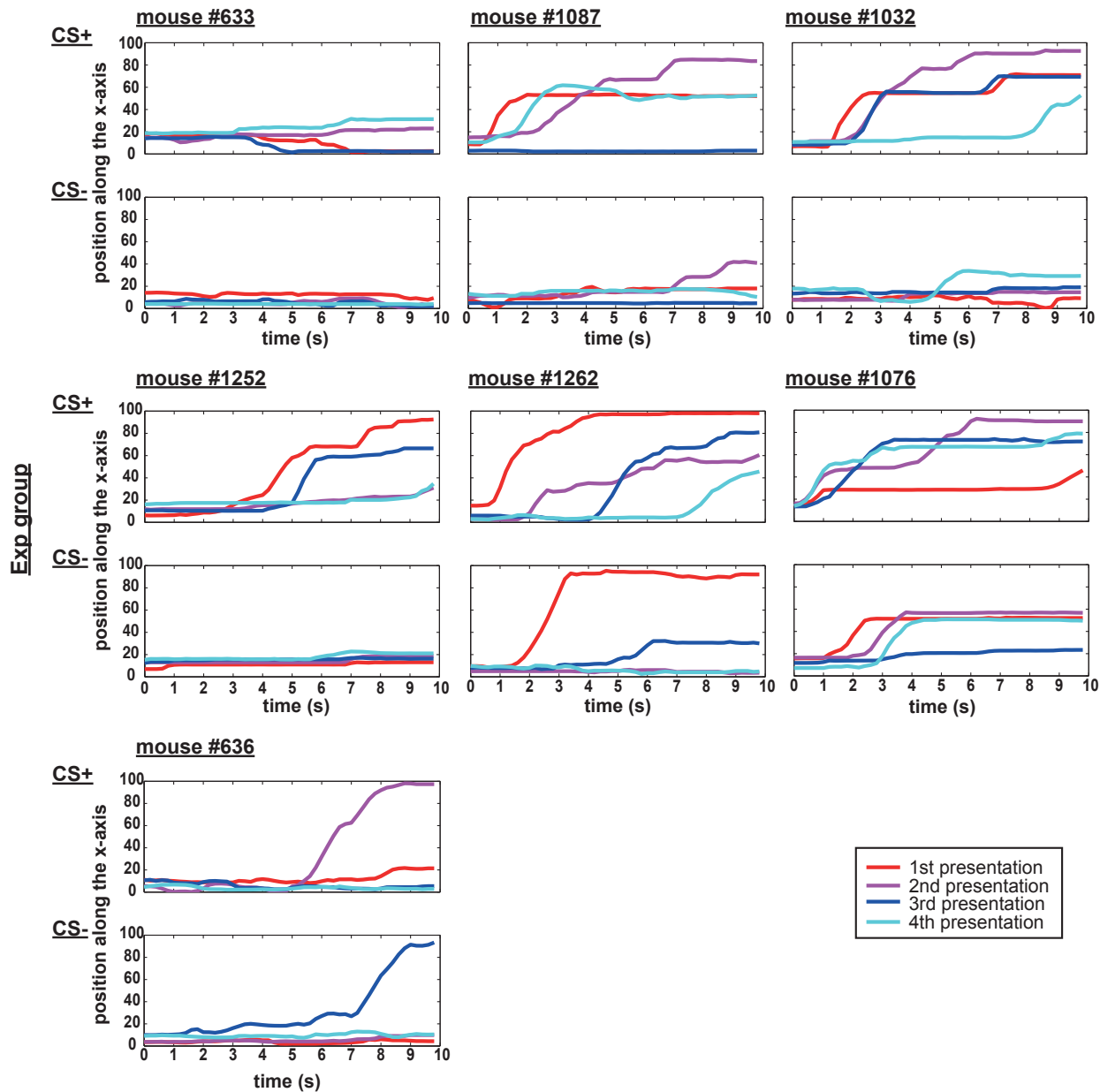


Figure 4.9 (b): **Position in the testing box as a function of time for each mouse after CS+ (top) or CS- (bottom) presentation:** first (red), second (purple), third (dark blue) or fourth (light blue) presentation. (A) cfos-tTA mice injected with AAV-hSyn-GCaMP (control GCaMP). (B) WT mice injected with AAV-tetO-hM4Di (control hM4Di). (C) cfos-tTA mice injected with AAV-tetO-hM4Di (exp. group).

Intact mobility

To assess if expression of hM4Di in Fos-expressing neurons lead to impaired motor processes or attentional levels, we calculated the median speed of each group of mice during the whole testing session (see Fig.4.7 B). There was no significant difference between groups ($H=1.751$, $p=0.433$). As already stated, all mice had a similar maximum velocity during the 7s which preceded odor presentation (CS+: $H=2.157$, $p=0.352$; CS-: $H=5.71$, $p=0.052$). Furthermore, all mice spent a similar amount of time in the left and right side of the testing box ($H=4.295$, $p=0.116$). Thus, the general mobility of mice from the experimental group was similar to the one of the control groups.

4.4 Memory deficits are odor-specific

Silencing any ensemble of piriform neurons could produce a more general disruption of piriform function and impair memory retrieval. We next verified if these memory deficits were specific to the ensemble of cells tagged during memory encoding, by expressing hM4Di in an odor-responsive ensemble that was not related to olfactory fear conditioning.

4.4.1 Experimental design

The experimental procedure was similar to the previous experiment, except that hM4Di is not expressed during olfactory fear conditioning but during simple odor exposure -or "tagging".

AAV-tetO-hM4Di was stereotaxically injected in both hemispheres of the PC of cfos-tTA transgenic male mice. Mice were then given ten days to recover, before being habituated on day 11 to the training and testing boxes (40 min and 10 min, respectively). Twenty-four hours after habituation, doxycycline was removed. Five days later, mice were exposed to an odor (odor "C" or "tagged" odor). Mice were put back on a doxycycline diet to avoid further expression of hM4Di. Two days later, mice were fear conditioned to an odor different from the tagged odor (CS+). One day later, memory retrieval was tested in the presence of CNO (see Fig.4.10 A). The fear memory should be retrieved, as neurons active during odor "C" presentation and not during learning were silenced. Two experiments were performed, using two different odors in two different contexts as odor "C":

- beta-citronellol (beta-cit.) presented with an olfactometer in the training box (6 times 8 s, 4 min intertrial interval, 25 min total).
- few μL of pure eugenol (eug.) on a cotton tip in a clean cage (15 min).

As there was no significant difference in the control groups in the previous experiment (see Fig.4.7), we decided to use only WT mice in which the AAV-tetO-hM4Di was injected as controls ($n=5$). The experimental group consisted of 12 cfos-tTA mice injected with tetO-hM4Di. As before, only mice who were bilaterally injected with at least all the posterior part of the pPC infected were included in the analysis.

4.4.2 Results

As expected, the control groups exhibited an escape behavior after CS+ presentation: mice ran towards the side opposite to the one where the odor was presented (averaged position of 61 and 74; 1.8 and 2.4-fold mean increase of the maximum velocity for eug. and beta-cit. respectively, see Figs.4.10 C,F). A similar behavioral response was observed for the experimental group tagged with beta-cit. (averaged position of 50, 1.7-fold increase of the maximum velocity, see Figs.4.10 C,F). For the experimental group tagged with eug., the behavioral response was more borderline: the average position 7s after CS+ presentation was 50 and the maximum velocity increased by 1.4, which is slightly below our threshold of 1.5 (see Figs.4.10 C,F). Nevertheless, there were no significant differences in the position of the experimental group 7s after CS+ presentation and its corresponding control (beta-cit.: $U=5$, $p=0.082$, eug.: $U=10$, $p=0.429$), as well as in the maximum velocity ratio before and after CS+ presentation (beta-cit.: $U=10$, $p=0.429$, eug.: $U=8$, $p=0.247$). The maximum velocity after CS+ presentation was similar between control and experimental group when mice were tagged with beta-cit. ($U=4$, $p=0.052$). However, when mice were tagged with eug., control mice had a higher maximum velocity ($U=3$, $p=0.030$).

As for the previous experiment, all mice were close to the odor port when CS+ odor presentation occurred ($t=1$ s, $H=7.522$, $p=0.057$), and had a similar maximum velocity during the 7s which preceded odor presentation ($H=0.647$, $p=0.886$). Fear responses were specific to the CS+ odor, as mice did not escape from the CS-, see Figs.4.10D,G (no significant difference between groups, position: $H=3.257$, $p=0.354$; velocity: $H=4.67$, $p=0.198$).

To conclude, we showed that inactivation of a population of piriform neurons that were active during presentation of a neutral odor did not have a strong effect on the retrieval of a learned association between an odor (etac) and an aversive stimulus. Nevertheless, quantitatively, when piriform neurons responding to eug. or beta-cit. were silenced, mice had a weaker escape response than controls. The values of the 3 parameters defining an escape behavior (position 7s after CS+ presentation, maximum velocity, maximum velocity ratio before/after) were lower for the "tagged" groups than for the control ones, but this difference was only significant for the maximum velocity of mice tagged with eug. This could be explained by the fact that a given neuron can respond to several odors, regardless of their structural similarity (Rennaker et al., 2007; Poo & Isaacson, 2009; Zhan & Luo, 2010). Roland et al., 2017 estimated by in vivo calcium imaging in anesthetized mice that around 10% of odor-responsive pPC neurons respond to 2 different odors, while 5% of them respond to 4 odors. Furthermore, they observed a substantial overlap between the population responses evoked by different odors (see also Bolding et al., 2017). It is therefore likely that the "tagged" odor representation partially overlaps with the CS+ odor representation, explaining the weaker escape response of mice in the experimental group. Overlap could be quantified by perfusing mice after the testing session to assess levels of co-expression of Fos with HA-hM4Di (but without CNO injection).

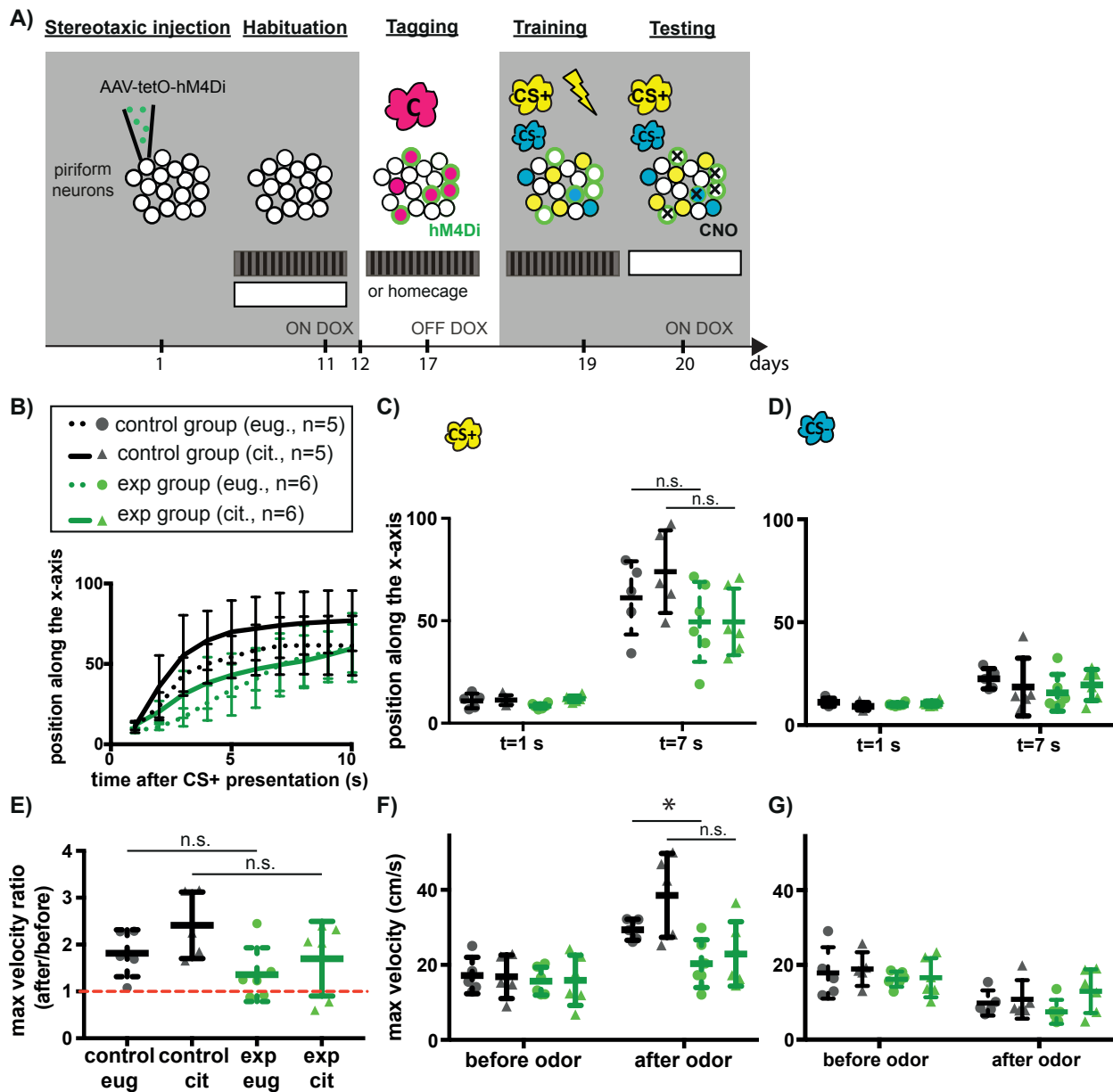


Figure 4.10: Odor specificity of fos-tagging and inactivation. (A) Experimental design: dissociating tagging and fear conditioning. Upon doxycycline (DOX) removal, mice are presented with an odor (eug. or beta-cit.). hM4Di expression (neurons surrounded by green) is induced in Fos-positive neurons (neurons filled in red). Mice are put back on DOX to avoid further expression of hM4Di. Mice are then fear-conditioned to etac (CS-: limonene and beta-cit. when tagged with eug., limonene and eug. when tagged with beta-cit.). One day later, memory retrieval is tested in the presence of CNO. CNO perturbs the activity of hM4Di-expressing neurons (black crosses). (B-G) Olfactory memory retrieval after CNO injection assessed by position in the testing box and maximum velocity. Memory retrieval was not significantly impaired in cfos-tTA mice expressing hM4Di in neurons that were active during a neutral odor presentation (exp group, * $p < 0.5$, ** $p < 0.01$). (B) Mouse position as a function of time after CS+ presentation. (C-D) Position along the x-axis 1s or 7s after CS+ (C) or CS- (D) presentation. (E) Maximum velocity ratio after/before CS+ presentation. (F-G) Maximum velocity during the 7s before and after odor presentation. CS+ (F) or CS- odor (G). Data are presented as mean \pm SD. * $p < 0.05$. n.s. not significant.

4.5 Preliminary results: Memory deficits are experience-dependent

As the mouse would be unable to detect etac if we would inactivate the epithelial sensory detectors, i.e. olfactory sensory neurons responding to etac, we could argue that mice do not perceive etac if we inactivate the neurons which are only two synapses away from the olfactory epithelium. The memory of the odor-shock association could be encoded in downstream areas of the PC. In the case of our CS+ etac for example, inactivating etac-responsive piriform neurons would simply be blocking the relay of information about odor identity to downstream areas involved in memory retrieval. Several arguments make this model unlikely. As stated in the Introduction, a large number of studies show that piriform odor representations are shaped by experience. Also, odor representations are not highly reliable (Roland et al., 2017; Bolding et al., 2017). Furthermore, due to the complexity of the odor space, when the mouse encounters an odor without behavioral meaning for the first time, it seems almost impossible that a representation of this odor preexists in the PC. To further support the functional relevance of PC in memory encoding, we dissociated expression of hM4Di in odor-responsive cells, and association of the same odor with a mild foot shock.

4.5.1 Experimental design

The experimental procedure was the same as in section 4.4, however in this particular case, the "tagged" odor was the CS+ (etac, see Fig.4.11A).

4.5.2 Preliminary results

Here the number of mice is not high enough to run a statistical test ($n=3$). However, for both the maximum velocity and position along the x-axis, the mean and standard deviations are in the range of the ones obtained from mice for which the tagged odor is different from the CS+ (see Fig.4.11 B-E). Thus, it seems that fos inactivation does affect memory retrieval itself, and not simply block the relay of sensory information to downstream areas involved in memory retrieval.

Results from this chapter (section 4.3 to 4.5) indicate that piriform neurons active during olfactory fear conditioning are necessary for memory retrieval and are therefore a component of the olfactory memory trace.

4.6 Artificially re-activating piriform neurons active during learning

Inactivation of the ensemble that was fos-tagged during learning specifically abolishes memory retrieval, indicating its necessity for olfactory memory. We next asked if this ensemble was

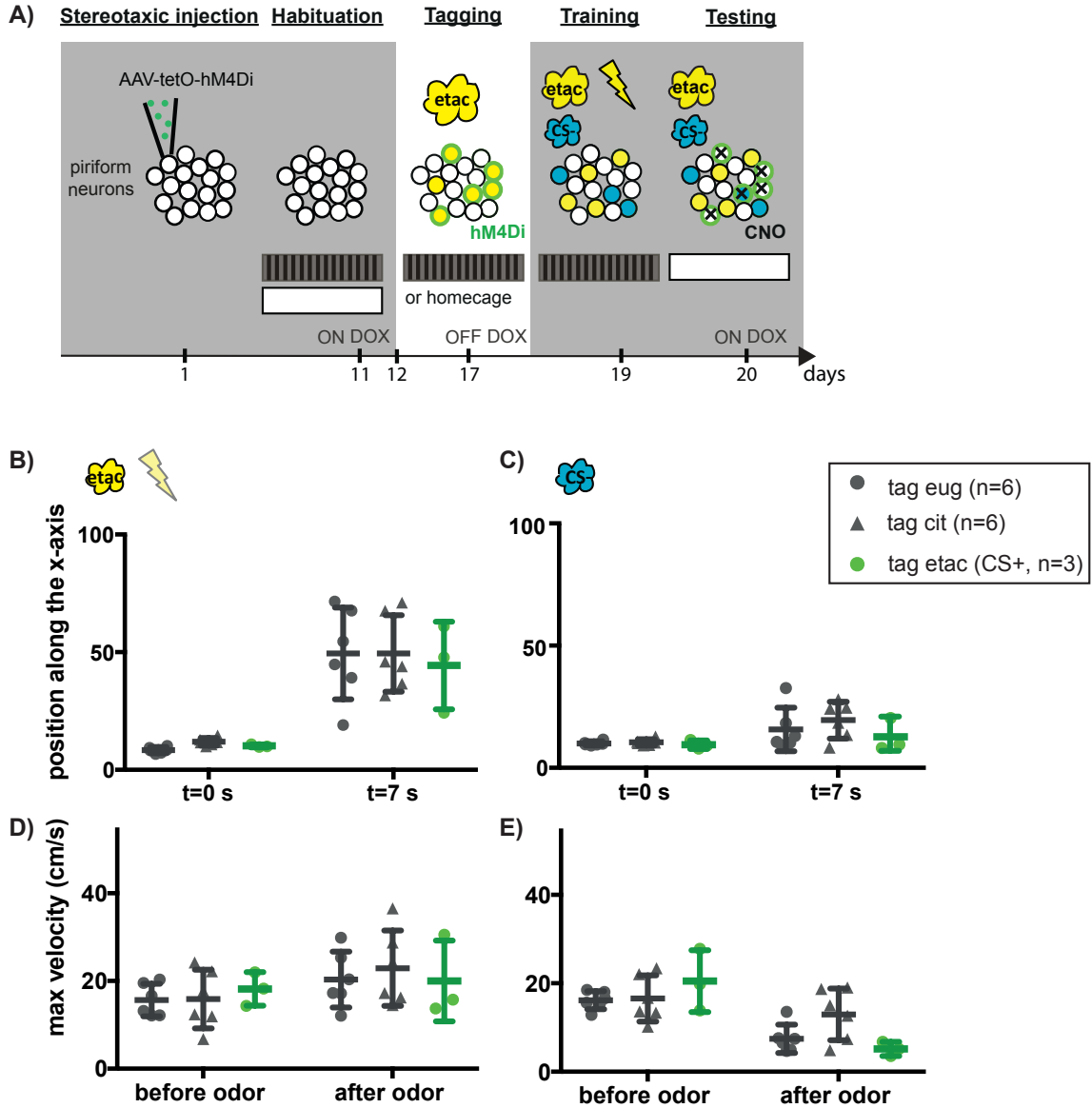


Figure 4.11: **Experience-dependence of fos-tagging and inactivation.** **A) Experimental design:** Dissociating tagging and fear conditioning. Same as Figure 4.10, except that the tagged odor is also the CS+ (etac). **(B-C)** Mouse position along the x-axis 1s or 7s after CS+ **(B)** or CS- **(C)** presentation. **(D-E)** Maximum velocity 7s before and 7s after odor presentation. CS+ **(D)** or CS- odor **(E)**. Data are presented as mean \pm SD. * $p < 0.05$. n.s. not significant.

sufficient to retrieve the memory. Can we artificially recall the memory by activating piriform neurons that were active during the encoding of an olfactory fear memory?

I chose to use hM3Dq in this experiment to be consistent in terms of tools with the silencing experiment (section 4.3 to 4.5). As DREADDs cannot be controlled on a very fine timescale, memory retrieval was tested by measuring the anxiety and locomotion of mice in an open field assay. Artificial memory retrieval of the feared odor could render mice anxious, and they would thus spend less time in the center of the open field and be less active (Bailey et al., 2009). However, the learned fear response is an escape response, which could also be reflected by mice being more active in the open field when memory is artificially retrieved.

4.6.1 Experimental procedure

First, cfos-tTA female mice were injected with AAV-tetO-hM3Dq. Mice were then given 10 days to recover, before being habituated on day 11 to the training and open field box (40 and 10 min respectively). The open field box consisted of a white Plexiglas (6 mm thickness) container (50 cm x 50 cm x 38 cm height). 24 h after habituation, doxycycline food was replaced by a regular food diet. Five days later, mice were fear conditioned to etac, and hM3Dq expression was induced in active piriform neurons. Two days later, baseline activity of mice in the open field box was assessed for 25 minutes, 5 min after i.p. injection of saline (testing 1). Mice were placed in the middle of the box at the start of the trial. The day after, mice were then randomly assigned to one of the two following groups: a control group (n=5), where saline was again i.p injected, and an experimental group (n=8), where CNO was i.p injected (testing 2). Thus, in the latter group, neurons that were active during learning were reactivated. 5 min after i.p injection, activity of mice in the open field box was assessed for 25 minutes, see Fig.4.12 A. One hour after the start of the experiment, mice were sacrificed for levels of Fos expression. Open field sessions were video recorded. In the control group, 1 mouse had its left PC infected, 2 mice had both hemispheres infected, and 2 mice had no visible hM3Dq expression. In the experimental group, 4 mice had their left PC infected, and 4 mice had both hemispheres infected.

4.6.2 Results

CNO-induced activity in hM3Dq-expressing neurons

One hour after the start of the last open field session (testing 2), CNO-induced neuronal activation was assessed by examining Fos expression in hM3Dq-expressing cells (see Chapter 3 for the counting method). 16% of hM3Dq neurons expressed Fos, see Fig.4.12 C,E and the total number of neurons co-expressing Fos and hM3Dq was significantly above chance level ($W=36$, $p=0.0078$), Fig.4.12 F. The chance level is the probability to observe a neuron that co-expresses hM3Dq and Fos, knowing the number of hM3Dq and Fos-positive neurons (as a reminder, $\text{chance}=(\text{hM3Dq neurons}/\text{total number neurons})*(\text{Fos neurons}/\text{total number neurons})*100$). Indeed, the more hM3Dq and Fos-positive neurons, the higher the probability to get a double-labeled

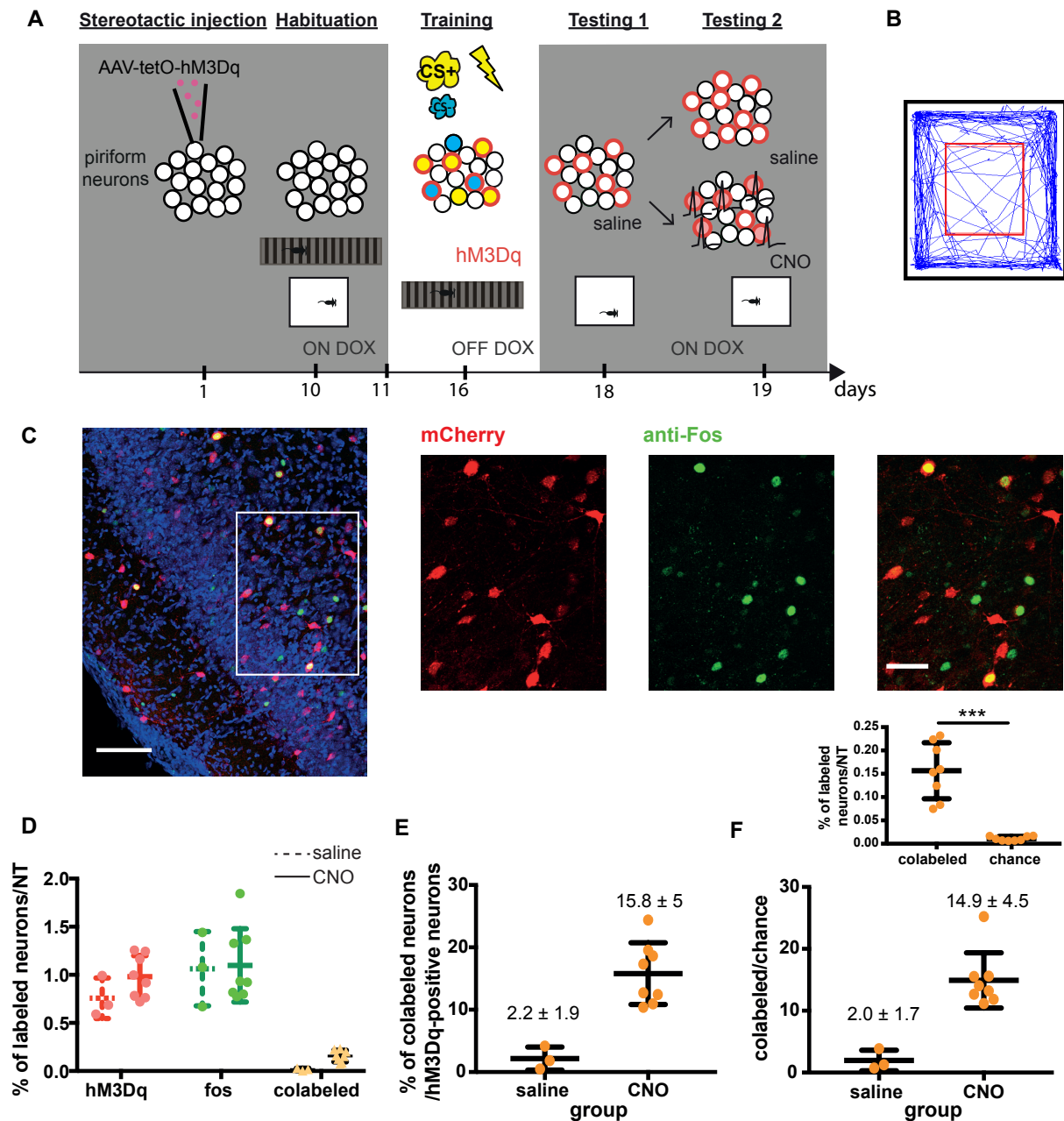


Figure 4.12: Artificial reactivation of fos-tagged ensembles: experimental design and histology. (A) Experimental design: cfos-tTA transgenic mice are stereotactically injected with AAV-tetO-hM3Dq (red dots) in both hemispheres of the PC. Mice are then habituated to the training and open field boxes. Upon doxycycline (DOX) removal, mice are trained to associate one odor with a foot shock (CS+ odor, etc). Training includes presentation of two other odors which are not paired with foot shock (CS- odor, eug. and beta-cit.). During training, hM3Dq expression (neurons surrounded by red) is induced in Fos-positive neurons (neurons filled in blue and yellow). Two days later, mice baseline activity in an open field is measured for 25 min, 5 min after i.p. injection of saline (testing 1). One day later, mice are randomly separated in two groups, receiving either an i.p injection of saline or CNO. 5 min after i.p. injection, mice activity in the open field is measured again for 25 min (testing 2). Mice are perfused 1 hour after i.p. injection to assess levels of Fos expression. (B) Representative tracksheet of an open field testing session. The red square delineates the center of the open field. (C-F) Fos immunostaining confirms that CNO activates piriform neurons in vivo. (C) Expression of Fos and hM3Dq after CNO injection. Neurotrace counterstain in blue. Scale bar: 100 μ m. High magnification of the region within the rectangle, Scale bar: 50 μ m (D) Quantification of Fos positive cells, hM3Dq-positive cells and double-labeled cells after saline (dashed lines) or CNO injection (full lines). (E) Percentage of hM3Dq-tagged neurons reactivated after saline or CNO injection. (F) Reactivation of hM3Dq-tagged neurons over chance level. *** $p < 0.01$.

neuron.

85% of Fos-positive cells did not express hM3Dq. These cells could have been responding to background odors (experimenter, open-field box, room....) or be activated by hM3Dq-expressing neurons via associative connections.

To better estimate the effectiveness of CNO to induce activity in hM3Dq-expressing neurons, we compared the number of co-labeled neurons after CNO and saline injection, even though we have only 3 mice in the control group (saline injection). Mice in both groups had a similar number of Fos expressing neurons ($1.1 \pm 0.4\%$ and $1.1 \pm 0.4\%$ after saline and CNO injection, respectively). Nevertheless, despite the small sample size in the control group, CNO injection induced a 7-fold increase in the number of hM3Dq-expressing cells co-expressing Fos (see Fig.4.12 E). Furthermore, the number of total neurons expressing both hM3Dq and Fos was 8-fold increased after CNO injection ($0.02 \pm 0.01\%$ and $0.16 \pm 0.06\%$ after saline and CNO injection respectively, see Fig. 4.12D).

The pattern of neuronal activation in vivo further supports our in vitro electrophysiological recordings. Nevertheless, previous studies in other brain regions found a higher number of hM3Dq-positive neurons expressing Fos after CNO injection, with doses ranging from 1 mg/kg to 5 mg/kg and perfusing mice between 60 and 90 minutes after induction (arcuate nucleus and nucleus tractus solitarius, Zhan et al., 2013; dorsal horn, Peirs et al., 2015; hippocampus, Garner et al., 2012). Expression of hM3Dq receptors might be lower in piriform neurons or CNO-induced piriform neural activation might be subthreshold to induce Fos expression.

Transient increase in locomotor activity

We next quantified activity in the open field (distance traveled and time spent in the middle). The first 5 min in the open field were excluded from the analysis. During the 20 remaining minutes, for both testing sessions, the control and experimental groups traveled a similar distance (testing 1: $U=12$, $p=0.284$; testing 2: $U=11$, $p=0.222$, see Fig.4.13A). They also spent a similar amount of time in the middle of the open field (testing 1: $U=13$, $p=0.354$; testing 2: $U=19$, $p=0.943$, see Fig.4.13A). However, Alexander et al. (2009) have shown by in vivo electrophysiology that the increase in hippocampal neuronal activity after CNO i.p. injection as well as its time course is dose-dependent. The highest dose they tested was 1 mg/kg, for which they saw an effect 15 minutes after injection (as a reminder, we use 3 mg/kg). Furthermore, even though CNO effects last for several hours, the brain could adapt to the sustained elevated activity of fos-tagged piriform neurons. Finally, the baseline level of anxiety can vary between mice, and could render differences between the two testing sessions difficult to see. For these reasons, I computed each parameter on smaller time intervals (every 2 minutes) for both testing sessions. I then divided each value of the distance traveled obtained on the second testing day by the one of the first testing day and subtracted each value of the time spent in the middle obtained on the first testing day from the one of the second testing day. A significant difference in the distance traveled by the control and experimental group emerged 22 minutes after CNO injection ($U=0$, $p=0.0016$, as a comparison, at $t=12$ min., $U=18$, $p=0.833$, see Figs.4.13C, D). However, there was no significant difference in the time spent in the middle ($t=22$ min, $U=6$, $p=0.0505$; $t=12$ min, $U=13$, $p=0.3318$, see Fig.4.13 B).

From the 8 mice in the experimental group, 4 were unilaterally injected in the left PC, and 4 were bilaterally injected, but there was no difference in the ratio of distance traveled between these two subgroups (see Figs.4.13 E, F).

Experimental mice were thus transiently more active, as if they were escaping from an "imaginary" odor. To further support this idea, we are reproducing the experiment in non-injected WT mice, and will present a long-lasting odor stimulus above the openfield during the second testing day. For half of the mice, the presented odor will be the CS+, to mimick the CNO effect, and for the other half, mineral oil will be used as a neutral stimulus (see Fig.4.13 G).

The olfactory memory can be artificially retrieved by activating piriform neurons that were active during learning. Nevertheless, the loss of temporal information in the activity pattern (neurons activated as soon as CNO binds to hM3Dq) as well as the long-lasting effect of CNO could explain why we observe an effect that lasts only a few minutes. We could also measure stress hormones levels like ACTH (adrenocorticotrophic hormone) and corticosterone (Kondoh et al, 2016) in both groups, as a readout of elevated stress levels. I chose to use hM3Dq in this experiment to be consistent with the silencing experiment (sections 4.3, 4.4 and 4.5). However, optogenetics (ChR2) might provide an easier way to interpret behavioral readout. Indeed, during fear conditioning, ChR2 could be expressed in active piriform neurons. Mice could then be tested in the testing box, as done in sections 4.3, 4.4 and 4.5. Photostimulation near the odor port would mimick odor presentation, and escape behavior of the mice could be measured. Nevertheless, the fos-tagged piriform neurons would still be activated all at once (no temporal information).

4.7 Reactivation of fos-tagged ensembles during memory retrieval

As piriform ensembles that were fos-tagged during memory encoding were required for memory retrieval, we next sought to quantify the number of piriform neurons that were active during both memory processes. For this purpose, we used hM3Dq to tag neurons that were active during fear conditioning and endogenous Fos expression to identify neurons active during memory retrieval. We used the hM3Dq receptor and not hM4Di to be able to compare numbers with the artificial reactivation described in the previous section.

4.7.1 Experimental design

AAV-tetO-hM3Dq-mCherry was stereotaxically injected in both hemispheres of the PC of cfos-tTA transgenic mice. Mice were then given 10 days to recover, before being habituated on day 11 to the training and testing boxes (40 and 10 min respectively). 24 h after habituation, doxycycline was removed and replaced by a normal food diet. 5 days later, mice were fear conditioned, and active neurons labeled with hM3Dq-mCherry. Mice were then put back on a doxycycline diet to avoid further expression of hM3Dq. 2 days later, memory retrieval was tested, and mice (n=4)

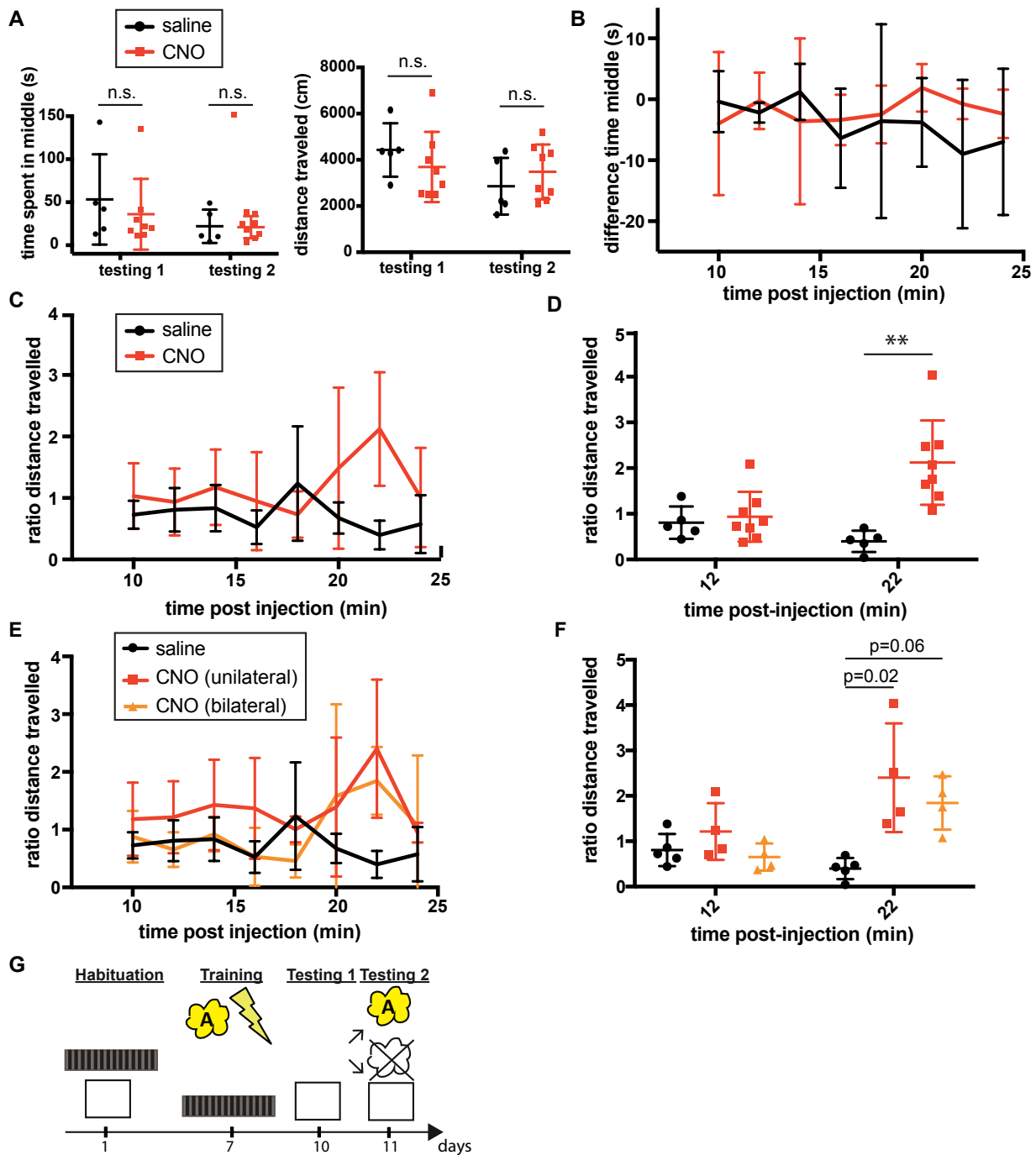


Figure 4.13: **Artificial reactivation of fos-tagged ensembles: behavior** (A) The total distance travelled (left) and the time spent in the center of the open field (right) are similar between the 2 groups (injection of CNO -red dots and lines- or saline -black dots and lines- for each testing session). (B) The time spent in the center is computed every two minutes. The obtained value on testing 1 subtracted from its corresponding one on testing 2 is plotted against the time post injection. There is no significant effect of CNO injection during testing 2. (C-D) The distance travelled is computed every two minutes. The obtained value on testing 2 divided by its corresponding one on testing 1 is plotted against the time post injection. The whole session (C) or a subset of time points (t=12 min and t=22 min, D) is shown. A significant effect of CNO injection was observed at t=22 min (** $p < 0.01$). (E-F) Same plots than (C-D), except that the group injected with CNO is split depending on whether hM3Dq expression is predominant in one or both hemispheres. (G) Does mouse activity during CS+ odor presentation resembles mouse activity during artificial reactivation? Similar experimental design than in Fig.4.12A, except that memory retrieval is tested in presence or absence of the CS+ in the open field.

were perfused 1 h after the start of the testing session to determine Fos expression levels (Fig.4.14 A).

For each mouse (n=4), the PC was delineated on 4 coronal sections, spaced 600 microns apart, and hM3Dq-mCherry positive, Fos positive and double labeled neurons were counted with an automated Fiji plugin (see Chapter 3 for details).

4.7.2 Results

As expected, mice exhibited an escape behavior after CS+ presentation: mice ran towards the side opposite to the one where the odor was presented (averaged position of 83; 3.8-fold increase of the maximum velocity, see Fig.4.14 B). We could therefore proceed to the quantification of overlap between the pattern of neural activity during memory encoding and retrieval. A similar amount of neurons was activated during memory encoding ($0.8 \pm 0.1\%$ of piriform neurons) and retrieval ($1.0 \pm 0.04\%$ of piriform neurons). Fig.4.14 F shows the percentage of reactivated neurons in TetTag mice relative to chance level. Reactivation was not significantly greater than chance ($W=10$, $p=0.125$). Furthermore, the percentage of hM3Dq-positive cells that were reactivated was very low ($1.7 \pm 0.8\%$). We compared reactivation in mice fear conditioned to etac and tested for memory retrieval ("retrieval" group), and mice fear conditioned to etac but then exposed to odors unrelated to fear conditioning ("different" group, see Fig.4.14 A). We used the group of mice from the open field experiment injected with saline (n=3), as background odors (odors from the new environment, open-field box, experimenter) were sufficient to induce similar levels of Fos expression than CS+ and CS- presentation. There was no striking difference in the percentage of reactivated hM3Dq-positive neurons between the two groups, see Fig.4.14 E.

Several -non-exclusive- hypotheses can be made to account for these results. First, more neurons might be reactivated, but their spiking pattern during memory retrieval did not induce Fos expression. Second, we are likely "over-tagging" neurons. To the basal levels of neurons tagged (see section 4.1), we can add neurons whose activity is driven by background odors (e.g. when transported from the housing room to the behavioral room, or in the behavioral room itself...) and is unrelated to fear conditioning. We are also "tagging" neurons responding to the CS- odors. Furthermore, all the neurons active during learning might not participate in the formation of a memory trace, and memory retrieval would thus only recruit a subpopulation of neurons during the initial learning. In line with this hypothesis, sparsening of odor representations has been observed in the aPC after reward learning (Shakhawat et al., 2014). This could be due in part by the sparsening of the mitral cells inputs which has been observed over several days when an odor is presented several times (Kato et al., 2012). As a consequence, the critical information needed to drive the appropriate behavior could be contained in the small percentage of reactivated neurons.

However, it should be noted that even if not significant, the mean reactivation of neurons was 1.7 fold above chance level, which is in the range of what was observed in hippocampus (between 1.5 and 2 depending on the subregion, Tayler et al., 2013).

We could also compare reactivation in a retrieval group tagged with hM4Di with reactivation

when CNO is injected before the testing session (section 4.3). However, i.p. injections, as well as the 20 min between CNO injection and start of the testing session are likely to induce background of Fos activity. Thus, we would need to inject saline in the hM4Di-tagged retrieval group for a rigorous comparison.

4.8 Discussion

Main results: piriform olfactory memory traces

Piriform odor representations are thought to encode odor identity and have been shown to be shaped by learning and experience, yet their function in olfactory learning and memory remains unknown (see Chapter 2). We used the TetTag inducible system to induce expression of DREADDs in piriform neurons that were active during olfactory fear conditioning. By directly manipulating their activity in subsequent memory retrieval, we were able for the first time to test their functional relevance: neurons tagged during fear conditioning are both necessary and sufficient for memory retrieval. Thus, one of the fundamental criteria required for an ensemble of neurons to qualify as a memory trace is met.

Silencing piriform neurons that were active during learning impaired memory retrieval. Nevertheless, this effect might not be limited to neurons active during memory encoding. For this reason, we dissociated the "tagging" from the fear conditioning: before fear conditioning and subsequent memory retrieval, expression of the inhibitory DREADD was induced while mice were exposed to a neutral unrelated odor. Silencing this "unrelated" piriform ensemble did not significantly impair memory retrieval, confirming the specificity of fos-tagging and inactivation.

Conversely, chemogenetically reactivating piriform neurons that were active during learning lead to a significant transient increase in the motor activity of mice in an open field. One possible interpretation of this observation is that mice were escaping to an "imaginary odor". This suggests that the relevant information encoded in our tagged ensembles is population-based rather than temporally-based. Indeed, the sequence of neuronal activation within the ensembles and spike-timing are lost with artificial means of reactivation, be it chemogenetics or optogenetics. This is coherent with recent *in vivo* calcium imaging and electrophysiology data in both anesthetized and awake mice: Bolding et al., 2017 and Roland et al., 2017 report that the spatial pattern of activity was sufficient to decode odor identity, with no additional information provided by temporal properties.

We found that a subset of piriform neurons that were active during learning must be reactivated for olfactory fear memories to be retrieved. Surprisingly, however, we could not see a significant reactivation of neurons tagged during fear conditioning. For possible explanations, the reader is referred to the related Results section.

Finally, we have indicated in Chapter 2 the heterogeneity of the PC along its antero-posterior axis. The features which make the PC a region well-suited for the encoding of memory traces are

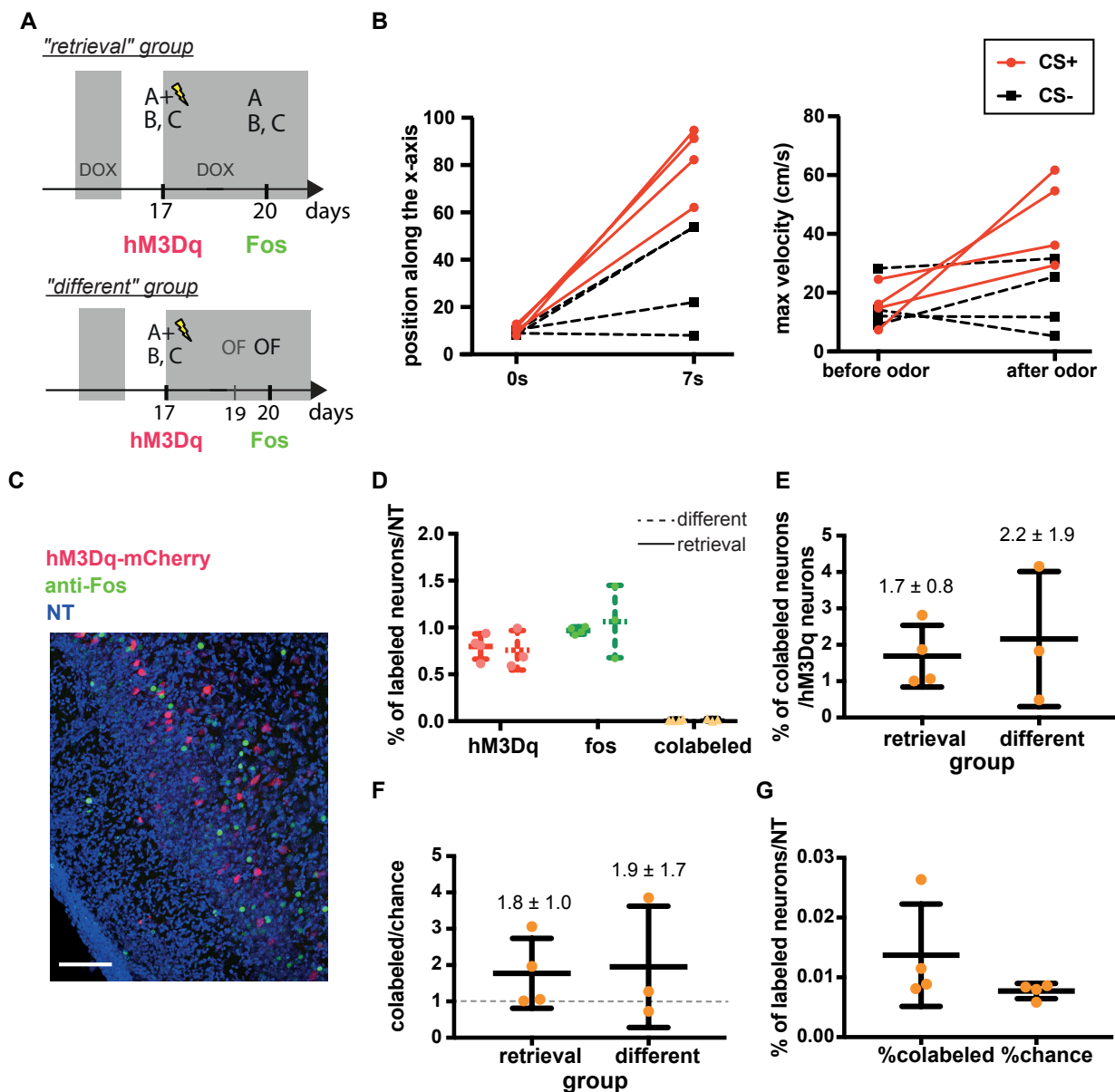


Figure 4.14: **Reactivation of piriform neurons during memory retrieval.** (A) Mice injected with AAV-tetO-hM3Dq-mCherry are subjected to olfactory fear conditioning. Three days later, mice are exposed either to the CS+ and CS- odors ("retrieval" group, n=4) either to odors unrelated to fear conditioning ("different" group, n=3, see text for more details). Mice were perfused 1 hour after the start of the testing session. Neurons active during learning are tagged with hM3Dq-mCherry, neurons active during memory retrieval are labeled with an anti-Fos antibody. odor A or CS+= etac. odor B and C or CS-= eug. and beta-cit. (B) Behavioral response of mice in the "retrieval" group. (C) hM3Dq (red) and Fos (green) expression after memory retrieval. NeuroTrace counterstain in blue. Scale bar, 100 μ m. (D-G) Neurons active during olfactory memory retrieval were not reactivated above chance levels during memory retrieval. (D) Percentage of hM3Dq-positive, Fos-positive or colabeled neurons. (E) Percentage of hM3Dq-positive neurons which are reactivated during memory retrieval. (F) Percentage of reactivated neurons compared to chance levels. (G) Percentage of colabeled neurons after memory retrieval and percentage of neurons colabeled by chance in the "retrieval" group.

more developed in the pPC. In our study, silencing of the aPC was partial, while silencing of pPC was almost complete, confirming the role of the pPC in olfactory memory.

Olfactory versus hippocampal memory traces: a comparison between TetTag studies.

The hippocampus and the PC are two allocortical brain regions that share similar features. They are both three-layered structures, with a relative sparse population coding and high recurrent connectivity, and have been shown to perform pattern completion. Therefore, it is interesting to put our results into perspective with recent findings on hippocampal memory traces (see Chapter 1).

Hippocampal TetTag studies have targeted subregions of the hippocampus which are smaller than the PC, making it possible to use optogenetics to manipulate neural activity. Due to the high temporal resolution of optogenetic interventions, memory retrieval can be assessed with and without memory trace manipulation in the same test session, in a within-subject design (Denny et al., 2014; Liu et al., 2012). Another difference between hippocampal TetTag studies and our study lies in the regional specificity of the TetTag system. First, the TetTag system may be less leaky in the hippocampus than in the PC, as all published studies report no basal level of expression of the transgene of interest (fluorescent proteins or receptors) when the mice are on doxycycline (Liu et al., 2012; Reijmers et al., 2007). Furthermore, TetTag-driven protein expression after contextual fear conditioning appears to be restricted to excitatory neurons (Liu et al., 2012; Tanaka et al., 2014; Tayler et al., 2013), which is not the case in the PC. Recent studies have highlighted the necessity and function of GABAergic neurons in memory trace formation (Stefanelli et al., 2016; Letzkus et al., 2011; Lovett-Barron et al., 2014), yet their role in memory retrieval remains largely unknown.

Despite the aforementioned differences, hippocampal neurons and piriform neurons tagged during contextual fear conditioning and olfactory fear conditioning, respectively, were both necessary and sufficient for memory retrieval (Liu et al., 2012; Tanaka et al., 2014), suggesting common mechanisms of memory formation and retrieval. First, Fos-expressing neurons active during fear conditioning encode fear memory traces, and depending on the nature of the CS, brain regions are differently involved. Second, the spatial code contained in the memory trace is sufficient to recall the natural event. Therefore, we hope that a deeper understanding of both PC and hippocampal memory traces will shed light on fundamental anatomical, functional and organizational principles of circuits involved in mnemonic processes.

Olfactory memory traces: a distributed network?

Current views suggest that the formation of memory traces, their storage and reactivation depends on the coordinated activity of neural ensembles that are distributed across several brain regions, including sensory cortices (Weinberger et al., 2004). We can take advantage of transgenic mice expressing the long-lasting green fluorescent protein H2BGFP under the control of the tetO operator to investigate how piriform inactivation affects other brain regions. This would require replacing the green mCitrine tag on our pAAV-hM4Di plasmid by a red fluorescent mCherry tag. As a consequence, piriform neurons active during fear conditioning would be "tagged" with

H2BGFP and hM4Di-mCherry, but most importantly, neurons active in other brain regions would be "tagged" with H2GFP as well. Silencing piriform "tagged" neurons during memory retrieval might impair reactivation of "tagged" neurons in other brain regions (see also Tanaka et al. in the hippocampus). One region of interest is the amygdala, which plays a key role in both contextual and cued fear conditioning (see Chapter 1). This would give us a better understanding about how different brain regions contribute to the overall olfactory fear memory trace.

Fos-expressing cells in the piriform cortex: who are they?

Fear-conditioned mice are presented several times with 3 different odors, one of them being paired with foot-shock. In these mice, the number of Fos-positive neurons or fos-tagged DREADDs-expressing neurons do not exceed 1% of the total number of piriform cells. As a point of comparison, *in vivo* calcium imaging and electrophysiological recordings indicate that odors activate between 5 and 20% of piriform neurons depending on the wakefulness of the mouse, the recording technique and the odor presented (Stettler et al., 2009; Roland et al., 2017; Bolding et al., 2017; Zhan et Luo, 2010). However, in these experiments, a large fraction of cells -even though not strictly quantified- exhibited low firing rates and low changes in fluorescence. Therefore, the Fos population could represent a subset of neurons strongly activated by the odor (see Schoenenberger et al., 2009).

Auditory stimuli (Varga et al., 2013) as well as visual stimuli previously associated with an odor (Mandairon et al., 2014) can elicit piriform activity. Furthermore, foot-shock can elicit responses in non-somatosensory cortices like the auditory cortex (activation of inhibitory neurons, Letkus et al., 2011). Therefore, it is not unlikely that our population of fos-tagged neurons includes odor-responsive neurons as well as foot-shock responsive neurons. The convergence of an olfactory stimuli and foot shock could modulate piriform activity, and in turn affect fos expression.

Clearly, further investigation is needed to determine the nature of piriform fos-tagged neurons and how Fos expression is induced in the PC.

As an example, Fos expression could be quantified in response to different stimuli (foot-shock alone/odor alone/paired odor and foot-shock) and colabeled with different markers of inhibitory neurons (PV, SST, etc... see Suzukki and Bekkers, 2010). We can now also take advantage of the recent developments in miniature microscopy (microendoscopes), which allow to record simultaneously the activity of more than thousands neurons in freely-moving mice (Ghosh et al., 2011). Integrated endoscopes can repeatedly image neuronal populations for several weeks (Ziv et al., 2013). As a consequence, by virally co-injecting the calcium indicator GCaMP and tetO-mCherry in the PC, the response properties of fos-tagged piriform ensembles could be characterized over time in both naïve and fear conditioned mice. Emergence of Fos ensembles could be correlated with the past history of neuronal activity and improve our understanding of how Fos expression is related to the neuron's physiological properties.

What comes next

We have demonstrated that manipulating piriform neurons that were active during olfactory fear conditioning affects memory retrieval. This supports our working hypothesis that PC encodes

olfactory memory traces (see Chapter 2). Nevertheless, to qualify as a memory trace, an ensemble of cells must also demonstrate learning-induced changes in cellular or network properties (see Chapter 1). Therefore, we will present in Chapter 5 a working hypothesis of olfactory memory trace formation, based on the assumption that the connections between "odor memory" cells are strengthened.

Furthermore, the TetTag has several limitations. First, the "tagged" neurons are a mixed population containing the "memory trace" cells, but also a large number of cells activated by unrelated events both during and outside the "tagging" window. Second, once expressed, target protein expression is gone by 30 days. Sacco et al., 2010 have shown a time-dependent role of PC in memory retrieval. It would thus be interesting to manipulate the memory trace at several time points.

Limitations of the TetTag system might be partly overcome with the TRAP system (see Chapter 1, Guenther et al., 2013), where activity is more tightly regulated and expression of the target protein, once induced, is permanent. As a consequence, we will investigate in Chapter 6 if the TRAP system can be used as a more efficient way to label olfactory memory traces.

Chapter 5

Mechanisms of memory trace formation.

5.1 Hypothesis

In chapters 3 and 4, we have established an experimental approach to persistently tag and manipulate "odor memory cells". We have shown the functional relevance of piriform neurons in memory formation and retrieval. These results open a range of new horizons in understanding the mechanisms of odor coding and memory. This chapter explores in a preliminary way how learning shapes piriform network properties.

Synaptic transmission is a stochastic process (Branco et al., 2009), and instability of neuronal representations has been reported in several brain regions, including the piriform cortex (Ziv et al., 2013; Roland et al., 2017). Since Hebb's postulate in 1949, changes in synaptic strength have been suggested to be a core mechanism for the formation of memory traces (see Chapter 1). During learning, if the probability that the presynaptic neuron activates the postsynaptic neuron increases, this could be reflected at the network level by the formation of a stable ensemble of neurons encoding the event which induced plasticity (the CS-US association in the case of classical conditioning for example, Lütcke et al., 2013). In line with this idea, recent studies indicate that learning stabilizes hippocampal spatial representations (Kentros et al., 2004; Wang et al., 2012).

Furthermore, recent studies hint towards a role of neuromodulation in the induction of synaptic plasticity (Pawlak et al., 2010, see Chapter 1). We have already mentioned in Chapter 2 the modulation of olfactory learning and piriform plasticity by acetylcholine (ACh). We want to briefly review here evidence for the role of ACh during fear learning in other brain regions. Optogenetically silencing the cholinergic inputs to the BLA during auditory fear conditioning impaired memory formation. In support of ACh contribution to fear learning, *ex vivo* electrophysiological recordings showed an enhanced excitability of BLA neurons and enhanced cortico-amygdalar plasticity after cholinergic stimulation (Jiang et al. 2016). In the auditory cortex, infusion of ACh receptor antagonists 15 minutes before fear conditioning impaired memory formation and strongly reduced foot-shock mediated activation of interneurons (Letzkus et al., 2011). Intra-hippocampal infusion of a cholinergic antagonist impaired contextual fear learning, but not cued fear learning

(Gale et al., 2001). As a consequence, we postulate the following hypothesis, see Fig.5.1:

Odor representations are stabilized by learning via the neuromodulatory signal ACh.

We present here preliminary results, investigating first if piriform ACh plays a role in the formation of olfactory fear memories, and then if piriform odor representations are more stable after fear conditioning.

5.2 Role of Acetylcholine in olfactory learning

To address the role of ACh in olfactory learning, we developed local drug infusion in the PC during our olfactory fear conditioning procedure. There are two main classes of acetylcholine receptors: muscarinic and nicotinic receptors. I chose to infuse scopolamine hydrobromide, a muscarinic antagonist, as it has been shown to affect olfactory fear learning (Pavesi et al., 2012).

5.2.1 Experimental procedure

The following ACh experiment was performed by Agatha Anet, an internship bachelor student, under my supervision.

Guide cannulas (26 gauge, 4.5 mm, Plastics One) were implanted bilaterally at the following coordinates: -0.6 AP, +/-4 ML and 3.5 DV. Then cannulas were fixed to the skull with dental cement and SuperBond. Dummy cannulas without projection were screwed to the guide cannula to prevent clogging and infection. Mice (males) were allowed between 5 and 7 days to recover from the surgery, and were handled 2-3 times during this period to habituate them to the experimentalist. One day after habituation to the training and testing boxes, mice were fear conditioned to etac. Three days later, memory retrieval was tested (see Fig.5.2A). Scopolamine infusion (1 $\mu\text{g}/\text{L}$) was performed twenty minutes before fear conditioning (experimental group, $n=6$). Internal cannulas with a 1 mm projection (Plastics One) were connected to a 10 μL Hamilton syringe via a Polyethylene tubing and inserted into the guide cannulas. A volume of 1 μL (1, 2 or 8 μg of scopolamine) was injected in each hemisphere using a microinfusion pump (rate of 0.2 μL per min, visual check that the solution is moving in the tubing). The internal cannula was left in place for an additional 5 mins and slowly withdrawn. Control mice ($n=6$) were injected with saline solution.

At the end of the experiment, to check that drugs were infused in the correct brain region, mice were infused with FastGreen. Mice were killed 30 minutes later to mimick the timeline of the testing session.

As we can see on Fig.5.2B, the spread of the drugs seemed to be restricted to the PC and did not diffuse to neighbouring regions like the BLA.

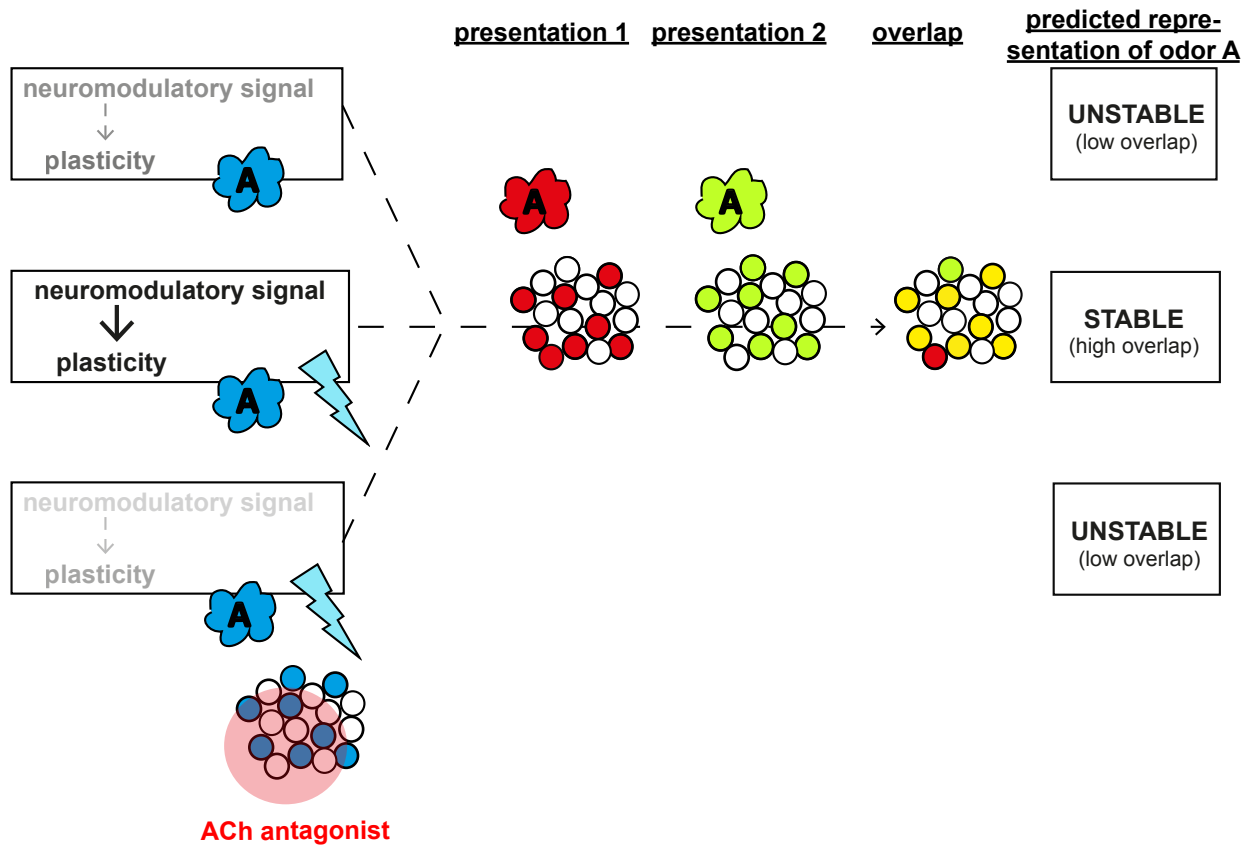


Figure 5.1: **Hypothesis:** Learning stabilizes odor representations via the neuromodulatory signal ACh.

5.2.2 Preliminary results

Acetylcholine neuromodulation was blocked during olfactory fear conditioning. As can be seen in Figs.5.2C, D, mice in both groups exhibited an escape behavior. However, two mice in the control group seem to behave as outliers, as they did not show any significant change in their position in the box or increase of speed after CS+ presentation. Furthermore, within the experimental group, three different concentrations of scopolamine were tested. Thus, more numbers of mice infused with the same concentration of scopolamine are needed to reach conclusive results.

Nevertheless, preliminary results indicate that scopolamine infusion in the PC does not alter olfactory learning. This does not exclude a role of ACh in olfactory fear learning via activation of the nicotinic ACh receptors, which are also found in the PC (Parker et al., 2004, Shipley and Ennis, 1996). Nicotinic ACh receptors in the auditory cortex have been shown to play a role in auditory fear conditioning (Letzkus et al. 2011).

Other neuromodulators could also be at play: the PC receives input from both the dopaminergic midbrain nuclei and the noradrenergic locus coeruleus (Shipley and Ennis, 1996; Datiche and Cattarelli, 1996). Dopamine and noradrenaline have been shown to be required for fear memory formation (Fadok et al., 2009; Johansen et al., 2014) and to modulate piriform response properties (Hasselmo et al., 1997; Bouret and Sara, 2002; Gellman et al., 1993).

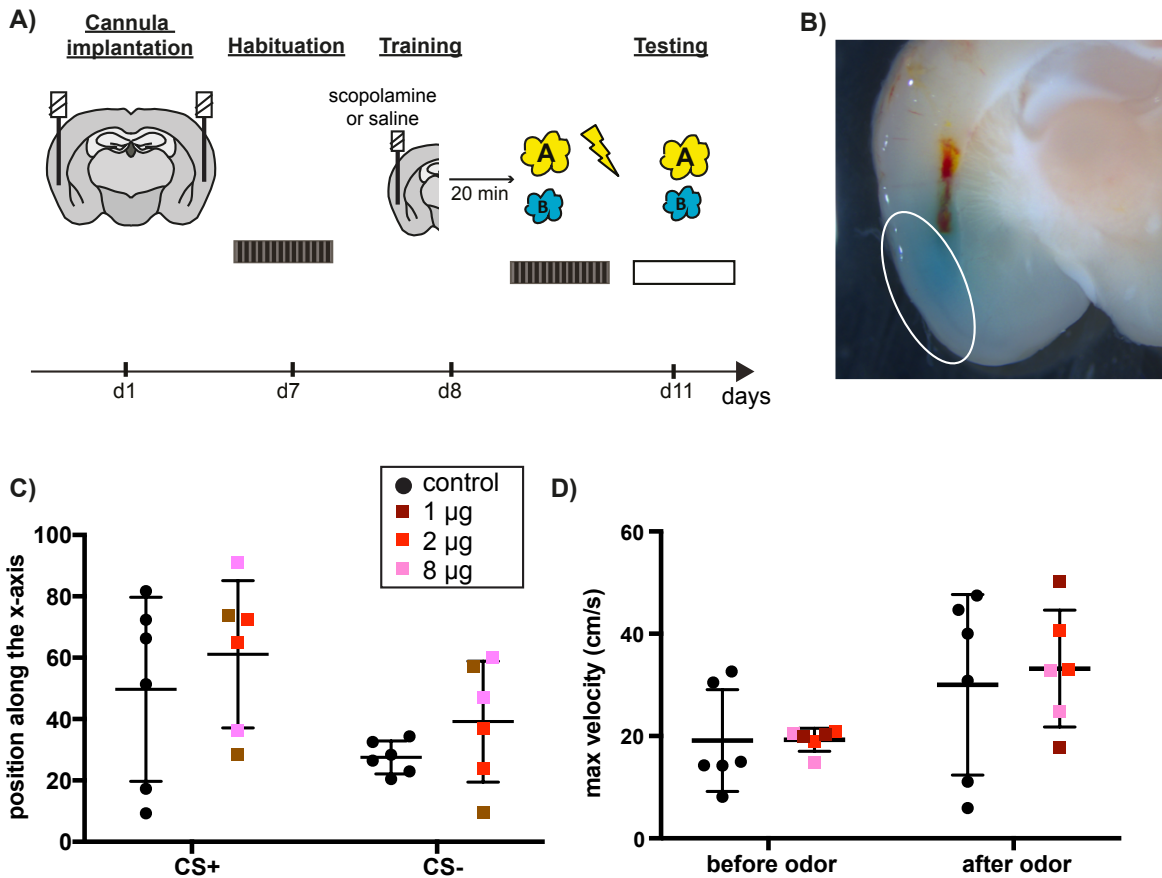


Figure 5.2: **Blocking acetylcholine neuromodulation in the PC during olfactory fear conditioning.** (A) Drug infusion in the PC. Scopolamine was infused 20 min before training. (B) Histological verification of cannula placement: Fast Green was infused after testing to check the site of drug infusion. (C) Position along the x-axis 7s after CS+ or CS- presentation. (D) Maximum velocity after CS+ presentation (7s time-window). The concentration of scopolamine is color-coded.

5.3 Stabilization of odor representation after learning?

We present in this section preliminary results about stability of odor representations in animals in which an odor is given valence by its association with a mild foot shock.

5.3.1 Experimental design

We used the tetO-hM3Dq-mCherry as a fluorescent marker to specifically tag odor-responsive piriform neurons. *cfos*-tTA male mice were bilaterally stereotaxically injected with AAV-tetO-hM3Dq. Ten days later, they were habituated to the training and "tagging" boxes (25 min each). One day later, mice in the "shock" group were fear conditioned to etac. Mice in the control group ("no shock") were exposed to the same odors, except that etac was not paired with a foot shock. Before putting mice back in their homecage, doxycycline was switched to a regular diet, to open the tagging window. Three days later, mice were exposed to 4 brief presentations of etac (8s),

interspaced by a minimum of 3 min (total of 20 min, "presentation 1"). Neurons active during this session of etac presentation were tagged with hM3Dq. Odors were delivered via an olfactometer in the box used to test memory retrieval, to be able to quantify escape responses. Before putting mice back in their homecage, the regular food was replaced by doxycycline, to avoid further expression of hM3Dq. Three days later, exposition to etac was repeated (same as for presentation 1), and mice perfused 1 h after start of the experiment to assess levels of endogenous fos ("presentation 2"). Therefore, the overlap between the hM3Dq-tagged and Fos-positive ensemble of neurons will inform us about the stability of the representation (see Fig.5.3B).

We designed our control group to have a mean of comparison with the study of Shakhawat et al., 2014. The authors looked at the stability of peppermint odor (PP) in the aPC after rats learned to associate PP with a water reward and to disregard presentation of a vanilin odor (VA) (see Fig.5.3A). Control rats received the same odor presentations, but paired with random water delivery. Shakhawat et al. (2014) looked at overlap between two representations of PP, with odor presentations spaced 30 min apart using the catFISH technique. CatFISH or Cellular compartment analysis of temporal activity by Fluorescence In Situ Hybridization takes advantage of the time-dependent localization of the IEG Arc RNA after neuronal activation: Arc RNA signal is nuclear a few min after neuronal activation for up to 15 min and becomes cytoplasmic 20–45 min after activation.

This experimental design also reduces the "over-tagging" of neurons, which likely occurs in the reactivation experiment (see Chapter 4.7).

5.3.2 Preliminary results

On average, mice in the "shock" group escaped during both sessions of etac presentation, while mice in the "no shock" group did not exhibit any change in behavior upon etac presentation (see Figs.5.3C, D). Nevertheless, we did not observe any difference in the number of reactivated neurons between the "shock" and "no shock" group, meaning that etac piriform representation was not stabilized by learning, see Figs.5.3E-G. These preliminary results go against our hypothesis and contrasts with the results of Shakhawat et al., 2014, who observed an increased stability of PP odor representation after associative learning.

Nevertheless, differences between our results and the ones of Shakhawat et al. (2014) might come from the difference in the immediate early gene used as a marker of neural activity (Arc versus Fos). Representations might also be transiently more stable on short timescales (30 min between two presentations versus 3 days). Also, as briefly mentioned in the introduction, during memory retrieval, the memory trace enters a labile state and is then reconsolidated, which could explain why we do not see a high overlap between the two etac representations.

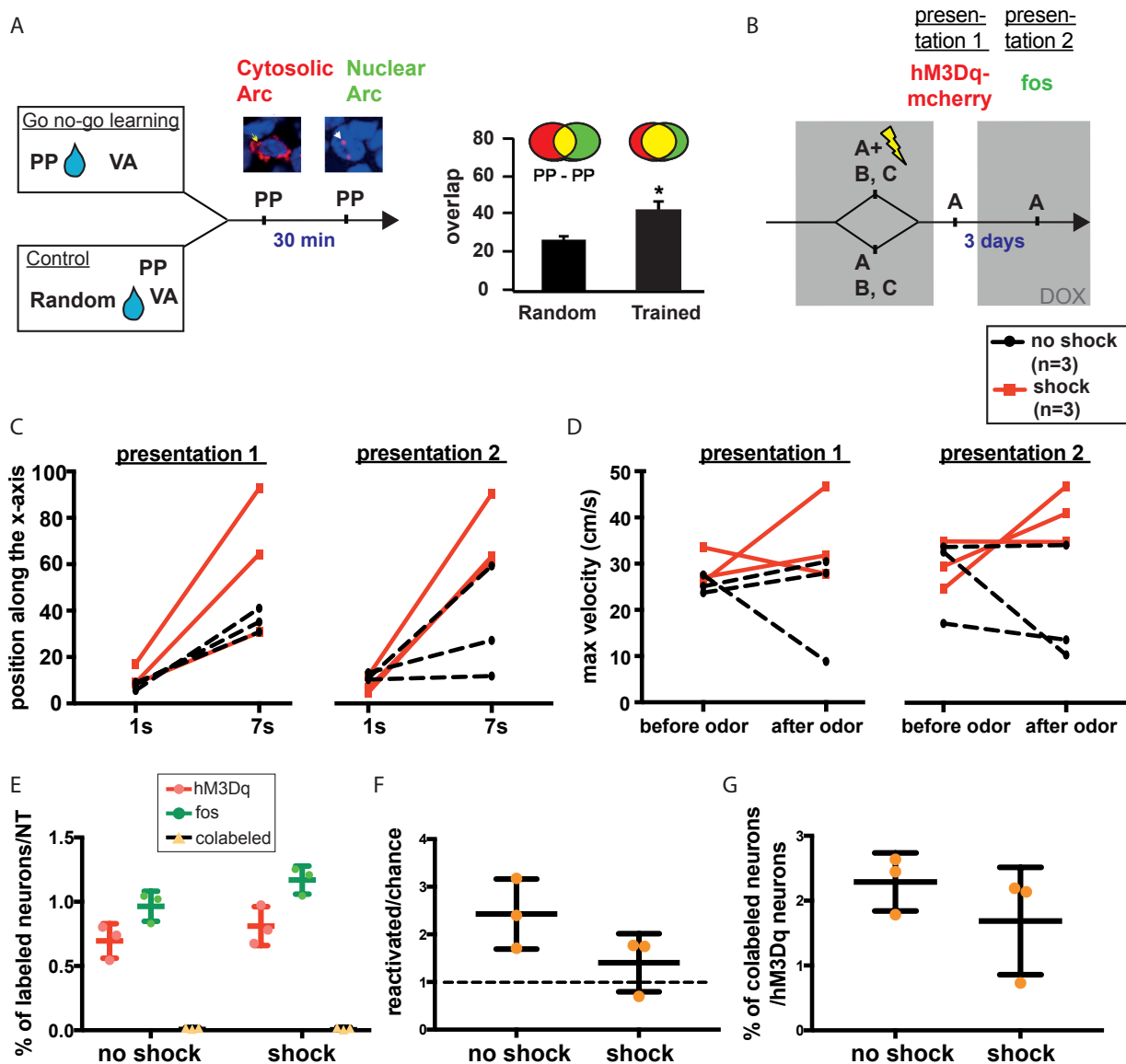


Figure 5.3: **Stability of odor representations after learning.** (A) Data redrawn from Shakhawat et al., 2014, see text for more details. Overlap is defined as the proportion of cells with double staining relative to the total number of Arc-positive cells) (B) Experimental procedure. Mice are presented with 3 odors (A=etac, B=eug., C=cit). In the 'shock' group, one of these odors (odor A=etac) is paired with foot shock. 3 days later, odor A is presented and active piriform neurons are tagged with hM3Dq (presentation 1). 3 days later, odor A is presented again, and active neurons express Fos (presentation 2). Neurons which were active during both sessions of odor presentation will co-express hM3Dq and Fos. (C-D) For both presentation sessions, mice fear conditioned to odor A (n=3) showed an overall avoidance of the side where the odor was presented (C) as well as an increase in maximum velocity after odor presentation (D). (E-G) Odor representations do not seem to be stabilized after aversive conditioning. (E) Quantification of Fos-positive cells, hM3Dq-positive cells and double-labeled cells. NT=Neurotrace counterstained piriform neurons. (F) Reactivation of hM3Dq-positive neurons during presentation 2 relative to chance level. (G) Percentage of hM3Dq-positive neurons which are reactivated.

Chapter 6

TRAPing piriform neurons

We have highlighted in Chapter 4 some limitations of the TetTag system. In this Chapter, we characterize the TRAP system (see Chapter 1 & Fig.6.1A) in the PC after odor stimuli. Then, we test if behavioral results obtained with the TetTag system can be reproduced. We finish by summarizing the advantages and disadvantages of both systems for labeling active piriform neurons.

6.1 TRAPing odor-responsive neurons

We will refer to the manuscript by Guenther et al. (2013), in which the authors describe the FosCreER^{T2} transgenic mice they generated. They crossed these mice with tdTomato mice in which the red fluorescent protein tdTomato is expressed ubiquitously in a Cre-dependent manner (Madisen et al., 2010). Using the same system, we characterized tdTomato expression in the PC in different conditions, Fig.6.1 A and Fig.6.3. All mice were sacrificed 5 days after 4-OHT injection (50 mg/kg), unless otherwise stated. This is based on the observation of Guenther et al. (2013) that levels of tdTomato expression 3 days after injection almost reached the levels of expression observed 7 days after injection.

First, we confirmed very low levels of background tdTomato expression in homecage mice i.p injected with saline (saline group, n=1, Figs.6.1 B, 6.3 B). Despite CreER^{T2} expression in Fos-positive neurons throughout the mouse's life, very few cells were TRAPed in the absence of 4-OHT.

Intraperitoneal injections require to pick up the mouse and take it out of its homecage for a few seconds. Consequently, multiple odor sources (experimenter, room...) likely induce neuronal activity in the PC. To account for these background odors, one group of mice received 4-OHT i.p injections in their homecage ("HC" group, n=5): 0.79% of piriform neurons were TRAPed (see Figs.6.1C, 6.3B). This is consistent with background activity observed in homecage controls in Guenther et al. (2013).

We then investigated if odors delivered in a controlled way via an olfactometer could generate a significant increase in the amount of TRAPed cells. One group of mice explored for 30 min a box

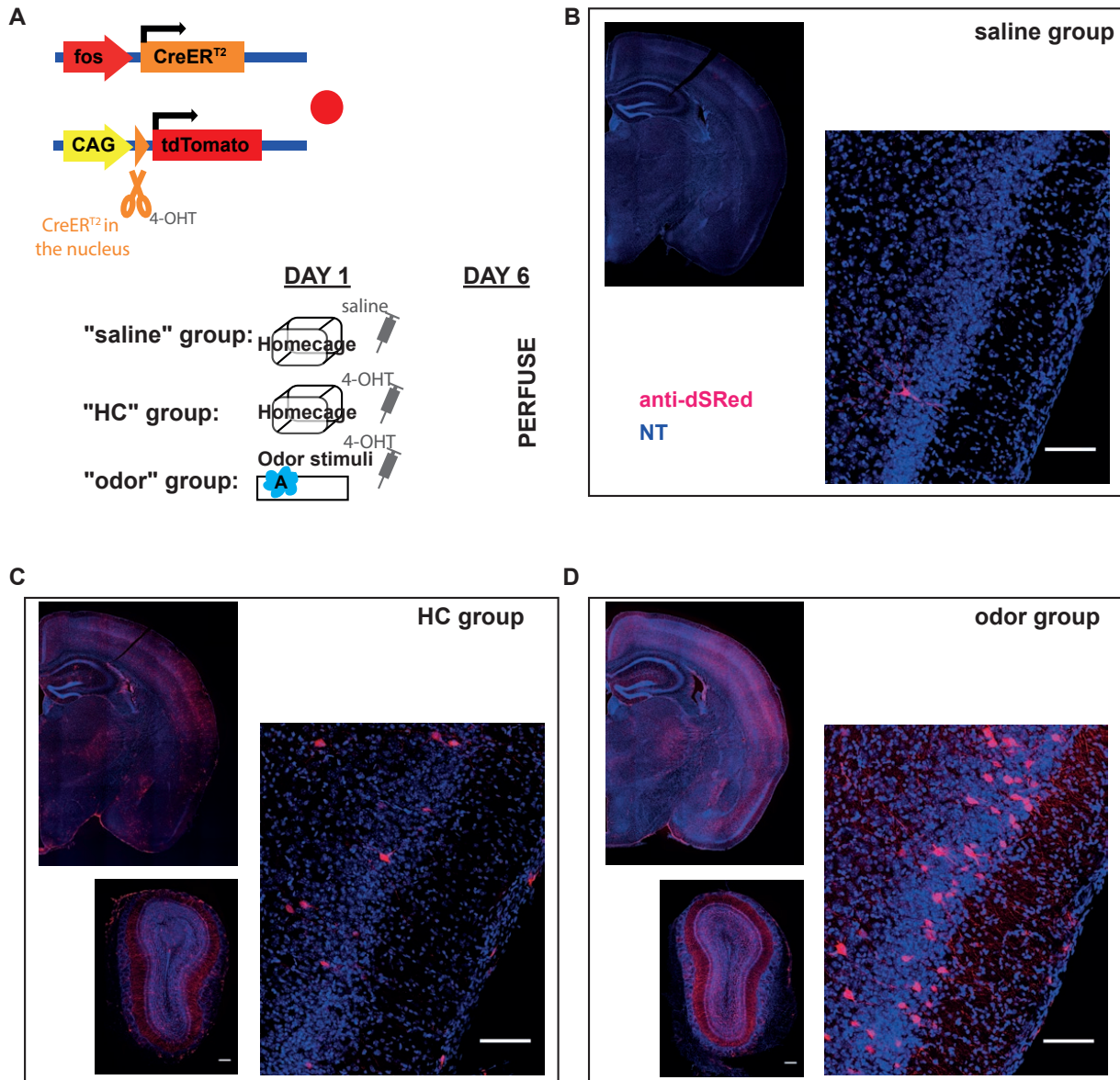


Figure 6.1: Histological characterization of fos-TRAPed piriform ensembles. (A) (Up) The «TRAP» system: CreER^{T2} is under the control of the activity-dependent cfos promoter. tdTomato is expressed in a Cre-dependent manner. In the absence of 4-OHT, active neurons express CreER^{T2} which is retained in the cytoplasm. In the presence of 4-OHT, CreER^{T2} translocates in the nucleus of active neurons and tdTomato is expressed. (Down) Experimental timeline: Homecage mice were injected with either saline ("saline" group) or 4-OHT ("HC" group). Mice in the "odor" group explored a box for 30 minutes and during these 30 min, etac was delivered 8 times during 8s. In this case, 4-OHT was injected 20 min before start of the exploration. All mice were perfused five days after injection to assess levels of recombination. (B-D) Coronal section of a mouse brain (top left) and high magnification of the PC (bottom right, scale bar = 100 μ m): example of a mouse from the "saline" group (B), from the "HC" group (C), and from the "odor" group (D). (C-D) Coronal section of the olfactory bulb (bottom left, scale bar=200 μ m): example of a mouse from the "HC" group (C), and from the "odor" group (D).

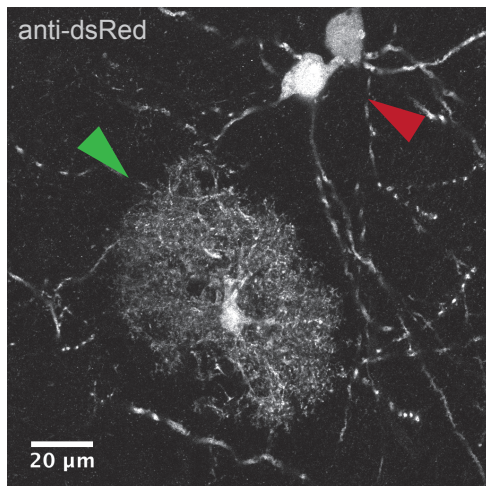


Figure 6.2: **Morphology of TRAPed cells.** TRAPed cells include a majority of neurons (red arrow) and very few astrocytes (green arrow).

to which they had been habituated the day before for 30 min ("box" group, n=7). Another group of mice received in addition 8 presentations of etac while being in the box. Each presentation lasted for 8s, with a mean time of 4 min between presentations ("odor" group, n=8), see Fig.6.3A. In the "box" and "odor" group, half of the mice were injected with 4-OHT and left undisturbed in their homecage for 20 min before the start of the 30 min box exploration. The other half were injected with 4-OHT just after the 30 min box exploration (color code on Fig. 6.3B). Odor stimuli induced a moderate but significant increase in the numbers of TRAPed cells compared to 4-OHT-injected homecage controls (1.4-fold increase, U=8, p= 0.043, Figs.6.1C, 6.3B). As a comparison, Guenther et al. (2013) observed a 1.9-fold increase in the numbers of TRAPed cells in the PC after a 2 hours exploration of a novel environment, with i.p injection of 4-OHT at the start of the second hour of exploration. In Fig.6.3, we see that the number of TRAPed cells in the "box" group overlaps with the ones in the HC and "odor" group. This correlates with the presence of additional background odors (box odors...) compared to the HC group, and with the absence of brief controlled odor stimuli compared to the "odor" group. Furthermore, data points in the "odor" and "box" group did not cluster relative to the timing of 4-OHT injection.

tdTomato fills cell bodies and processes, which provides an opportunity to determine the morphology of the cells, and thus can provide information about cell type identity. By visual inspection, the majority of TRAPed cells were neurons, with a few astrocytes detected (see Fig.6.2).

As seen with endogenous Fos expression (see Chapter 4), there was no significant difference in the percentage of TRAPed piriform neurons between the left and right hemisphere (see Fig.6.3C). Furthermore, the number of TRAPed cells decreased along the rostro-caudal axis (see Fig.6.3D). This is in line with Datiche et al. (2001), who observed a higher number of Fos-positive cells in aPC compared to pPC. In Fig.6.3D, the approximate end of aPC/beginning of pPC is indicated by a dotted line.

Finally, we identified the time course of tdTomato expression after TRAPing. Contrary to Guenther et al. (2013), we saw tdTomato expression in piriform already 24 h after odor stimulation and 4-OHT injection ('odor 1day' group). However, contrary to Guenther et al. (2013), we used an anti-dsRed antibody to amplify tdTomato signal. The fact that they looked in visual

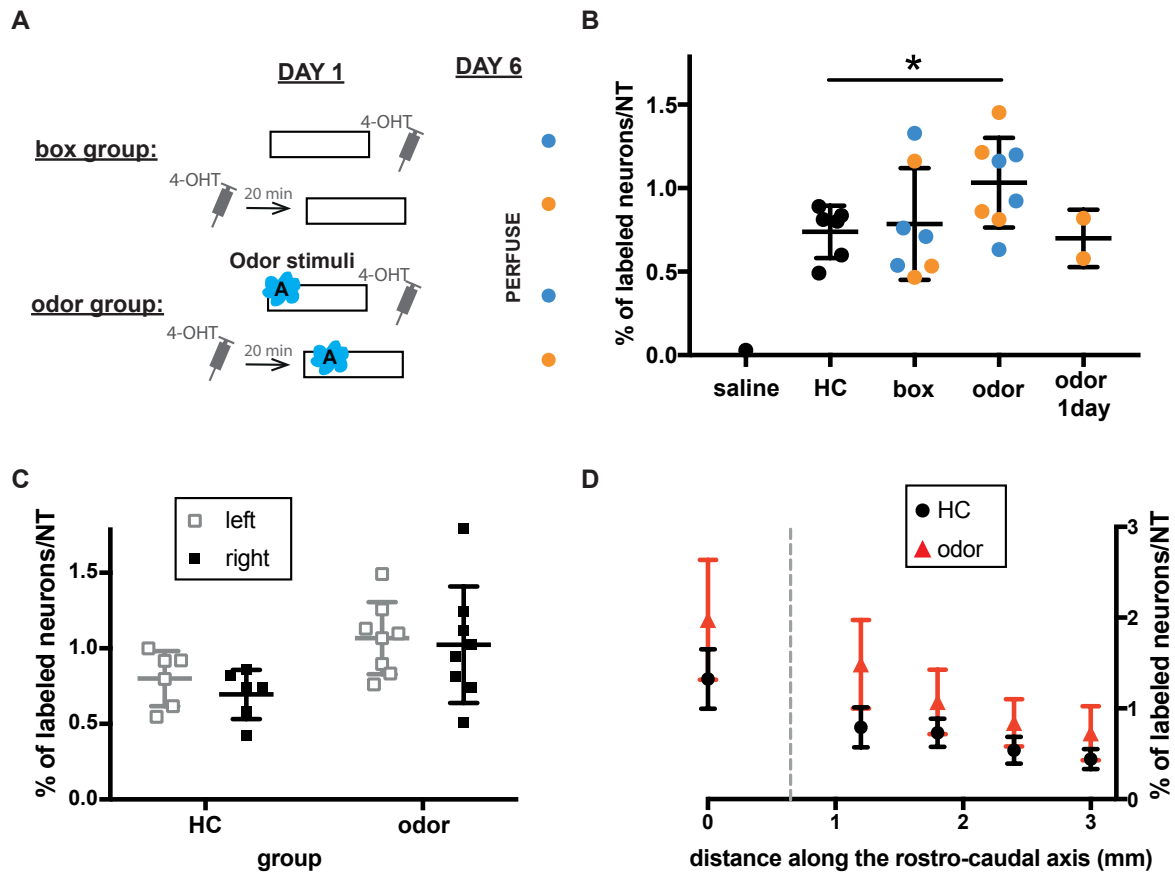


Figure 6.3: **TRAPing in the PC after odor stimulation** (A) Experimental scheme: Mice in the "box" and "odor" groups explored a box for 30 minutes during which mice in the "odor" group received 8 short (8 s) presentation of etac. 4-OHT was injected 20 min before start of the exploration or just after. This is denoted on the figure by a filled orange circle and a blue one, respectively. (B) Percent of TRAPed neurons in different conditions (see A, Fig.6.1 and text). Time of 4-OHT injection is color-coded as in A. Odor stimuli induced a significant increase in the numbers of TRAPed cells in comparison to 4-OHT injected homecage controls. * $p < 0.05$. (C) TRAPing does not differ between brain hemispheres. (D) The number of piriform TRAPed cells decreases along the rostro-caudal axis. The position of the first section along the rostro-caudal axis was set to 0, and the dotted line indicates the border between aPC and pPC. NT=NeuroTrace counterstain

cortex after visual stimulation could also explain this difference. Automated cell counting yielded numbers of TRAPed cells similar to the mean percent of TRAPed cells in the "HC" group. Nevertheless, for one of the 2 mice from this group, signal intensity seemed lower than for mice from the "HC" group (data not shown).

6.2 Inactivating neurons TRAPed during fear conditioning

We next tested if TRAPing piriform neurons during olfactory fear conditioning and inactivating them during memory retrieval would impair memory retrieval, as was the case with the TetTag system. However, instead of testing memory retrieval 3 days after learning, we decided to wait

1 week. Indeed, Guenther et al. (2013) found that levels of tdTomato were sufficiently high to be reliably identified 72h after 4-OHT injection. Furthermore, in our case, waiting 5 days yielded significant labeling of piriform neurons, and patterns of TRAPed piriform neurons resembled patterns of endogenous Fos expression (see Chapter 4.1). tdTomato is a cytosolic protein, while hM4Di is a membrane protein. We thus decided to wait two more days to allow for membrane integration¹.

6.2.1 Experimental design

AAV-floxed-hM4Di-mCherry was stereotaxically injected in both hemispheres of the PC of FosCreER^{T2} transgenic male mice. Mice were then given ten days to recover, before being habituated on day 11 to the training and testing boxes (40 and 10 min respectively). Two days later, mice were trained to associate beta-cit. with foot shock (see Chapter 3 for more details). Just after the training session, mice were injected with 4-OHT to induce expression of hM4Di. One week later, memory retrieval was tested in the presence of CNO to silence neurons that were active during learning (see Fig.6.5A).

One control group was used: WT mice injected with the floxed-hM4Di AAV (n=7). The experimental group consisted of fosCreER^{T2} mice injected with AAV-floxed-hM4Di (n=23). 1 mouse had to be excluded from the analysis as it was too stressed during testing and stayed in the middle of the box. After histological posthoc analysis, only mice in which expression of mCherry could be detected in at least all the posterior part of the PC (both hemispheres) were included in the analysis (see Fig.6.4). As a consequence, 16 further mice were excluded from the analysis

6.2.2 Results

The control group exhibited an escape behavior after CS+ presentation (averaged position of 86, 3.0-fold increase of the maximum velocity). Similarly, the experimental group escaped after CS+ presentation (averaged position of 76, 2.4-fold increase of the maximum velocity) (Figs.6.5 C,D,F,G). There was no significant difference in the position of the mice 7s after CS+ presentation between control and experimental groups (U=10, p=0.138), as well as in the maximum velocity after CS+ presentation (U=20, p=0.945) and the maximum velocity ratio (U=16, p=0.534).

All mice were close to the odor port when the CS+ odor was presented (U=24, p=0.694), and had a similar maximum velocity during the 7s that preceded odor presentation (U=18, p=0.281). This excludes any inherent differences between groups due to how the CS+ was presented.

Learning was associative, as none of the mice escaped to the CS-. Mice stayed on the side where the odor was presented, and had a similar maximum velocity before and after CS- presentation (Figs.6.5E, H).

¹A pilot experiment indicates that the number of TRAPed hM4Di-mCherry cells is 1.5-fold increased 1 week after 4-OHT injection (n=2), compared to 72 hours (n=2).

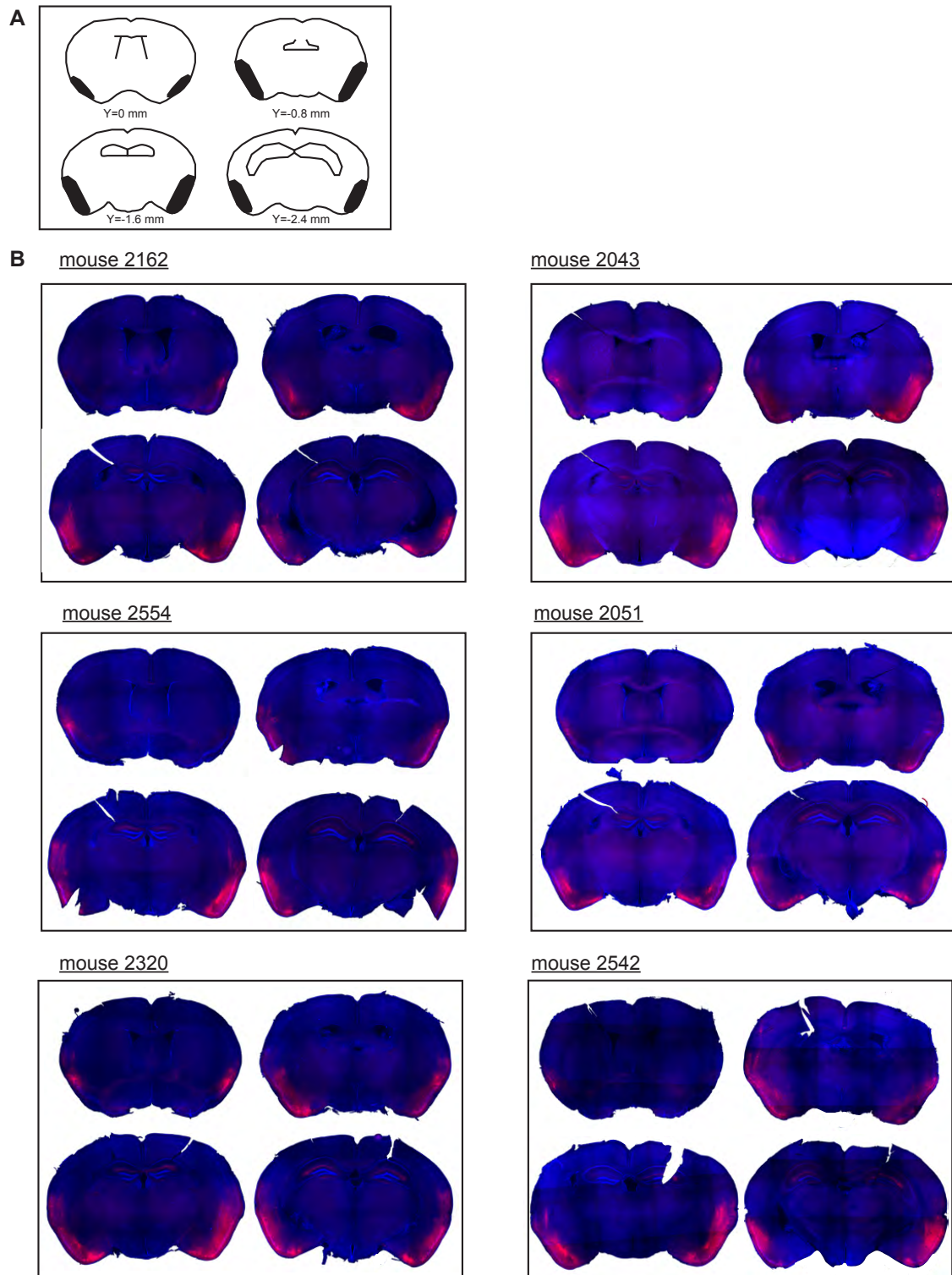


Figure 6.4: **Histological confirmation of hM4Di expression in the PC.** (A) Four $200\mu\text{m}$ coronal sections spaced $800\mu\text{m}$ apart were taken from each mouse to determine the extent of the viral infection. The PC is highlighted in black, and position of the section relative from bregma along the anterior-posterior axis (Y) is indicated. The anterior PC ends around $Y=0$ mm. (B) hM4Di-mCherry expression (anti-dsRed, in red) in the PC of fear-conditioned fosCreER^{T2} mice. All the posterior PC was labeled. The anterior PC was only partly infected. Images were acquired using an Axio Zoom microscope (Zeiss). NeuroTrace counterstaining in blue.

6.3 Discussion

We will first compare the TetTag and TRAP system for labeling odor-responsive piriform neurons, and then give some possible interpretations of the behavioral results.

Comparison of cfos-tTA and FosCreER mouse line

In the TRAP system, gene expression is induced by 4-OHT i.p injection, while in the TetTag system, gene expression is induced by doxycycline removal. Doxycycline is an antibiotic with a half-life of 2 days delivered via rodent chow, and has thus to be removed for at least 2 days to enable induction of the target gene. 4-OHT can be i.p injected, and minimal TRAPing occurs when stimulation precedes or follows 4-OHT injections by 6 hours (Guenther et al., 2013). As a consequence, the TRAP system has better temporal control, with likely less labeling of cells active prior or after presentation of the experimental stimuli. In both cases, the labeled population depends on tTA/CreER^{T2} protein stability and doxycycline/4-OHT metabolism.

Another advantage of the TRAP system is that CreER^{T2} activity is tightly regulated by 4-OHT, as seen with the zero-percent of TRAPed neurons in mice injected with saline (see Figs.6.1 & 6.3). In contrast, mice that are on doxycycline exhibit a non-negligible number of tagged neurons (see Fig. 4.1B-C and Chapter 4.1). The TetTag system seems thus more leaky than the TRAP system in the PC.

Another difference between the two systems is that in the TRAP system, once recombined, the target protein is permanently expressed. In the TetTag system, binding of tTA to tetO will generate mRNA and protein, which will be subject to degradation. Thus, in the latter case, experimental manipulation or characterization of the labeled population is limited in time. Nevertheless, the TetTag system might allow the study of the labeled population with a shorter delay than the TRAP system.

Nevertheless, the major advantage of the TetTag system is that it has been used extensively (see references in Chapter 1). To our knowledge, apart from the study describing the generation of the FosCreER^{T2} transgenic mouse, no other study using the TRAP system has been published since.

Behavioral results: how can they be explained?

Results obtained with the TetTag system could not be reproduced with the TRAP system: inactivation of piriform neurons that were active during olfactory fear conditioning did not impair memory retrieval.

First, we should consider that the two systems, despite depending on activation of the cfos promoter, might label different neuronal ensembles during fear conditioning. Indeed, the downstream pathways leading to the expression of the target protein (DREADDs) are different. The timing of 4-OHT injections relative to fear conditioning might also not be TRAPing the relevant cells. A simple experiment to compare the labeled ensembles is to look at the proportion of different cell types in each ensemble. Among others, we know from immunohistochemistry and electrophysiology that a non-negligible amount of TetTag cells are inhibitory (see Chapter 4). We have not

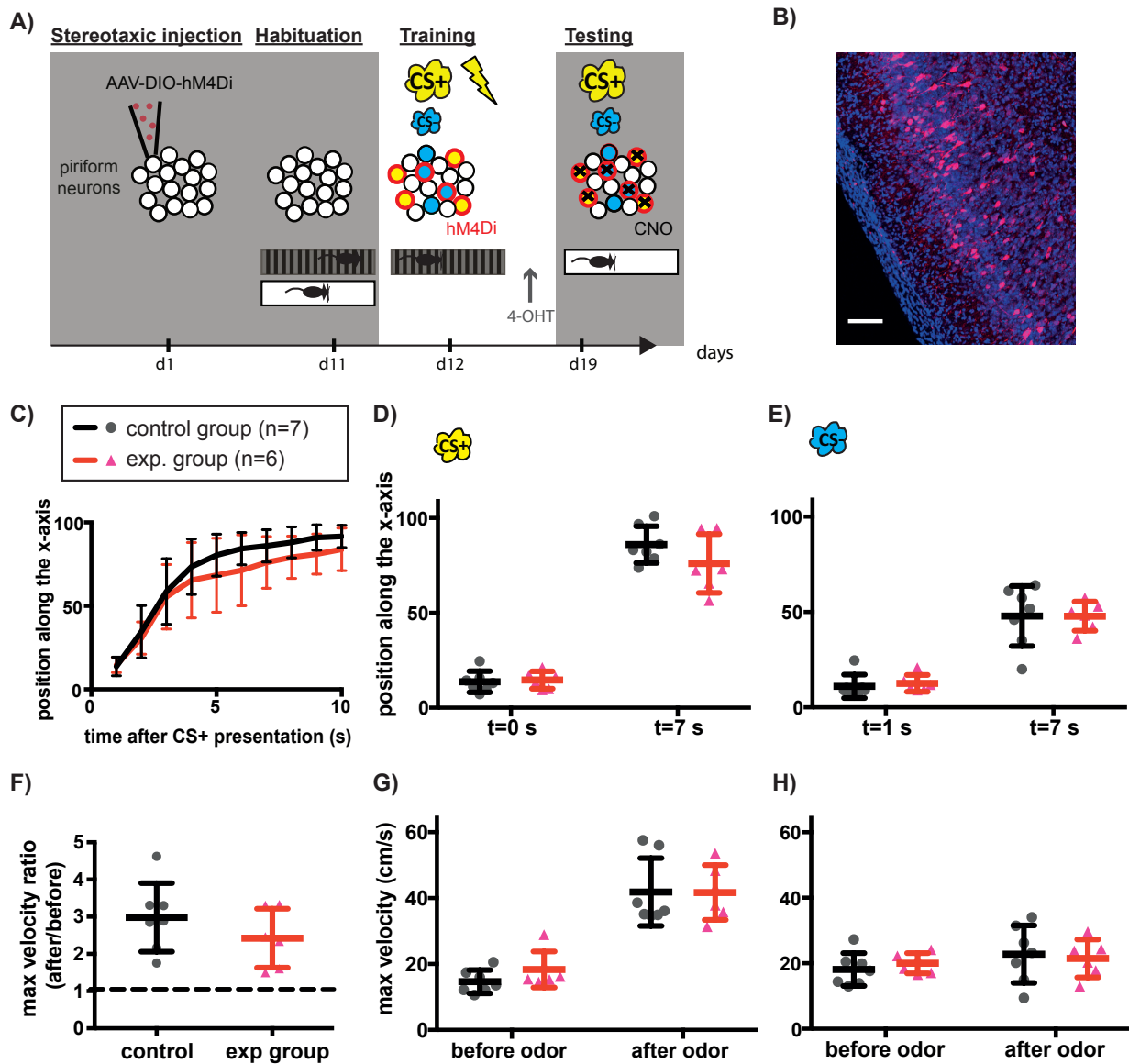


Figure 6.5: **Inactivation of fos-TRAPed ensembles during memory retrieval.** (A) Experimental design: *fosCreER^{T2}* transgenic mice are stereotaxically injected with AAV-DIO-hM4Di-mCherry in both hemispheres of the PC. Mice are then habituated to the training and testing boxes. Just before 4-OHT i.p. injection, mice are trained to associate one odor with a foot shock (CS+ odor, beta-cit.). Training includes presentation of two other odors which are not paired with foot shock (CS- odor, eug. and etac). During training, hM4Di expression (neurons surrounded by red) is induced in Fos-positive neurons (neurons filled in blue and yellow). Seven days later, memory retrieval is tested in the presence of CNO. CNO silences the activity of hM4Di-expressing neurons (black crosses). (B) hM4Di-mCherry expression in *fosCreER* mice during memory retrieval. NeuroTrace counterstain in blue. Scale bar, 100 μm . (C to H) Olfactory memory retrieval after CNO injection assessed by position in the testing box and maximum velocity. There was no significant difference between the 2 groups tested: *fos-CreER^{T2}* mice (exp group, n=8) or WT mice (control group, n=7) were injected with AAV-DIO-hM4Di. (C) Position of the mouse in the box (0 being the extremity of the box where the odor is presented, 100 the opposite side) as a function of time after CS+ presentation. (D-E) Mouse position along the x-axis 1s or 7s after CS+ (D) or CS- (E) presentation. (F) Maximum velocity ratio after/before CS+ presentation. (G-H) Maximum velocity during the 7s before and after odor presentation. CS+ (G) or CS- odor (H). Data are presented as mean \pm SD.

performed GABA staining on TRAPed piriform ensembles.

Second, hM4Di might not be expressed at levels sufficiently high for in vivo silencing of the TRAPed neurons. We are using an anti-dsRed antibody to detect TRAPed cells, as considerable quenching of mCherry fluorescence occurs after overnight fixation (compared to 4 h used for detecting the TetTag hM3Dq-mCherry). Therefore, fluorescence intensity does not reflect levels of receptor expression. It might be informative to quantify levels of hM4Di expression by quantitative Western Blots in both the TRAPed and TetTag system, at different time points after conditioning (e.g. 3 days, 5 and 7 days). If similar levels are found at one time point, then it might be worth repeating the experiment in both systems to test memory retrieval at this particular time point. Differential results would then confirm an intrinsic difference in the cells labeled in both systems.

Finally, if we assume that the labeled populations are similar in both systems, one difference between the two experiments is the time at which we tested memory retrieval: 3 days after fear conditioning for TetTag, 7 days for TRAP. This could hint towards a time-dependent role of the PC in memory retrieval: the PC would be necessary for the retrieval of recent but not remote memories. As described in Chapter 3, the hippocampus and the PC are two allocortical circuits with a similarity in circuit connectivity and operations performed. General principles of memory encoding might be similarly conserved, including the temporary necessity of these structures in memory retrieval. Kim and Fanselow (1992) showed that while freezing in the conditioned chamber was completely abolished when the hippocampus was lesioned 1 day after contextual fear conditioning, some freezing was observed for lesions occurring 7 days after fear conditioning. However, this goes against the results of Sacco et al. (2010) who showed that excitotoxic lesion of the PC affects retrieval of remote but not recent olfactory memories (1 month vs 1 day).

Part IV

Modeling project

Chapter 7

Predict synaptic plasticity using dendritic recordings

From Chapter 2 to 6, we have searched for the memory trace, at a behavioral and network level, using an experimental approach. While synaptic plasticity has been correlated to learning and memory, more recent studies have started to unravel a causal link between these two processes (Nabavi et al., 2014, Ryan et al., 2015). We will now investigate synaptic plasticity at a cellular level in a theoretical framework. This work has been done in EPFL, Lausanne under the supervision of Wulfram Gerstner. I visited his lab for 2 months in 2014 and 2 weeks in 2017.

7.1 Introduction

There is now a very large body of studies investigating synaptic plasticity in different brain areas, using different protocols. This leads sometimes to results which seems at first contradictory (Birtoli et al., 2004; Froemke et al., 2005). Thus, developing models predicting synaptic plasticity can help extract underlying unifying principles. However, few models take into account the complex morphology of neurons. Indeed, the majority of the excitatory synapses contact the postsynaptic neuron on its dendrites. Besides passively conducting the voltage, dendrites have also active properties, which can vary along the dendritic tree, creating dendritic domains defined by morphology, excitability and input specificity (Spruston, 2008). As a consequence, dendritic nonlinearities could explain different plasticity results.

Hebbian plasticity depends on the correlation between the firing of pre- and postsynaptic neurons: the pre- and postsynaptic neurons are active within some short time window. The postsynaptic depolarization was first thought to be provided by the back propagation of an action potential into the dendritic tree. Nevertheless, several recent studies challenge this view (Kampa et al., 2007; Lisman et al., 2005 and 2010). The increasing availability of dendritic recordings during LTP induction allows now to investigate and model the precise nature of the postsynaptic depolarization. In some studies, dendritic spikes appeared to be necessary for the induction of plasticity in

various brain regions (Kampa et al., 2006; Brandalise et al., 2016, Humeau et al., 2006). Among others, plasticity with dendritic spikes could happen with only one pairing (Remy et al., 2007; Holthoff et al., 2004).

We decided to use experimental voltage traces recorded close to the 'plastic' synapse and see if a voltage-based model could predict the experimentally measured plasticity. We took advantage of a recent phenomenological model of voltage-based plasticity by Clopath et al (2010), which we combined with a 'veto' concept as in Rubin et al. (2005). The 'veto' concept translates the competition between the LTP and the LTD pathway at a molecular level. We showed that this combined voltage-based model of synaptic plasticity could predict synaptic plasticity, both in neocortex and allocortex. We could also explain the dependence of synaptic plasticity on spatial and morphological properties of the neuron.

7.2 Methods

7.2.1 Voltage-based model of synaptic plasticity

The plasticity model is a combination of the voltage-based model of Clopath et al. (2010) and the veto concept of Rubin et al. (2005).

Potentiation is induced as in Clopath et al.(2010): if both the postsynaptic voltage u and its low-pass filtered trace \bar{u}_+ are above a threshold θ_+ and θ_- respectively, after a presynaptic spike X has occurred. The latter leaves a "trace" at the synapse for a certain duration defined by the time constant τ_x .

$$\frac{d}{dt}w_{LTP}(t) = A_{LTP}\bar{x}(t)[u(t) - \theta_+][\bar{u}_+(t) - \theta_-] \quad (7.1)$$

with

$$\tau_+ \frac{d}{dt}\bar{u}_+(t) = -\bar{u}_+(t) + u(t) \quad (7.2)$$

and

$$\tau_x \frac{d}{dt}\bar{x}(t) = -\bar{x}(t) + X(t) \quad (7.3)$$

A_{LTP} is an amplitude. If $\bar{u}_+(t) < \theta_-$ then $[\bar{u}_+(t) - \theta_-]$ equals 0.

Depression is induced if a low-pass filtered trace \bar{u}_- is above a threshold θ_- while a presynaptic "trace" remains. Thus, the mathematical formalization is slightly different from Clopath et al.(replace $X(t)$ by $\bar{x}(t)$, see equation in Clopath et al. (2010)). This is the only way to have LTD with pre-post pairs at low pairing frequencies (see Letzkus et al., 2006 as an example). It seems conceivable, as biological events are rarely "point-like events".

$$\frac{d}{dt}w_{LTD}(t) = A_{LTD}\bar{x}(t)[\bar{u}_-(t) - \theta_-] \quad (7.4)$$

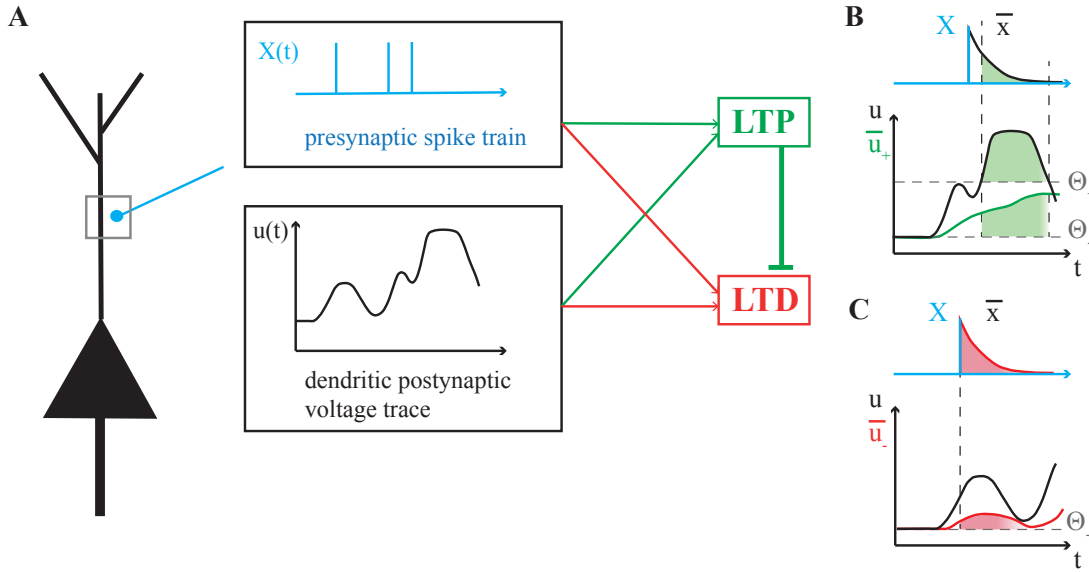


Figure 7.1: Scheme of the model. (A) The activity of the presynaptic neurons X induces local dendritic voltage changes u in the postsynaptic neurons. Depending on the timing of the presynaptic spike, and the voltage in the dendrite, either LTP or LTD are induced. When LTP is induced, LTD cannot occur. (B) LTP induction. (C) LTD induction (see text for more details).

with

$$\tau_- \frac{d}{dt} \bar{u}_-(t) = -\bar{u}_-(t) + u(t) \quad (7.5)$$

and

$$\tau_x \frac{d}{dt} \bar{x}(t) = -\bar{x}(t) + X(t) \quad (7.6)$$

Amplitudes, thresholds and time constants are defined for one type of neuron. Indeed, a layer 5 pyramidal neuron in neocortex may have different synaptic plasticity rules than one in hippocampus region CA1 or CA3. Furthermore, differences in preparations (temperature, ion concentrations in the bath, and potential pharmacological manipulations) could affect plasticity rules.

Finally, the total synaptic change is the contribution of either depression or potentiation, but not both. This parallels the 'veto' concept of the Rubin et al. (2005) paper.

Thus, we have the following rule (cf Fig.7.1) :

If $u(t) > \theta_+$,

$$\frac{d}{dt} w = A_{LTP} \bar{x}(t) [u(t) - \theta_+] [\bar{u}_+(t) - \theta_-] \quad (7.7)$$

Else,

$$\frac{d}{dt} w = A_{LTD} \bar{x}(t) [\bar{u}_-(t) - \theta_-] \quad (7.8)$$

7.2.2 Postsynaptic voltage traces

To validate the new version of the voltage-based model, we used the same neuron model as

the one used by Clopath et al. (2010): the Adaptive Exponential Integrate and Fire model (Brette and Gerstner, 2005).

To then test the voltage-based model, we searched for plasticity papers where dendritic voltage recordings close to the "plastic" synapse were available. As the plasticity model has 6 free parameters, recordings in at least 6 different conditions had to be available. This was the case for two papers: Letzkus et al. 2006, Brandalise et al. 2014 and its follow up Brandalise et al. 2016. For Letzkus et al. 2006, we scaled the traces setting the resting potential to 0, as this potential differs between distal and proximal synapses.

7.2.3 Parameters

A model can only set a mathematical framework whereas parameter values may vary between different preparations. Therefore we used different sets of parameters, depending on the experiments we wanted to model.

We took the simulated or experimental voltage traces as input to our model. The 6 parameters of our model were fitted to the outcome of different experiments using the Matlab function `fmincon`. We minimized the error defined as the squared difference between experimental and theoretical plasticity value. θ_- was set empirically to a value near the resting membrane potential. All the parameters can be found in Table 7.1.

synapse	τ_x (ms)	τ_- (ms)	τ_+ (ms)	A_{LTD} (1/mV)	A_{LTP} (1/mV ²)	Θ_- (mV)	Θ_+ (mV)
L5-L5 neocortex (Sjöström)	10	8.1	6.8	$24 \cdot 10^{-5}$	$66 \cdot 10^{-4}$	3.5*	19.7*
L213-L5 neocortex (Letzkus)	10.7	167	2.5	$40 \cdot 10^{-3}$	$14 \cdot 10^{-5}$	3.5	59
rCA3 allocortex (Brandalise)	4.3	55	2.1	$32 \cdot 10^{-3}$	$18 \cdot 10^{-4}$	1.5	14.3 (sub.) 26(classic)

Table 7.1: Values of the parameters of the model obtained in the fit. Θ_- has been fixed empirically. The star indicates that the resting membrane potential has been subtracted. In the last column, for the rCA3 synapse, the two values for Θ_+ corresponds to two different protocols, see text for details

7.3 Results

7.3.1 Validation of the model

The voltage-based model can explain the results from experiments using different plasticity protocols in various brain regions:

- experiments in the visual cortex where the timing between pairs of presynaptic and postsynaptic spikes is varied, as well as the pairing frequency (Sjöström et al., 2001, cf Fig. 7.2).
- experiments in somatosensory cortex where presynaptic spikes are paired with bursts of postsynaptic spikes (Letzkus et al, 2006, see subsection 7.3.2 and Fig.7.3).

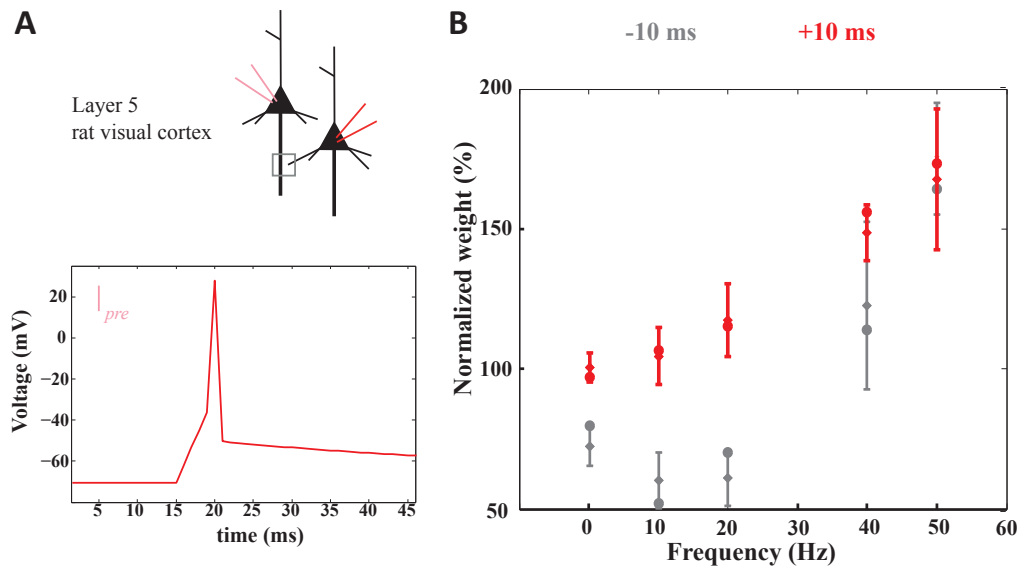


Figure 7.2: Plasticity experiments with pairings of presynaptic and postsynaptic spikes. A) Pairings in L5 neurons in rat visual cortex slices. Simulated postsynaptic voltage trace (pre-post, +5 ms). B) Synaptic weight change as a function of pairing frequency and spike-timing. Red indicates a time interval of +10 ms (pre-post), grey -10 ms (post-pre). Crosses with errorbars represent data from Sjöström et al. (2001) and dots simulations.

7.3.2 Dendritic voltage shapes synaptic plasticity in the neocortex

Necortical dendritic recordings during plasticity experiments can be found in Letzkus et al.(2006). The authors investigate plasticity both at proximal and distal synapses between layer 2/3 and layer 5 pyramidal neurons in slices from rat somatosensory cortex. Interestingly, they find that the learning rule varies with synapse location on the dendritic tree. Proximal EPSPs potentiate during pairing at +10 ms with postsynaptic bursts but depress after pairing at -10 ms. Conversely, distal EPSPs depress during pairing at +10 ms but potentiate during pairing at -10 ms. We fed dendritic recordings available in Letzkus et al. (2006) into our plasticity model to fit parameters to L5 neocortical pyramidal synapses. We find a set of parameters explaining both the plasticity rule at the proximal and the distal synapses (cf Fig.7.3 and Table 7.1). These further supports that the distance-dependent difference in the voltage traces could explain spatial differences in the learning rule, as suggested by the authors.

7.3.3 Dendritic voltage shapes synaptic plasticity in the allocortex

Allocortical dendritic recordings during plasticity experiments can be found in Brandalise et. al (2014 and 2016).

Brandalise et al. (2014 and 2016) investigate plasticity at CA3 recurrent synapses in rat hippocampus, using two different types of protocol. In the first one, the subthreshold pairing protocol, a recurrent CA3 EPSP is paired with a subthreshold mossy fibre (MF) stimulation (10 ms time interval, 60 pairings at 0.1Hz), see Fig.7.4 A, without generation of action potential. In the second

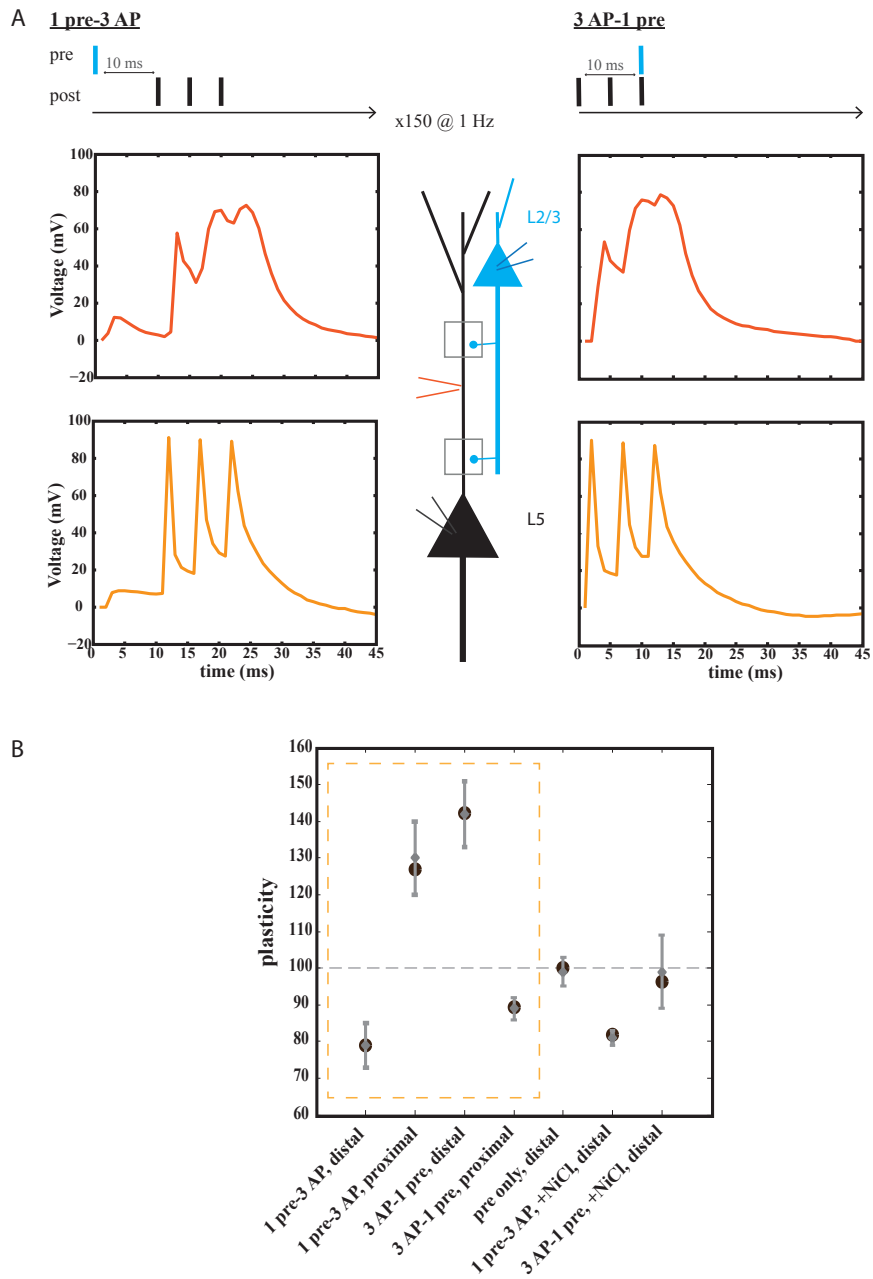


Figure 7.3: Distance-dependent STDP at synapses between layer 2/3 and layer 5 pyramidal neurons in somatosensory cortex. A) Experimental dendritic voltage trace: pre-post pair, +10 ms (left) and post-pre pair, -10 ms (right) at proximal (bottom) and distal (top) synapses, data redrawn from Letzkus et al.(2006). B) 6 out of 7 experiments : postsynaptic bursts (3 APs at 200 Hz) are paired with presynaptic action potentials (10 ms time interval, pairing frequency of 1 Hz). Plasticity is measured at distal and proximal synapses, in the presence or absence of NiCl (blocks T- and/or R-type voltage-gated calcium channels). Remaining experiment (pre only): trains of presynaptic action potentials are not paired with postsynaptic action potentials. Crosses with error bars represent data from Letzkus et al. (2006) and dots simulations.

one, the classic STDP protocol, they pair a recurrent CA3 EPSP with 3 APs at 200 Hz (10 ms time interval, 50 pairings at 0.3Hz), see Figure 7.4 C. We copied the voltage time course from the subthreshold experiments into our plasticity model with parameters adjusted to hippocampus. We found that our model with a fixed set of parameters can explain the outcome of the Brandalise

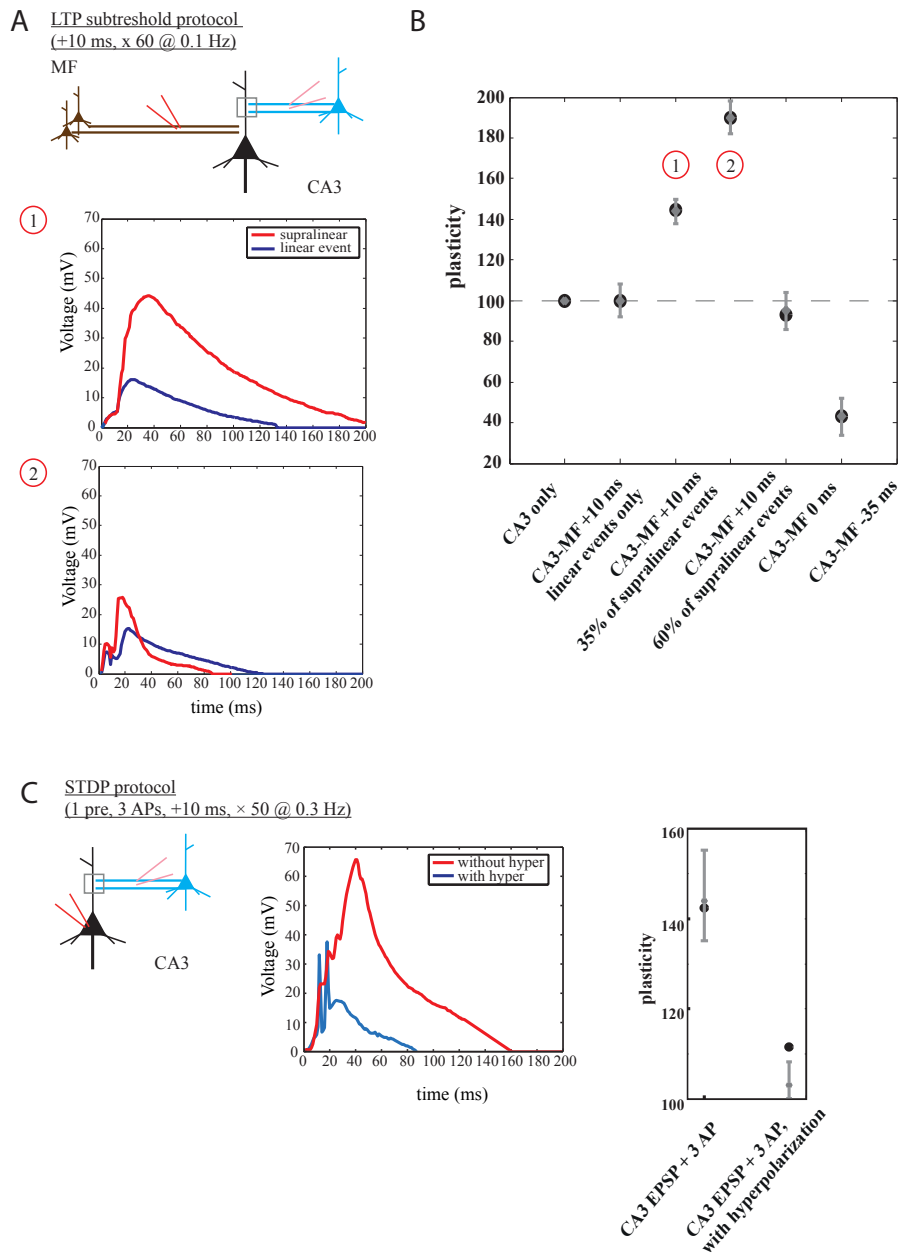


Figure 7.4: Plasticity in the hippocampus. A) Experimental voltage traces from the subthreshold protocol, data redrawn from Brandalise et al.(2014). Dendritic spikes (also named supralinear events, red) were evoked with a certain likelihood. B) First experiment : CA3 stimulation only, no pairing ; next 5 experiments : subthreshold protocol with different time intervals and different likelihood of generating a supralinear event. C) Experimental voltage traces from the STDP protocol, data redrawn from Brandalise et al.(2016). Dendritic spikes were completely abolished with a hyperpolarizing pulse (blue). STDP protocol with or without generation of a dendritic spike. Crosses with error bars represent data from Brandalise et al. and dots simulations.

subthreshold plasticity experiments, see Fig.7.4 B and Table 7.1. Using these parameters we then copied the voltage time course from the classic STDP experiment into our plasticity model adjust-

ing only the threshold Θ_+ .

7.3.4 Dendritic plateau potentials play an important role in the generation of plasticity

Letzkus et al. (2006) show that at distal locations, the peak amplitude of single backpropagating action potentials is twice smaller than at proximal locations. Furthermore, postsynaptic bursts at the soma generates dendritic calcium spikes at distal locations. In Brandalise et al., dendritic NMDA spikes are generated : they result from high frequency bursting during the STDP protocol (as in Letzkus et al., 2006), and from broad and long mossy-fiber evoked EPSPs during the subthreshold protocol.

Both Letzkus et al.(2006) and Brandalise et al.(2014 and 2016) show that long-term potentiation is abolished when dendritic spikes are blocked (pharmacologically or by hyperpolarizing the cell).

In our model, the voltage time course near the synapse determines whether LTP is induced. If the voltage threshold Θ_+ is not reached, then potentiation is impossible (cf Fig. 7.5 B). However, if the momentary voltage increases beyond the threshold Θ_+ , LTP induction can occur only if in addition also the low-pass filtered voltage reaches the threshold Θ_- (cf Fig.7.5 A). Thus a prolonged dendritic plateau potential is more efficient than a short and isolated dendritic depolarization.

7.4 Conclusion

Our results suggest that voltage traces can predict synaptic plasticity. In particular, experiments where no action potential are generated (Brandalise et al., 2014 & 2016) as well as synapse location-dependent plasticity (Letzkus et al., 2006) could be explained by our voltage-based model.

The strength of the voltage model using dendritic recordings close to the "plastic synapse" is that it captures the important role played by dendritic spikes for the induction of long-term plasticity, without excluding other types of depolarizing events. The importance of NMDAR-mediated long-lasting depolarization without somatic spiking in the generation of LTP has also recently been demonstrated in vivo (Gambino et al., 2014).

Dendritic recordings are very difficult to obtain in vivo, limiting our predictions to in vitro data. With the development of microendoscopes allowing dendritic calcium imaging in awake behaving mice, it might be interesting to see in the future, once data are available, if experimental calcium changes can predict plasticity in more physiological conditions.

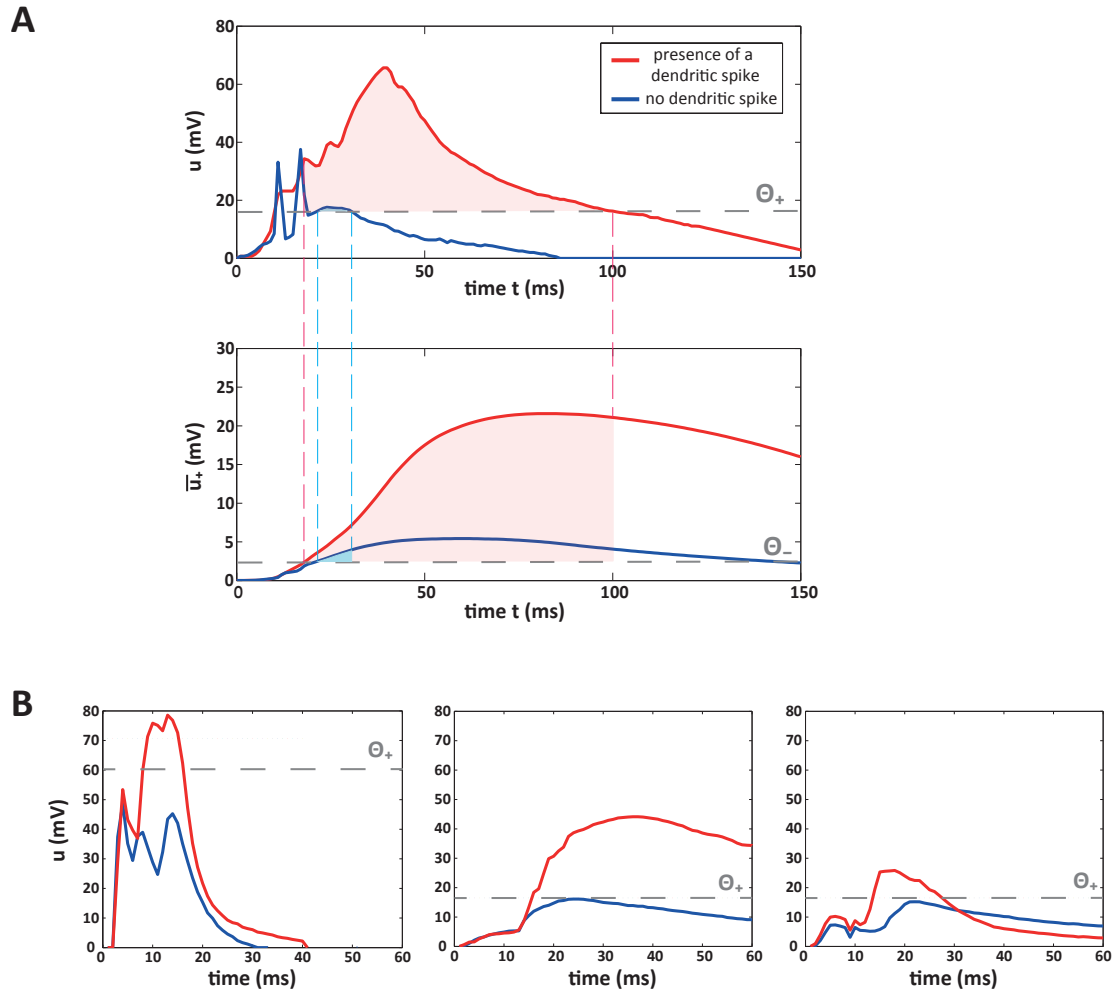


Figure 7.5: Necessity of dendritic spikes for the induction of LTP using different experimental protocols. A) The combination of u and $\bar{u}_+(t)$ reaching their respective threshold Θ_+ and Θ_- (dotted lines) determines the synaptic weight change (STDP protocol, Brandalise et al.). Red trace: presence of a dendritic spike ; blue trace: no dendritic spike. B) u exceeding the threshold Θ_+ is sufficient to detect the dendritic spike (left : Letzkus et al., middle and right : recordings from two different neurons during the subthreshold protocol in Brandalise et al. and courtesy of F.Brandalise)

Part V

Conclusion

Pairing an odor with an aversive stimuli resulted in the subsequent processing of this odor to produce a fear response rather than exploratory behavior. This reflects latent changes in the representation of this odor in the brain: an olfactory memory trace of the association emerged. The PC, a subdivision of the olfactory system, seems to be a good candidate for encoding olfactory memory traces for reasons highlighted in Chapter 2. I have described in Chapter 1 the characteristics of memory traces, from which one can extract two main criteria to assess if an ensemble of cells is part of a memory trace: -criteria #1: this ensemble contains all the information needed to retrieve the memory. -criteria #2: persistent changes in cellular or network properties of this ensemble occur following learning.

The TetTag system has been used extensively in studies of hippocampal memory traces, see Chapter 1. As the PC is a large area, I combined the TetTag system with DREADDs to test the functional relevance of the PC in memory formation and retrieval (see Chapter 3 for Material and Methods and Chapter 4 for Results). I first generated a tetO-hM4Di adenoassociated virus, and verified that piriform neuronal activity could be manipulated with DREADDs. Chemogenetically reactivating piriform neurons that were active during fear conditioning lead to memory retrieval in the absence of the conditioned odor. Conversely, inactivating these neurons impaired memory retrieval when the conditioned odor was presented alone. Furthermore, these memory deficits were specific to the conditioned odor. These results indicate that criteria #1 for finding memory traces is fulfilled. "Odor memory cells" can now be labeled, and this opens a range of new horizons in understanding the mechanisms of odor coding and memory. I have presented in Chapter 6 a possible follow-up line of research which also test criteria #2: the increased connectivity strength within a group of piriform neurons, enabled via a neuromodulatory signal, would result in the emergence of a stable representation of the conditioned odor, forming a neural correlate of the olfactory memory trace.

It should be noted that the choice of the four odors used throughout our study was pseudo-random. I picked these odors from a set of monomolecular odorants used in our laboratory and which activated a similar number of piriform neurons (in vivo two-photon Ca^{2+} imaging in anesthetized mice, B. Roland). I also checked that odors did not elicit an innate behavioral response by visually inspecting the behavior of the mice and quantifying the amount of time spent near the odor port when the odors were presented for the first time (data not shown, see also Kobayakawa et al., 2007; Root et al, 2014 for behavioral assays characterizing the innate valence of odors). It could be worthwhile replicating our findings using another set of odorants, especially that overlap between patterns of activity evoked by different odorants has now been quantified (Roland et al., 2017; see section 4.4).

I have presented in Chapter 1 the advantages in studying fear memories. I adopted a fear conditioning paradigm relying on the presentation of three odors, from which only one is paired with foot shock. Behavioral responses and training-induced changes in piriform odor responses differ from single-CS fear conditioning paradigm (Chen et al., 2011). It has been suggested that discriminating between odors with different valences presumably involves higher brain areas, which is one of the reason for choosing this paradigm. It would be interesting to see if the PC is needed

for "simpler" fear conditioning paradigm, and extend our findings to other types of learning (appetitive, social...).

I have highlighted some technical limitations of the TetTag system. Among others, the TetTag system seems to capture a non-negligible number of neurons which are not activated by the learning experience. I thus characterized a more recent transgenic mouse line which relies on an inducible recombinase, the TRAP system. I have shown that odor stimuli can induce significant labeling of neurons above background levels, but that inactivating neurons that were active during fear conditioning did not impair memory retrieval. However, as discussed in Chapter 6, memory retrieval was tested more remotely than with the TetTag system and other technical limitations of the TRAP system could explain this negative result.

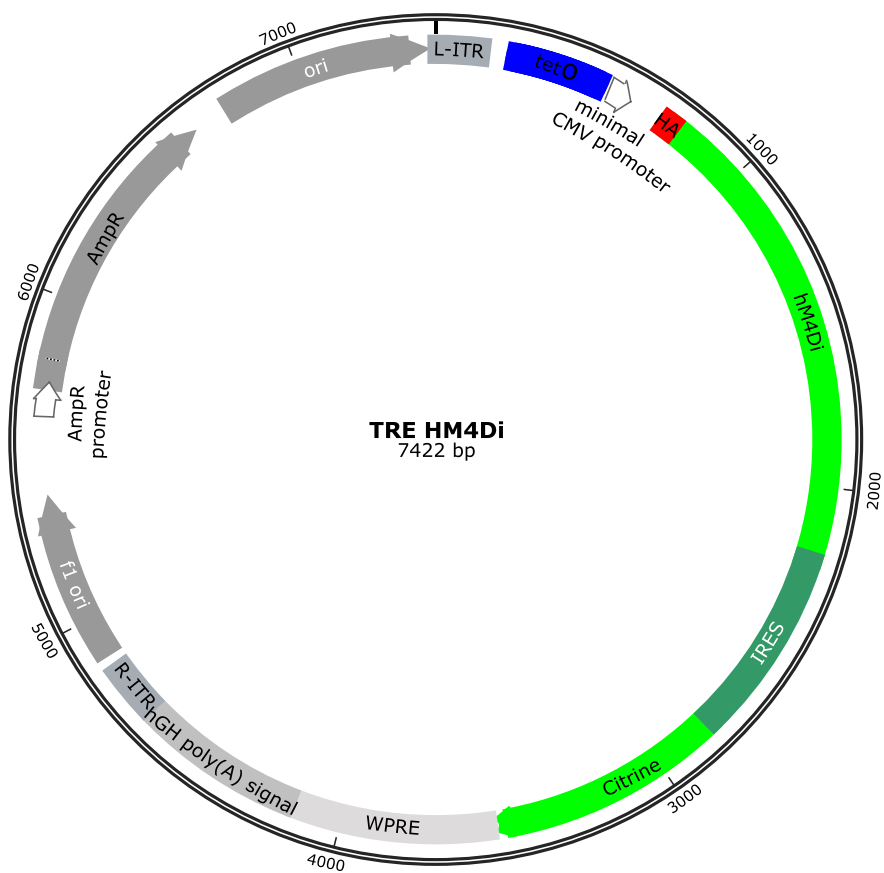
In both the TRAP and TetTag systems, DREADDs expression is under the control of the activity-dependent *cfos* promoter. Nevertheless the precise relationship between neuronal activity and Fos expression, as well as the role of Fos in memory formation remains to be elucidated. Thus, it seems essential to combine our findings with other methods of investigations. As an example, the recent development of *in vivo* Ca²⁺ imaging in awake behaving mice using miniature microscopy (Ghosh et al., 2011) will allow to follow live the formation of memories. Computational modeling can also help generating or testing predictions. I have illustrated this in Chapter 7: a voltage-based model of synaptic plasticity captures the important, recently emerging role played by dendritic spikes for the induction of LTP.

The results of my PhD work have important implications: put into perspective with findings on other types of memories in other brain regions, they will shed new light on the mechanisms underlying different memory processes. My findings could also have a potential valuable clinical impact, by providing a novel and powerful experimental model to study memory loss in Alzheimer disease, which prevalence is high and continues to increase. Indeed, olfactory deficits are one early symptom of this disease and strongly predict disease progression (Murphy, 1999). As a consequence, odor identification and memory tests are being developed as diagnostic tools, due to their non-invasiveness and affordable cost (Albers et al., 2016). Furthermore, piriform activity patterns have been shown to be disrupted in patients with Alzheimer's disease (Li et al., 2010). Combining "odor memory cells" labeling tools with mouse models of Alzheimer disease could help better understand the neural mechanisms underlying olfactory dysfunctions in this disease.

Part VI
Appendices

Appendix A:

Plasmid map of AAV-tetO-HA-hM4Di-IRES-mCitrine

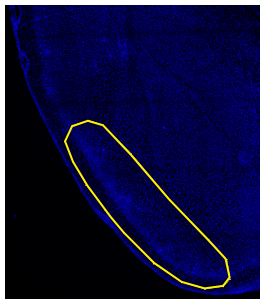


Appendix B: Automated cell counting

The reader is referred to Chapter 3. Z-projected images are shown, unless otherwise stated

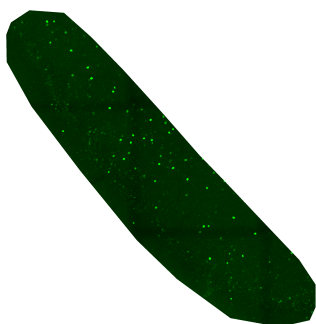
EXAMPLE 1: cfos-tTA mouse injected with AAV-tetO-hM3Dq-mCherry, endogenous fos 1 hour after CNO injection (open field, section 4.6)

Delineate PC

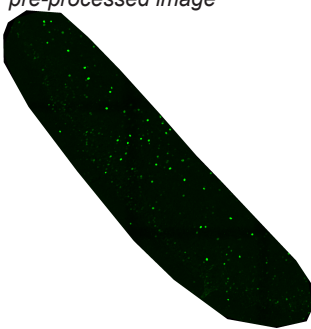


Nuclear staining (Fos)

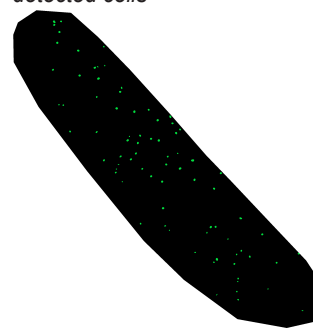
original image



pre-processed image



detected cells



Soma staining (mCherry)

original image



pre-processed image

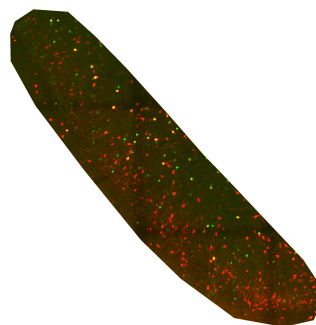


detected cells

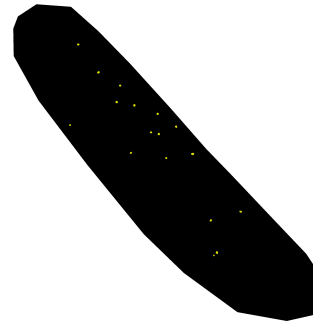


Overlap between the two previous images

original images



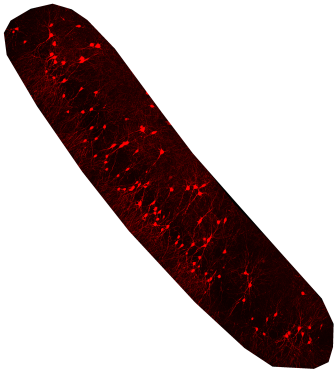
detected co-labeled cells



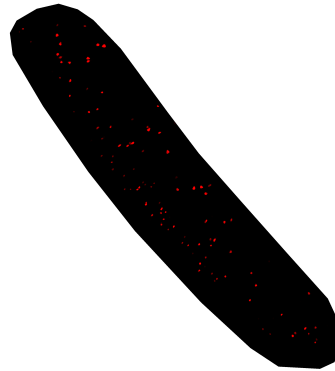
EXAMPLE 2: fosCreER-tdTomato mouse (chapter 6)

Soma+Fibers (tdtomato)

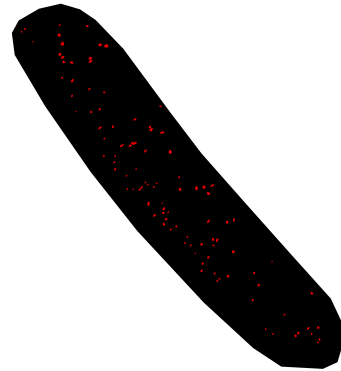
original image



pre-processed image

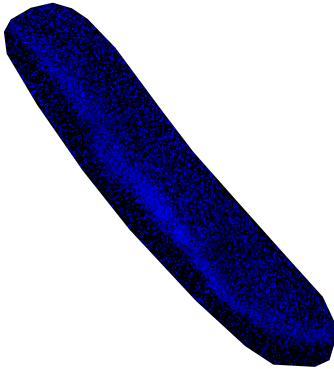


detected cells



NeuroTrace

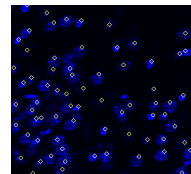
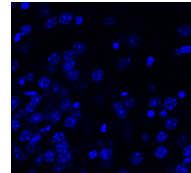
original image



one point per maximum



zoom of one slice



*yellow points:
local maximum*

Appendix C: Matlab code

The reader is referred to Chapter 3.

First step: ROI definition and stimuli onset definition

```
num_vid_toanal=input('How many videos to analyze?');
[num,filetoread,raw] = xlsread('videos1.xlsx');

for analis=1:num_vid_toanal

    filecell=filetoread(analis);
    filestring=filecell{1};
    vidObj = VideoReader(filestring); %read video
    filename=vidObj.Name;
    nombrestimuli=input('nombre de stimuli');
    [pathstr,namefich,ext] = fileparts(filename) ;

    mkdir(namefich);

    %% define ROI and scale box
    s(1).cdata=read(vidObj,4000);
    figure(2)
    image(s(1).cdata)
    rect=imrect;
    % wait for key pressed
    pause('on');
    pause;
    xy = rect.getPosition; %[xmin ymin width height].

    pos=[xy(1), xy(2)+xy(4)/2;xy(1)+xy(3),xy(2)+xy(4)];
    width=xy(3);
    height=xy(4);
    if pos(2,2)>pos(1,2)
        middle=[pos(2,1)-((pos(2,1)-pos(1,1))/2);pos(2,2)-(abs(pos(2,2)-pos(1,2))/2)];
    elseif pos(2,2)<pos(1,2)
        middle=[pos(2,1)-((pos(2,1)-pos(1,1))/2);pos(1,2)-(abs(pos(2,2)-pos(1,2))/2)];
    end

    yext=[xy(2) xy(2)+xy(4)];
    yext=sort(yext);

    %% define stimuli onset
    [d,sr] = audioread(filestring);

    num_stim=1;
    figure(1)
    specgram(d(:,1),1024,sr);
    data={};

    while num_stim<nombrestimuli+1
        dcmObj=datacursormode
            pause
        data{num_stim} = getCursorInfo(dcmObj);
        num_stim=num_stim+1;
    end

    cd(namefich);
    save(namefich,'middle', 'width','data','namefich','nombrestimuli','yext')
    cd ../
    clear middle pos width data namefich nombrestimuli filename
end
```

Second step: compute background, subtract background, detect mouse, estimate its centroid, and plot its position and velocity

```

num_vid_toanal=input('How many videos to analyze? ');
[num,filetoread,raw] = xlsread('videos1.xlsx');

for analis=1:num_vid_toanal
    %% import video
    filecell=filetoread(analis);
    filestring=filecell{1};
    vidObj = VideoReader(filestring);
    filename=vidObj.Name;
    numFrames=vidObj.NumberOfFrames;
    temps=vidObj.Duration; %en s
    [pathstr,namefich,ext] = fileparts(filename);

    cd(namefich)
    load(strcat(namefich, '.mat'))
    % scale box
    boxlength=57; % in cm

    vidHeight=vidObj.Height;
    vidWidth=vidObj.Width;

    s=struct('cdata',zeros(vidHeight,vidWidth,3,'uint8')); %color matrice, image 8 bits

    absnumFramespersecond=vidObj.FrameRate %FrameRate
    numFramespersecondtoconsider=0.5; % (1 frame every 2 seconds for global analysis)
    saut=floor(absnumFramespersecond/numFramespersecondtoconsider+0.0001)
    relnumFramespersecond=absnumFramespersecond/saut;
    tbetwframes=saut/absnumFramespersecond %must be equal to 0.5 if
    numFramespersecondtoconsider=0.5 and FrameRate=25

    k=numFrames;
    indtab=numFrames*30/temps;
    fram=1;

    while indtab<=k
        s(fram).cdata=read(vidObj,indtab);
        indtab=indtab+saut;
        fram=fram+1;
    end
    fram=fram-1;

    %% compute background

    %median value
    % to calculate background, consider just first 3 minutes
    cinq=numFramespersecondtoconsider*180;

    for he=1:vidHeight
        for we=1:vidWidth
            for ind=1:cinq %number of frames
                concat(ind,:)=s(ind).cdata(he,we,:);
            end

            background(he,we,:)=median(concat,1);
            clear concat
        end
        waitbar(he/vidHeight)
    end

    %% background subtraction and object detection

    t=struct('subtrac',zeros(vidHeight,vidWidth,3,'uint8'));

    for ind=1:fram %number of frames
        %threshold

```

```

        t(ind).subtrac=background-s(ind).cdata>40*ones(vidHeight,vidWidth,3); %40 black
mouse on white floor (20 for white mouse)
        t(ind).subtrac(t(ind).subtrac==1)=255;
        v = regionprops(t(ind).subtrac, 'all');
        souris=0;
        nombsup=0;
        %constraints
        for cherch=1:length(v)
            dimens=length(v(cherch).BoundingBox);
            if v(cherch).Area>5000 && v(cherch).BoundingBox(dimens/2+1)<1000 &&
v(cherch).Centroid(2)>yext(1) && v(cherch).Centroid(2)<yext(2)
                souris=cherch;
                nombsup=nombsup+1;
            end
        end
        %centroid
        if souris==0 || nombsup~=1 %manual detection
            image(s(ind).cdata)
            dcmObj=datacursormode
            pause
            prov = getCursorInfo(dcmObj);
            clf
            centroids(ind,1) = prov.Position(1);
            centroids(ind,2) = prov.Position(2);
        else
            centroids(ind,:) = cat(1, v(souris).Centroid);
        end
        clear v souris prov
    end

figure(3)
image(background)
saveas(gcf, strcat('bground', namefich), 'png')

%% compute position of mice (left or right side)
posit=zeros(fram,1);

for ind=1:fram
    if centroids(ind,1)>middle(1)
        posit(ind,1)=1; % left=1;
    else
        posit(ind,1)=0; % right=0;
    end
end

%% compute velocity of mice
delta=zeros(fram,1);
veloc=zeros(fram,1);

for ind=1:fram-1
    delta(ind,:)=(centroids(ind+1,:)-centroids(ind,:))*boxlength/width;
    veloc(ind)=sqrt(delta(ind,1)^2/tbetwframes^2+delta(ind,2)^2/tbetwframes^2);
end

%% plots, whole session

figure(5)
% Mouse localization in the box
ax1=subplot(2,1,2);
imagesc(posit)
colormap(ax1, jet)

```

```

% Velocity profile
maxv=max(veloc);
subplot(2,1,1)
xlim([0 length(veloc)])
plot(veloc)
for ks=1:nombrestimuli
    hold on
    line([time_f(ks) time_f(ks)],[0 maxv],'Color',[1 0 0])
end

saveas(gcf,strcat('profildevitesse',namefich),'png')
saveas(gcf,strcat('profildevitesse',namefich),'fig')

for extr=1:nombrestimuli
    timetoplot(extr)=data{extr}.Position(1)-30; % temps 0 =1
    time_f(extr)=round(timetoplot(extr)/tbetwframes);
end

% save mat file
save(strcat(namefich,'_background'),'background','-v7.3') ;
save(strcat(namefich,'_global'),'veloc','posit','s','timetoplot','t','centroids','-v7.3') ;
save(strcat(namefich,'_param_global'),'posit_compart','vitesse moy','vitesse med','tempsg_auche','temps droite','-v7.3') ;

clear s centroids background concat middle posit veloc t timetoplot
cd ../
close(h)
close all
end

```

Third step: in case of odor stimuli, define a time-window around the stimulus. Then, subtract background, detect mouse, estimate its centroid, and extract its position and velocity

```

num_vid_toanal=input('How many videos to analyze? ');
timewindow=input('time window?');
[num,filetoread,row] = xlsread('videos1.xlsx');

for analis=1:num_vid_toanal
    %% import video
    filecell=filetoread(analis);
    filestring=filecell{1};
    vidObj = VideoReader(filestring);
    %%vidObj properties
    filename=vidObj.Name;
    numFrames=vidObj.NumberOfFrames;
    vidHeight=vidObj.Height;
    vidWidth=vidObj.Width;
    absnumFramespersecond=vidObj.FrameRate;

    temps=vidObj.Duration; %in seconds

    [pathstr,namefich,ext] = fileparts(filename);
    cd(namefich)
    load(strcat(namefich,'.mat'))
    load(strcat(namefich,'_background.mat'))
    load(strcat(namefich,'_param_global.mat'))

    s_stim=struct('cdata',zeros(vidHeight,vidWidth,3,'uint8')); %color matrice, image 8
bits
    t_stim=struct('subtrac',zeros(vidHeight,vidWidth,3,'uint8'));

    h = waitbar(0,'Please wait...');

    if absnumFramespersecond==25
        numFramespersecondtoconsider=5;
    else
        disp('error')
    end

    saut_s=floor(absnumFramespersecond/numFramespersecondtoconsider); %must be an
integer
    relnumFramespersecond=absnumFramespersecond/saut_s;
    tbetwframes_s=saut_s/absnumFramespersecond; %must be equal to 0.2

    boxlength=57;

    fram_s=1;
    for extr=1:nombrestimuli
        timepoint(extr)=round(data{extr}.Position(1)*numFrames/temps)+1;

        iti=timewindow*numFrames/temps; % extract 10 s before, and 10 s after odor
stimulation if timewindow=10
        indtab=timepoint(extr)-iti;

        while indtab<=timepoint(extr)+iti
            s_stim(fram_s).cdata=read(vidObj,indtab);
            indtab=indtab+saut_s;
            fram_s=fram_s+1;
        end
        waitbar(extr/nombrestimuli)
    end

    fram_s=fram_s-1;
    fram_stim=fram_s/nombrestimuli;
    stim_pres=ceil(fram_stim/2);

    %% background subtraction and object detection

```

```

for ind=1:fram_s %number of frames
t_stim(ind).subtrac=background-s_stim(ind).cdata>40*ones(vidHeight,vidWidth,3);
t_stim(ind).subtrac(t_stim(ind).subtrac==1)=255;
v = regionprops(t_stim(ind).subtrac, 'all');
souris=0;
nombsup=0;
for cherch=1:length(v)
dimens=length(v(cherch).BoundingBox);
if v(cherch).Area>5000 && v(cherch).BoundingBox(dimens/2+1)<1000 &&
v(cherch).Centroid(2)>yext(1) && v(cherch).Centroid(2)<yext(2)
souris=cherch;
nombsup=nombsup+1;
end
end
if souris==0 || nombsup~=1;
image(s_stim(ind).cdata)
dcmObj=datacursormode
%
set(dcmObj,'DisplayStyle','datatip','SnapToDataVertex','on','Enable','on')
pause
prov = getCursorInfo(dcmObj);
clf
centroids_stim(ind,1) = prov.Position(1);
centroids_stim(ind,2) = prov.Position(2);
else
centroids_stim(ind,:) = cat(1, v(souris).Centroid(1:2));
end
clear v souris prov
waitbar(ind/fram_s)

end

posit_stim=zeros(fram_s,1);

for ind=1:fram_s
if centroids_stim(ind,1)>middle(1)
posit_stim(ind,1)=1; % left=1;
else
posit_stim(ind,1)=0; % right=0;
end
end

%% compute velocity of mice

veloc_stim=zeros(fram_s,1);
accel_stim=zeros(fram_s,1);
posit_nose=zeros(nombrestimuli,1);
kn=1;

for ind=1:fram_s-2
delta(ind,:)=abs(centroids_stim(ind+1,:)-
centroids_stim(ind,:))*boxlength/width;

veloc_stim(ind)=sqrt(delta(ind,1)^2/tbetwframes_s^2+delta(ind,2)^2/tbetwframes_s^2);
veloc_stim_x(ind)=delta(ind,1)/tbetwframes_s; %velocity along the x-axis
v_delta(ind,:)=((centroids_stim(ind+2,:)-
centroids_stim(ind+1,:))*boxlength/width)/tbetwframes_s-delta(ind,:)/tbetwframes_s;

accel_stim(ind)=sqrt(v_delta(ind,1)^2/tbetwframes_s^2+v_delta(ind,2)^2/tbetwframes_s^2)
;
if ind==fram_stim || ind==fram_stim*2 || ind==fram_stim*3 || ind==fram_stim*4
|| ind==fram_stim*5 || ind==fram_stim*6 || ind==fram_stim*7 || ind==fram_stim*8
veloc_stim(ind)=0;
veloc_stim_x(ind)=0;
accel_stim(ind)=0;
end
end

```

```

        end

    end

    %% extract parameters before/after odor stimuli

    maxvitesse_bef=zeros(nombrestimuli,1);
    maxvitesse_bef_x=zeros(nombrestimuli,1);
    maxvitesse_aft=zeros(nombrestimuli,1);
    maxvitesse_aft_x=zeros(nombrestimuli,1);

    timepoint=timepoint';

    for extr=1:nombrestimuli

        framiti=1;
        vitesse_bef=veloc_stim(fram_stim*(extr-1)+1:fram_stim*(extr-1)+stim_pres-1);
        vitesse_bef_x=veloc_stim(fram_stim*(extr-1)+1:fram_stim*(extr-1)+stim_pres-1);
        accel_bef=accel_stim(fram_stim*(extr-1)+1:fram_stim*(extr-1)+stim_pres-1);
        maxvitesse_bef(extr)=max(vitesse_bef);
        maxvitesse_bef_x(extr)=max(vitesse_bef_x);

        vitesse_aft=veloc_stim(fram_stim*(extr-1)+stim_pres+1:fram_stim*extr-2);
        vitesse_aft_x=veloc_stim(fram_stim*(extr-1)+stim_pres+1:fram_stim*extr-2);
        accel_aft=accel_stim(fram_stim*(extr-1)+stim_pres+1:fram_stim*extr-2);
        maxvitesse_aft(extr)=max(vitesse_aft);
        maxvitesse_aft_x(extr)=max(vitesse_aft_x);

    end

    raw_posit=zeros(nombrestimuli,stim_pres-1); %position along x-axis

    for extr=1:nombrestimuli
        k=1;
        if centroids_stim(fram_stim*(extr-1)+stim_pres,1)>middle(1)
            ref=middle(1)+width/2;
        elseif centroids_stim(fram_stim*(extr-1)+stim_pres,1)<middle(1)
            ref=middle(1)-width/2;
        else
            disp('erreur');
        end

        for it=1:stim_pres-1
            raw_posit(extr,k)=100*abs(ref-centroids_stim(fram_stim*(extr-
1)+stim_pres+it,1))/width;
            k=k+1;
        end

    end

    %%save in excel file
    xlswrite(strcat(namefich,'_odor'),[maxvitesse_bef maxvitesse_aft maxvitesse_bef_x
maxvitesse_aft_x max_accel_bef max_accel_aft timepoint])

    save(strcat(namefich,'_odor'),'veloc_stim','rawposit','vitesse_bef','vitesse_aft','vite
sse_bef_x','vitesse_aft_x','fram_stim','posit_stim','s_stim',
't_stim','centroids_stim','-v7.3') ;
    clear veloc_stim fram_stim posit_stim s_stim t_stim centroids_stim vitesse_bef
vitesse_aft maxvitesse_bef maxvitesse_aft max_accel_bef max_accel_aft timepoint delta
v_delta
    close all
    cd ../

end

```

Part VII

Bibliography

CHAPTERS 1-6

Adolphs, R. (2013). The Biology of Fear. *Current Biology*, 23(2), R79–R93.

<https://doi.org/10.1016/j.cub.2012.11.055>

Albers, A. D., Asafu-Adjei, J., Delaney, M. K., Kelly, K. E., Gomez-Isla, T., Blacker, D., ... Albers, M. W. (2016). Episodic memory of odors stratifies Alzheimer biomarkers in normal elderly: POEM: Odor Memory Biomarker in Normal Elderly. *Annals of Neurology*, 80(6), 846–857.

<https://doi.org/10.1002/ana.24792>

Alexander, G. M., Rogan, S. C., Abbas, A. I., Armbruster, B. N., Pei, Y., Allen, J. A., ... Roth, B. L. (2009). Remote Control of Neuronal Activity in Transgenic Mice Expressing Evolved G Protein-Coupled Receptors. *Neuron*, 63(1), 27–39. <https://doi.org/10.1016/j.neuron.2009.06.014>

Anagnostaras, S. G., Maren, S., Sage, J. R., Goodrich, S., & Fanselow, M. S. (1999). Scopolamine and Pavlovian fear conditioning in rats: dose-effect analysis. *Neuropsychopharmacology*, 21(6), 731–744.

Apicella, A., Yuan, Q., Scanziani, M., & Isaacson, J. S. (2010). Pyramidal Cells in Piriform Cortex Receive Convergent Input from Distinct Olfactory Bulb Glomeruli. *Journal of Neuroscience*, 30(42), 14255–14260. <https://doi.org/10.1523/JNEUROSCI.2747-10.2010>

Armbruster, B. N., Li, X., Pausch, M. H., Herlitze, S., & Roth, B. L. (2007). Evolving the lock to fit the key to create a family of G protein-coupled receptors potently activated by an inert ligand. *Proceedings of the National Academy of Sciences*, 104(12), 5163–5168.

Attwell, D., Buchan, A. M., Charpak, S., Lauritzen, M., MacVicar, B. A., & Newman, E. A. (2010). Glial and neuronal control of brain blood flow. *Nature*, 468(7321), 232–243. <https://doi.org/10.1038/nature09613>

Auffarth, B. (2013). Understanding smell—The olfactory stimulus problem. *Neuroscience & Biobehavioral Reviews*, 37(8), 1667–1679. <https://doi.org/10.1016/j.neubiorev.2013.06.009>

Bailey KR, Crawley JN. Anxiety-Related Behaviors in Mice. (2009) In: Buccafusco JJ, editor. *Methods of Behavior Analysis in Neuroscience*. 2nd edition. Boca Raton (FL): CRC Press/Taylor & Francis; Chapter 5.

Barnett SA. (2009) *The Rat. A study in behavior* New Brunswick and London: Aldine Transaction.

Barnes, D. C., Chapuis, J., Chaudhury, D., & Wilson, D. A. (2011). Odor Fear Conditioning Modifies Piriform Cortex Local Field Potentials Both during Conditioning and during Post-Conditioning Sleep. *PLoS ONE*, 6(3), e18130. <https://doi.org/10.1371/journal.pone.0018130>

- Bekkers, J. M., & Suzuki, N. (2013). Neurons and circuits for odor processing in the piriform cortex. *Trends in Neurosciences*, 36(7), 429–438. <https://doi.org/10.1016/j.tins.2013.04.005>
- Ben-Yakov, A., Dudai, Y., & Mayford, M. R. (2015). Memory Retrieval in Mice and Men. *Cold Spring Harbor Perspectives in Biology*, a021790. <https://doi.org/10.1101/cshperspect.a021790>
- Blair, H. T. (2001). Synaptic Plasticity in the Lateral Amygdala: A Cellular Hypothesis of Fear Conditioning. *Learning & Memory*, 8(5), 229–242. <https://doi.org/10.1101/lm.30901>
- Bergstrom, H. C. (2016). The neurocircuitry of remote cued fear memory. *Neuroscience & Biobehavioral Reviews*, 71, 409–417. <https://doi.org/10.1016/j.neubiorev.2016.09.028>
- Bliss, T. V., & Lømo, T. (1973). Long-lasting potentiation of synaptic transmission in the dentate area of the anaesthetized rabbit following stimulation of the perforant path. *The Journal of Physiology*, 232(2), 331–356.
- Bolding, K.A. & Franks, K.M. (2017). Complementary codes for odor identity and intensity in olfactory cortex. *eLife*, 6: e22630 <https://doi.org/10.7554/eLife.22630.001>
- Bouret, S. & Sara, S.J.(2002) Locus coeruleus activation modulates firing rate and temporal organization of odour-induced single-cell responses in rat piriform cortex *Eur. J. Neurosci.*, 16 , pp. 2371-2382
- Branco, T., & Staras, K. (2009). The probability of neurotransmitter release: variability and feedback control at single synapses. *Nature Reviews. Neuroscience*, 10(5), 373.
- Chapuis, J., & Wilson, D. A. (2011). Bidirectional plasticity of cortical pattern recognition and behavioral sensory acuity. *Nature Neuroscience*, 15(1), 155–161. <https://doi.org/10.1038/nn.2966>
- Chapuis, J., & Wilson, D. A. (2013a). Cholinergic modulation of olfactory pattern separation. *Neuroscience Letters*, 545, 50–53. <https://doi.org/10.1016/j.neulet.2013.04.015>
- Chapuis, J., Cohen, Y., He, X., Zhang, Z., Jin, S., Xu, F., & Wilson, D. A. (2013b). Lateral Entorhinal Modulation of Piriform Cortical Activity and Fine Odor Discrimination. *Journal of Neuroscience*, 33(33), 13449–13459. <https://doi.org/10.1523/JNEUROSCI.1387-13.2013>
- Chen, C.-F. F., Barnes, D. C., & Wilson, D. A. (2011). Generalized vs. stimulus-specific learned fear differentially modifies stimulus encoding in primary sensory cortex of awake rats. *Journal of Neurophysiology*, 106(6), 3136–3144. <https://doi.org/10.1152/jn.00721.2011>
- Chen, Chien-Fu F., Zou, D.-J., Altomare, C. G., Xu, L., Greer, C. A., & Firestein, S. J. (2014). Nonsensory target-dependent organization of piriform cortex. *Proceedings of the National Academy of Sciences*, 111(47), 16931–16936.
- Choi, G. B., Stettler, D. D., Kallman, B. R., Bhaskar, S. T., Fleischmann, A., & Axel, R. (2011).

Driving Opposing Behaviors with Ensembles of Piriform Neurons. *Cell*, 146(6), 1004–1015. <https://doi.org/10.1016/j.cell.2011.07.041>

Chu, S., and Downes, J.J. (2000). Odour-evoked autobiographical memories: psychological investigations of Proustian phenomena. *Chem. Senses* 25, 111–116.

Cole, A. J., Saffen, D. W., Baraban, I. & Worley, P. F. (1989) Rapid increase of an immediate-early gene messenger RNA in hippocampal neurons by synaptic NMDA receptor activation. *Nature*, 340, 474-476.

Counet, C., Callemien, D., Ouwerx, C., & Collin, S. (2002). Use of Gas Chromatography-Olfactometry To Identify Key Odorant Compounds in Dark Chocolate. Comparison of Samples before and after Conching. *Journal of Agricultural and Food Chemistry*, 50(8), 2385-2391. <https://doi.org/10.1021/jf0114177>

Cowansage, K. K., Shuman, T., Dillingham, B. C., Chang, A., Golshani, P., & Mayford, M. (2014). Direct Reactivation of a Coherent Neocortical Memory of Context. *Neuron*, 84(2), 432–441. <https://doi.org/10.1016/j.neuron.2014.09.022>

Curran, T. & Verma, I.M. (1984). FBR murine osteosarcoma virus. I. Molecular analysis and characterization of a 75,000-Da gag-fos fusion product. *Virology* 135, 218-228.

Datiche, F., & Cattarelli, M. (1996). Catecholamine innervation of the piriform cortex: a tracing and immunohistochemical study in the rat. *BrainRes.* 710, 69–78.

Datiche, F., Rouillet, F., & Cattarelli, M. (2001). Expression of Fos in the piriform cortex after acquisition of olfactory learning: an immunohistochemical study in the rat. *Brain Research Bulletin*, 55(1), 95–99.

Davis, R. L. (2004). Olfactory learning. *Neuron*, 44(1), 31–48.

DeBose, J.L., Nevitt, G.A., 2008. The use of odors at different spatial scales: comparing birds with fish. *Journal of Chemical Ecology* 34 (July (7)), 867–881.

De Rosa, E., & Hasselmo, M. E. (2000). Muscarinic cholinergic neuromodulation reduces proactive interference between stored odor memories during associative learning in rats. *Behavioral Neuroscience*, 114(1), 32–41. <https://doi.org/10.1037//0735-7044.114.1.32>

Deisseroth, K. (2011). Optogenetics. *Nature Methods*, 8(1), 26–29. <https://doi.org/10.1038/nmeth.f.324>

Denny, C. A., Kheirbek, M. A., Alba, E. L., Tanaka, K. F., Brachman, R. A., Laughman, K. B., ... Hen, R. (2014). Hippocampal Memory Traces Are Differentially Modulated by Experience, Time, and Adult Neurogenesis. *Neuron*, 83(1), 189–201. <https://doi.org/10.1016/j.neuron.2014.05.018>

Diodato, A., Ruinart de Brimont, M., Yim, Y. S., Derian, N., Perrin, S., Pouch, J., ... Fleischmann, A. (2016). Molecular signatures of neural connectivity in the olfactory cortex. *Nature*

Communications, 7, 12238. <https://doi.org/10.1038/ncomms12238>

Dong, S., Allen, J. A., Farrell, M., & Roth, B. L. (2010). A chemical-genetic approach for precise spatio-temporal control of cellular signaling. *Molecular BioSystems*, 6(8), 1376.

<https://doi.org/10.1039/c002568m>

Dragunow M et Faull R. (1989). The use of c-fos as a metabolic marker in neuronal pathway tracing. *J Neurosci Methods* 29, 261-265.

Dudai, Y., Karni, A., & Born, J. (2015). The Consolidation and Transformation of Memory. *Neuron*, 88(1), 20–32. <https://doi.org/10.1016/j.neuron.2015.09.004>

Dudek, S. M., & Bear, M. F. (1993). Bidirectional long-term modification of synaptic effectiveness in the adult and immature hippocampus. *Journal of Neuroscience*, 13(7), 2910–2918.

Eichenbaum, H. (2000). A cortical-hippocampal system for declarative memory. *Nature Reviews. Neuroscience*, 1(1), 41.

Fadok, J. P., Dickerson, T. M. K., & Palmiter, R. D. (2009). Dopamine Is Necessary for Cue-Dependent Fear Conditioning. *Journal of Neuroscience*, 29(36), 11089–11097. <https://doi.org/10.1523/JNEUROSCI.1616-09.2009>

Ferguson, S. M., Eskenazi, D., Ishikawa, M., Wanat, M. J., Phillips, P. E. M., Dong, Y., ... Neumaier, J. F. (2011). Transient neuronal inhibition reveals opposing roles of indirect and direct pathways in sensitization. *Nature Neuroscience*, 14(1), 22–24. <https://doi.org/10.1038/nn.2703>

Fields, R. D., Eshete, F., Stevens, B., & Itoh, K. (1997). Action potential-dependent regulation of gene expression: temporal specificity in Ca²⁺, cAMP-responsive element binding proteins, and mitogen-activated protein kinase signaling. *Journal of Neuroscience*, 17(19), 7252–7266.

Fleischmann, A., Hvalby, O., Jensen, V., Strekalova, T., Zacher, C., Layer, L. E., ... others. (2003). Impaired long-term memory and NR2A-type NMDA receptor-dependent synaptic plasticity in mice lacking c-Fos in the CNS. *Journal of Neuroscience*, 23(27), 9116–9122.

Fletcher, M. L. (2012). Olfactory aversive conditioning alters olfactory bulb mitral/ tufted cell glomerular odor responses. *Frontiers in Systems Neuroscience*, 6. <https://doi.org/10.3389/fnsys.2012.00016>

Franks, K. M., Russo, M. J., Sosulski, D. L., Mulligan, A. A., Siegelbaum, S. A., & Axel, R. (2011). Recurrent Circuitry Dynamically Shapes the Activation of Piriform Cortex. *Neuron*, 72(1), 49–56. <https://doi.org/10.1016/j.neuron.2011.08.020>

Gale, G. D. (2004). Role of the Basolateral Amygdala in the Storage of Fear Memories across the Adult Lifetime of Rats. *Journal of Neuroscience*, 24(15), 3810–3815. <https://doi.org/10.1523/JNEUROSCI.4100-03.2004>

Gale, Greg D., Anagnostaras, S. G., & Fanselow, M. S. (2001). Cholinergic modulation of pavlo-

vian fear conditioning: effects of intrahippocampal scopolamine infusion. *Hippocampus*, 11(4), 371–376.

Garner, A. R., Rowland, D. C., Hwang, S. Y., Baumgaertel, K., Roth, B. L., Kentros, C., & Mayford, M. (2012). Generation of a Synthetic Memory Trace. *Science*, 335(6075), 1513–1516. <https://doi.org/10.1126/science.1214985>

Gdalyahu, A., Tring, E., Polack, P.-O., Gruver, R., Golshani, P., Fanselow, M. S., ... Trachtenberg, J. T. (2012). Associative Fear Learning Enhances Sparse Network Coding in Primary Sensory Cortex. *Neuron*, 75(1), 121–132. <https://doi.org/10.1016/j.neuron.2012.04.035>

Gellman, R.L., & Aghajanian, G.K. (1993). Pyramidal cells in piriform cortex receive a convergence of inputs from monoamine activated GABAergic interneurons. *BrainRes.* 600, 63–73.

Ghosh, S., Larson, S. D., Hefzi, H., Marnoy, Z., Cutforth, T., Dokka, K., & Baldwin, K. K. (2011). Sensory maps in the olfactory cortex defined by long-range viral tracing of single neurons. *Nature*, 472(7342), 217–220. <https://doi.org/10.1038/nature09945>

Giessel, A. J., & Datta, S. R. (2014). Olfactory maps, circuits and computations. *Current Opinion in Neurobiology*, 24, 120–132. <https://doi.org/10.1016/j.conb.2013.09.010>

Gore, F., Schwartz, E. C., Brangers, B. C., Aladi, S., Stujenske, J. M., Likhtik, E., ... Axel, R. (2015). Neural Representations of Unconditioned Stimuli in Basolateral Amygdala Mediate Innate and Learned Responses. *Cell*, 162(1), 134–145. <https://doi.org/10.1016/j.cell.2015.06.027>

Goshen, I., Brodsky, M., Prakash, R., Wallace, J., Gradinaru, V., Ramakrishnan, C., & Deisseroth, K. (2011). Dynamics of Retrieval Strategies for Remote Memories. *Cell*, 147(3), 678–689. <https://doi.org/10.1016/j.cell.2011.09.033>

Gottfried, J. A. (2010). Central mechanisms of odour object perception. *Nature Reviews Neuroscience*, 11(9), 628–641. <https://doi.org/10.1038/nrn2883>

Gourdon, H. C., & Lagrutta, A. A. (1988a). The primate hippocampal formation: evidence for a time-limited role in memory storage. *Biochim. Biophys. Acta*, 966, 84.

Grewe, B. F., Gründemann, J., Kitch, L. J., Lecoq, J. A., Parker, J. G., Marshall, J. D., ... Schnitzer, M. J. (2017). Neural ensemble dynamics underlying a long-term associative memory. *Nature*, 543(7647), 670–675. <https://doi.org/10.1038/nature21682>

Guenther, C. J., Miyamichi, K., Yang, H. H., Heller, H. C., & Luo, L. (2013). Permanent Genetic Access to Transiently Active Neurons via TRAP: Targeted Recombination in Active Populations. *Neuron*, 78(5), 773–784. <https://doi.org/10.1016/j.neuron.2013.03.025>

Guzowski, J. F. (2002). Insights into immediate-early gene function in hippocampal memory consolidation using antisense oligonucleotide and fluorescent imaging approaches. *Hippocampus*, 12(1), 86–104. <https://doi.org/10.1002/hipo.10010>

Guzowski, J. F., Timlin, J. A., Roysam, B., McNaughton, B. L., Worley, P. F., & Barnes, C. A. (2005). Mapping behaviorally relevant neural circuits with immediate-early gene expression. *Current Opinion in Neurobiology*, 15(5), 599–606. <https://doi.org/10.1016/j.conb.2005.08.018>

Haberly LB. (1985). Neuronal circuitry in olfactory cortex: anatomy and functional implications. *Chem Senses* 10, 219-238.

Haberly LB. (2001). Parallel-distributed processing in olfactory cortex: new insights from morphological and physiological analysis of neuronal circuitry. *Chem Senses* 26, 551-576.

Hagiwara, A., Pal, S. K., Sato, T. F., Wienisch, M., & Murthy, V. N. (2012). Optophysiological analysis of associational circuits in the olfactory cortex. *Frontiers in Neural Circuits*, 6. <https://doi.org/10.3389/fncir.2012.00018>

Hansson, B. S., & Stensmyr, M. C. (2011). Evolution of Insect Olfaction. *Neuron*, 72(5), 698–711. <https://doi.org/10.1016/j.neuron.2011.11.003>

Harris, J. A. (1998). Using c-fos as a neural marker of pain. *Brain Research Bulletin*, 45(1), 1–8.

Hasselmo, M. E., & Barkai, E. (1995a). Cholinergic modulation of activity-dependent synaptic plasticity in the piriform cortex and associative memory function in a network biophysical simulation. *Journal of Neuroscience*, 15(10), 6592–6604.

Hasselmo, M. E., Linster, C., Patil, M., Ma, D., & Cekic, M. (1997). Noradrenergic suppression of synaptic transmission may influence cortical signal-to-noise ratio. *Journal of Neurophysiology*, 77(6), 3326–3339.

Hebb, D.O. (1949). *The Organization of Behavior: A Neuropsychological Theory*. Wiley, ISBN 0805843000. <https://doi.org/10.2307/1418888>

Herdegen T et Leah JD. (1998). Inducible and constitutive transcription factors in the mammalian nervous system: control of gene expression by Jun, Fos and Krox, and CREB/ATF proteins. *Brain Res Brain Res Rev* 28, 370-490.

Herrera, D.G. & Robertson, H.A. (1996) Activation of c-fos in the brain. *Progress in Neurobiology*, Volume 50(2–3) 83-107. [https://doi.org/10.1016/S0301-0082\(96\)00021-4](https://doi.org/10.1016/S0301-0082(96)00021-4)

Herry, C., & Johansen, J. P. (2014). Encoding of fear learning and memory in distributed neuronal circuits. *Nature Neuroscience*, 17(12), 1644–1654. <https://doi.org/10.1038/nn.3869>

Illig, K. R., & Haberly, L. B. (2003). Odor-evoked activity is spatially distributed in piriform cortex. *The Journal of Comparative Neurology*, 457(4), 361–373. <https://doi.org/10.1002/cne.10557>

Jiang, L., Kundu, S., Lederman, J. D., López-Hernández, G. Y., Ballinger, E. C., Wang, S., ... Role, L. W. (2016). Cholinergic Signaling Controls Conditioned Fear Behaviors and Enhances Plasticity of Cortical-Amygdala Circuits. *Neuron*, 90(5), 1057–1070.

<https://doi.org/10.1016/j.neuron.2016.04.028>

Johansen, J. P., Diaz-Mataix, L., Hamanaka, H., Ozawa, T., Ycu, E., Koivumaa, J., ... LeDoux, J. E. (2014a). Hebbian and neuromodulatory mechanisms interact to trigger associative memory formation. *Proceedings of the National Academy of Sciences*, 111(51), E5584–E5592. <https://doi.org/10.1073/pnas.1421304111>

Johanning, F. W., Beed, P. S., Trimbuch, T., Bendels, M. H. K., Winterer, J., & Schmitz, D. (2009). Dendritic Compartment and Neuronal Output Mode Determine Pathway-Specific Long-Term Potentiation in the Piriform Cortex. *Journal of Neuroscience*, 29(43), 13649–13661. <https://doi.org/10.1523/JNEUROSCI.2672-09.2009>

Johnson, D. M., Illig, K. R., Behan, M., & Haberly, L. B. (2000). New features of connectivity in piriform cortex visualized by intracellular injection of pyramidal cells suggest that “primary” olfactory cortex functions like “association” cortex in other sensory systems. *Journal of Neuroscience*, 20(18), 6974–6982.

Jones, S. V., Choi, D. C., Davis, M., & Ressler, K. J. (2008). Learning-Dependent Structural Plasticity in the Adult Olfactory Pathway. *Journal of Neuroscience*, 28(49), 13106–13111. <https://doi.org/10.1523/JNEUROSCI.4465-08.2008> josselyn-et-al-2015.pdf. (n.d.).

Josh Huang, Z., & Zeng, H. (2013). Genetic Approaches to Neural Circuits in the Mouse. *Annual Review of Neuroscience*, 36(1), 183–215.

<https://doi.org/10.1146/annurev-neuro-062012-170307>

Josselyn, S. A., Köhler, S., & Frankland, P. W. (2015). Finding the engram. *Nature Reviews Neuroscience*, 16(9), 521–534. <https://doi.org/10.1038/nrn4000>

Kandel, E. R. & Tauc, L. (1964). Mechanism of prolonged heterosynaptic facilitation, *Nature*, 202, 145.

Kanter, E. D. & Haberly, L. B. (1993). Associative long-term potentiation in piriform cortex slices requires GABAA blockade. *Journal of Neuroscience*, 13(6), 2477–2482.

Kanter ED et Haberly LB. (1990). NMDA-dependent induction of long-term potentiation in afferent and association fiber systems of piriform cortex in vitro. *Brain Res* 525, 175-179.

Kass, M.D., Rosenthal, M.C., Pottackal, J., and McGann, J.P. (2013) Fear learning enhances neural responses to threat-predictive stimuli. *Science* 342:1389-92. <https://doi.org/10.1126/science.1244916>.

Kato, H.K., Chu, M.W., Isaacson, J.S., Komiyama, T., 2012. Dynamic sensory representations in the olfactory bulb: modulation by wakefulness and experience. *Neuron* 76, 962–75. <https://doi.org/10.1016/j.neuron.2012.09.037>

Kaupp, U. B. (2010). Olfactory signalling in vertebrates and insects: differences and commonalities. *Nature Reviews Neuroscience*. <https://doi.org/10.1038/nrn2789>

- Kentros, C. G., Agnihotri, N. T., Streater, S., Hawkins, R. D., & Kandel, E. R. (2004). Increased attention to spatial context increases both place field stability and spatial memory. *Neuron*, 42(2), 283–295.
- Kim, J.J. & Fanselow, M. S. (1992) Modality-specific retrograde amnesia of fear. *Science*, 256(5057): 675-677, <https://doi.org/10.1126/science.1585183>
- Kitamura, T., Ogawa, S. K., Roy, D. S., Okuyama, T., Morrissey, M. D., Smith, L. M., ... Tonegawa, S. (2017). Engrams and circuits crucial for systems consolidation of a memory. *Science*, 356(6333), 73–78.
- Kobayakawa, K., Kobayakawa, R., Matsumoto, H., Oka, Y., Imai, T., Ikawa, M., ... Sakano, H. (2007). Innate versus learned odour processing in the mouse olfactory bulb. *Nature*, 450(7169), 503–508. <https://doi.org/10.1038/nature06281>
- Kovacs, K.J. (1998) c-Fos as a transcription factor: a stressful (re)view from a functional map. *Neurochem Int* 33:287–297.
- Krashes, M. J., Koda, S., Ye, C., Rogan, S. C., Adams, A. C., Cusher, D. S., ... Lowell, B. B. (2011). Rapid, reversible activation of AgRP neurons drives feeding behavior in mice. *Journal of Clinical Investigation*, 121(4), 1424–1428. <https://doi.org/10.1172/JCI46229>
- Krettek J.E. & Price J.L. (1978) Amygdaloid projections to subcortical structures within the basal forebrain and brainstem in the rat and cat *J. Comp. Neurol.*, 178:225-254
- Larsson, M., & Willander, J., 2009. Autobiographical odor memory. *Annals of the New York Academy of Sciences*, 1170, 318–323.
- Lashley, K. S. (1929). *Brain Mechanisms and Intelligence. A Quantitative Study of Injuries to the Brain*. Chicago: University of Chicago Press.
- LeDoux, J. E. (1997). Emotion, memory and the brain. *Scientific American*, 7(1), 68–75.
- Letzkus, J. J., Wolff, S. B. E., Meyer, E. M. M., Tovote, P., Courtin, J., Herry, C., & Lüthi, A. (2011). A disinhibitory microcircuit for associative fear learning in the auditory cortex. *Nature*, 480(7377), 331–335. <https://doi.org/10.1038/nature10674>
- Li, W., Howard, J. D., & Gottfried, J. A. (2010). Disruption of odour quality coding in piriform cortex mediates olfactory deficits in Alzheimer’s disease. *Brain*, 133(9), 2714–2726. <https://doi.org/10.1093/brain/awq209>
- Li, W., Howard, J. D., Parrish, T. B., & Gottfried, J. A. (2008). Aversive Learning Enhances Perceptual and Cortical Discrimination of Indiscriminable Odor Cues. *Science*, 319(5871), 1842–1845. <https://doi.org/10.1126/science.1152837>
- Litaudon, P., Mouly, A.-M., Sullivan, R., Gervais, R., & Cattarelli, M. (1997). Learning-induced changes in rat piriform cortex activity mapped using multisite recording with voltage sensitive dye. *European Journal of Neuroscience*, 9(8), 1593–1602.

- Liu, X., Ramirez, S., Pang, P. T., Puryear, C. B., Govindarajan, A., Deisseroth, K., & Tonegawa, S. (2012). Optogenetic stimulation of a hippocampal engram activates fear memory recall. *Nature*. <https://doi.org/10.1038/nature11028>
- Lovett-Barron, M., Kaifosh, P., Kheirbek, M. A., Danielson, N., Zaremba, J. D., Reardon, T. R., ... Losonczy, A. (2014). Dendritic Inhibition in the Hippocampus Supports Fear Learning. *Science*, 343(6173), 857–863. <https://doi.org/10.1126/science.1247485>
- Luna, V.M., & Morozov, A. (2012). Input-specific excitation of olfactory cortex microcircuits. *Front. Neural Circuits* 6:69. <https://doi.org/10.3389/fncir.2012.00069>
- Lütcke, H., Margolis, D. J., & Helmchen, F. (2013). Steady or changing? Long-term monitoring of neuronal population activity. *Trends in Neurosciences*, 36(7), 375–384. <https://doi.org/10.1016/j.tins.2013.03.008>
- Madisen, L., Zwingman, T. A., Sunkin, S. M., Oh, S. W., Zariwala, H. A., Gu, H., ... Zeng, H. (2010). A robust and high-throughput Cre reporting and characterization system for the whole mouse brain. *Nature Neuroscience*, 13(1), 133–140. <https://doi.org/10.1038/nn.2467>
- Majak, K., Ronkko, S., Kemppainen, S., & Pitkanen, A. (2004). Projections from the amygdaloid complex to the piriform cortex: a PHA-L study in the rat. *J. Comp. Neurol.* 476, 414–428. <https://doi.org/10.1002/cne.20233>
- Mandairon, N., Kermen, F., Charpentier, C., Sacquet, J., Linster, C., & Didier, A. (2014). Context-driven activation of odor representations in the absence of olfactory stimuli in the olfactory bulb and piriform cortex. *Frontiers in Behavioral Neuroscience*, 8. <https://doi.org/10.3389/fnbeh.2014.00138>
- Maren S, Aharonov G & Fanselow MS. (1996). Retrograde abolition of conditional fear after excitotoxic lesions in the basolateral amygdala of rats: absence of a temporal gradient. *Behav. Neurosci.* 110:718–26
- Maren, S. (2005). Synaptic Mechanisms of Associative Memory in the Amygdala. *Neuron*, 47(6), 783–786. <https://doi.org/10.1016/j.neuron.2005.08.009>
- Markram, H., Lübke, J., Frotscher, M., & Sakmann, B. (1997). Regulation of synaptic efficacy by coincidence of postsynaptic APs and EPSPs. *Science* 275, 213–215.
- Markram, H. (2011). A history of spike-timing-dependent plasticity. *Frontiers in Synaptic Neuroscience*, 3. <https://doi.org/10.3389/fnsyn.2011.00004>
- Marr, D. (1971). Simple memory: a theory for archicortex. *Philosophical transactions of the Royal Society of London. Series B, Biological sciences*, 262(841):2381.
- Martin, S. J., Grimwood, P. D., & Morris, R. G. (2000). Synaptic plasticity and memory: an evaluation of the hypothesis. *Annual Review of Neuroscience*, 23(1), 649–711.
- Milanovic, S., Radulovic, J., Laban, O., Stiedl, O., Henn, F., & Spiess, J. (1998). Production of

- the Fos protein after contextual fear conditioning of C57BL/6N mice. *Brain Research*, 784(1), 37–47.
- Minatohara, K., Akiyoshi, M., & Okuno, H. (2016). Role of Immediate-Early Genes in Synaptic Plasticity and Neuronal Ensembles Underlying the Memory Trace. *Frontiers in Molecular Neuroscience*, 8. <https://doi.org/10.3389/fnmo.2015.00078>
- Miura, K., Mainen, Z. F., & Uchida, N. (2012). Odor Representations in Olfactory Cortex: Distributed Rate Coding and Decorrelated Population Activity. *Neuron*, 74(6), 1087–1098. <https://doi.org/10.1016/j.neuron.2012.04.021>
- Miyamichi, K., Amat, F., Moussavi, F., Wang, C., Wickersham, I., Wall, N. R., ... Luo, L. (2011). Cortical representations of olfactory input by trans-synaptic tracing. *Nature*, 472(7342), 191–196. <https://doi.org/10.1038/nature09714>
- Mombaerts, P., Wang, F., Dulac, C., Chao, S.K., Nemes, A., Mendelsohn, M., Edmondson, J. & Axel, R. (1996). Visualizing an olfactory sensory map. *Cell* 87, 675–686.
- Mori, K. (2006). Maps of Odorant Molecular Features in the Mammalian Olfactory Bulb. *Physiological Reviews*, 86(2), 409–433. <https://doi.org/10.1152/physrev.00021.2005>
- Mouly AM, Fort A, Ben-Boutayab N et Gervais R. (2001). Olfactory learning induces differential longlasting changes in rat central olfactory pathways. *Neuroscience* 102, 11-21.
- Murphy, C. (1999). Loss of olfactory function in dementing disease. *Physiology & Behavior*, 66(2), 177–182.
- Nabavi, S., Fox, R., Proulx, C. D., Lin, J. Y., Tsien, R. Y., & Malinow, R. (2014). Engineering a memory with LTD and LTP. *Nature*, 511(7509), 348–352. <https://doi.org/10.1038/nature13294>
- Otto, T., Cousens, G., & Herzog, C. (2000). Behavioral and neuropsychological foundations of olfactory fear conditioning. *Behavioural Brain Research*, 110(1), 119–128.
- Pastalkova, E., Serrano, P., Pinkhasova, D., Wallace, E., Fenton, A. A., & Sacktor, T. C. (2006). Storage of spatial information by the maintenance mechanism of LTP. *Science*, 313(5790), 1141–1144.
- Patil, M. M., Linster, C., Lubenov, E., & Hasselmo, M. E. (1998). Cholinergic agonist carbachol enables associative long-term potentiation in piriform cortex slices. *Journal of Neurophysiology*, 80(5), 2467–2474.
- Pavesi, E., Gooch, A., Lee, E., & Fletcher, M. L. (2012). Cholinergic modulation during acquisition of olfactory fear conditioning alters learning and stimulus generalization in mice. *Learning and Memory*, 20(1), 6–10. <https://doi.org/10.1101/lm.028324.112>
- Pawlak, V. Wickens, J.R., Kirkwood, A. & Kerr J.N.D. (2010). Timing is not everything: neuromodulation opens the STDP gate. *Frontiers in Synaptic Neuroscience*, 2. <https://doi.org/10.3389/fnsyn.2010.00146>

- Pedrosa, V., & Clopath, C. (2017). The Role of Neuromodulators in Cortical Plasticity. A Computational Perspective. *Frontiers in Synaptic Neuroscience*, 8. <https://doi.org/10.3389/fnsyn.2016.00038>
- Peirs, C., Williams, S.-P. G., Zhao, X., Walsh, C. E., Gedeon, J. Y., Cagle, N. E., ... Seal, R. P. (2015). Dorsal Horn Circuits for Persistent Mechanical Pain. *Neuron*, 87(4), 797–812. <https://doi.org/10.1016/j.neuron.2015.07.029>
- Phelps, E. A., & LeDoux, J. E. (2005). Contributions of the Amygdala to Emotion Processing: From Animal Models to Human Behavior. *Neuron*, 48(2), 175–187. <https://doi.org/10.1016/j.neuron.2005.09.025>
- Phillips, R. G. & LeDoux, J. E. (1992). Differential contribution of amygdala and hippocampus to cued and contextual fear conditioning. *Behav. Neurosci.* 106(2), 274-285. <https://dx.doi.org/10.1037/0735-7044.106.2.274>
- Pina, M. M., Young, E. A., Ryabinin, A. E., & Cunningham, C. L. (2015). The bed nucleus of the stria terminalis regulates ethanol-seeking behavior in mice. *Neuropharmacology*, 99, 627–638. <https://doi.org/10.1016/j.neuropharm.2015.08.033>
- Platenik J, Kuramoto N et Yoneda Y. (2000). Molecular mechanisms associated with long-term consolidation of the NMDA signals. *Life Sci* 67, 335-364.
- Poo, C., & Isaacson, J. S. (2009). Odor Representations in Olfactory Cortex: “Sparse” Coding, Global Inhibition, and Oscillations. *Neuron*, 62(6), 850–861. <https://doi.org/10.1016/j.neuron.2009.05.022>
- Poo, C., & Isaacson, J. S. (2011). A Major Role for Intracortical Circuits in the Strength and Tuning of Odor-Evoked Excitation in Olfactory Cortex. *Neuron*, 72(1), 41–48. <https://doi.org/10.1016/j.neuron.2011.08.015>
- Puig, M. V., Rose, J., Schmidt, R., & Freund, N. (2014). Dopamine modulation of learning and memory in the prefrontal cortex: insights from studies in primates, rodents, and birds. *Frontiers in Neural Circuits*, 8. <https://doi.org/10.3389/fncir.2014.00093>
- Radulovic, J., Kammermeier, J., & Spiess, J. (1998). Relationship between fos production and classical fear conditioning: effects of novelty, latent inhibition, and unconditioned stimulus pre-exposure. *Journal of Neuroscience*, 18(18), 7452–7461.
- Richardson, R. (2002). Extinction of conditioned odor potentiation of startle. *Neurobiology of Learning and Memory*, 78 (2), 426–440.
- Reijmers, L. (2009). Genetic control of active neural circuits. *Frontiers in Molecular Neuroscience*, 2. <https://doi.org/10.3389/neuro.02.027.2009>
- Reijmers, L. G., Perkins, B. L., Matsuo, N., & Mayford, M. (2007). Localization of a Stable Neural Correlate of Associative Memory. *Science*, 317(5842), 1230–1233.

<https://doi.org/10.1126/science.1143839>

Rennaker, R. L., Chen, C.-F. F., Ruyle, A. M., Sloan, A. M., & Wilson, D. A. (2007). Spatial and Temporal Distribution of Odorant-Evoked Activity in the Piriform Cortex. *Journal of Neuroscience*, 27(7), 1534–1542. <https://doi.org/10.1523/JNEUROSCI.4072-06.2007>

Ressler, K. J., Paschall, G., Zhou, X., & Davis, M. (2002). Regulation of synaptic plasticity genes during consolidation of fear conditioning. *Journal of Neuroscience*, 22(18), 7892–7902.

Rodrigues, S. M., Schafe, G. E., & LeDoux, J. E. (2004). Molecular mechanisms underlying emotional learning and memory in the lateral amygdala. *Neuron*, 44(1), 75–91.

Roesch MR, Stalnaker TA, Schoenbaum G. (2006) Associative encoding in anterior piriform cortex versus orbitofrontal cortex during odor discrimination and reversal learning. *Cereb Cortex*. <https://doi.org/10.1093/cercor/bhk009>

Roland, B., Deneux, T., Franks, K.M., Bathellier, B. & Fleischmann, A. (2017). Odor identity coding by distributed ensembles of neurons in the mouse olfactory cortex. *eLife*. 6: e26337. <https://doi.org/10.7554/eLife.26337>

Root, C. M., Denny, C. A., Hen, R., & Axel, R. (2014). The participation of cortical amygdala in innate, odour-driven behaviour. *Nature*, 515(7526), 269–273. <https://doi.org/10.1038/nature13897>

Roman, F.S., Chaillan, F.A. & Soumireu-Mourat, B. (1993a). Long-term potentiation in rat piriform cortex following discrimination learning. *Brain Res* 601, 265-272.

Roman, F.S., Simonetto, I. & Soumireu-Mourat, B. (1993b). Learning and memory of odor-reward association: selective impairment following horizontal diagonal band lesions. *Behav Neurosci* 107, 72-81.

Romanski, L. M. & LeDoux, J. E. Bilateral destruction of neocortical and perirhinal projection targets of the acoustic thalamus does not disrupt auditory fear conditioning. *Neurosci. Lett.* 142, 228–232 (1992).

Rosenkranz, J.A. & Grace, A.A. (2002). Dopamine-mediated modulation of odour-evoked amygdala potentials during pavlovian conditioning. *Nature*, 417, 282-287. <https://doi.org/10.1038/417282a>

Ryan, T. J., Roy, D. S., Pignatelli, M., Arons, A., and Tonegawa, S. (2015). Engram cells retain memory under retrograde amnesia. *Science* 348, 1007–1013. <https://doi.org/10.1126/science.aaa5542>

Sacco, T., & Sacchetti, B. (2010). Role of Secondary Sensory Cortices in Emotional Memory Storage and Retrieval in Rats. *Science*, 329(5992), 649–656. <https://doi.org/10.1126/science.1183165>

Sadrian, B., & Wilson, D. A. (2015). Optogenetic Stimulation of Lateral Amygdala Input to

Posterior Piriform Cortex Modulates Single-Unit and Ensemble Odor Processing. *Frontiers in Neural Circuits*, 9. <https://doi.org/10.3389/fncir.2015.00081>

Schoenbaum, G. (2003). Lesions of Orbitofrontal Cortex and Basolateral Amygdala Complex Disrupt Acquisition of Odor-Guided Discriminations and Reversals. *Learning & Memory*, 10(2), 129–140. <https://doi.org/10.1101/lm.55203>

Schoenenberger, P., Gerosa, D., & Oertner, T. G. (2009). Temporal control of immediate early gene induction by light. *PloS One*, 4(12), e8185.

Semon, R. *The Mneme* (G. Allen & Unwin, 1921).

Seoane, A., Tinsley, C. J., & Brown, M. W. (2012). Interfering with Fos expression in rat perirhinal cortex impairs recognition memory. *Hippocampus*, 22(11), 2101–2113. <https://doi.org/10.1002/hipo.22028>

Sevelinges Y, Gervais R, Messaoudi B, Granjon L et Mouly A. (2004). Olfactory fear conditioning induces field potential potentiation in rat olfactory cortex and amygdala. *Learn Mem Nov* 10.

Shakhawat, A. M., Harley, C. W., & Yuan, Q. (2014). Arc Visualization of Odor Objects Reveals Experience-Dependent Ensemble Sharpening, Separation, and Merging in Anterior Piriform Cortex in Adult Rat. *Journal of Neuroscience*, 34(31), 10206–10210. <https://doi.org/10.1523/JNEUROSCI.1942-14.2014>

Sharp, F. R., Gonzalez, M. F., Sharp, J. W., & Sagar, S. M. (1989). c-fos expression and (14C) 2-deoxyglucose uptake in the caudal cerebellum of the rat during motor/sensory cortex stimulation. *Journal of Comparative Neurology*, 284(4), 621–636.

Sheng M et Greenberg ME. (1990). The regulation and function of c-fos and other immediate early genes in the nervous system. *Neuron* 4, 477-485.

Sjostrom, P. J., Rancz, E. A., Roth, A., & Häusser, M. (2008). Dendritic Excitability and Synaptic Plasticity. *Physiological Reviews*, 88(2), 769–840. <https://doi.org/10.1152/physrev.00016.2007>

Slotnick, B. (2001). Animal cognition and the rat olfactory system. *Trends in Cognitive Sciences*, 5(5), 216–222.

Sosulski, D. L., Lissitsyna Bloom, M., Cutforth, T., Axel, R., & Datta, S. R. (2011). Distinct representations of olfactory information in different cortical centres. *Nature*, 472(7342), 213–216. <https://doi.org/10.1038/nature09868>

Squire, L. R. (2004). Memory systems of the brain: A brief history and current perspective. *Neurobiology of Learning and Memory*, 82(3), 171–177. <https://doi.org/10.1016/j.nlm.2004.06.005>

Squire, L. R. (2009). The Legacy of Patient H.M. for Neuroscience. *Neuron*, 61(1), 6–9.

<https://doi.org/10.1016/j.neuron.2008.12.023>

Staubli U, Schottler F et Nejat-Bina D. (1987b). Role of dorsomedial thalamic nucleus and piriform cortex in processing olfactory information. *Behav Brain Res* 25, 117-129

Stefanelli, T., Bertollini, C., Lüscher, C., Muller, D., & Mendez, P. (2016). Hippocampal Somatostatin Interneurons Control the Size of Neuronal Memory Ensembles. *Neuron*, 89(5), 1074–1085. <https://doi.org/10.1016/j.neuron.2016.01.024>

Stettler, D. D., & Axel, R. (2009). Representations of Odor in the Piriform Cortex. *Neuron*, 63(6), 854–864. <https://doi.org/10.1016/j.neuron.2009.09.005>

Suzuki, N., & Bekkers, J. M. (2010). Inhibitory neurons in the anterior piriform cortex of the mouse: Classification using molecular markers. *The Journal of Comparative Neurology*, 518(10), 1670–1687. <https://doi.org/10.1002/cne.22295>

Suzuki, N., & Bekkers, J. M. (2012). Microcircuits Mediating Feedforward and Feedback Synaptic Inhibition in the Piriform Cortex. *Journal of Neuroscience*, 32(3), 919–931. <https://doi.org/10.1523/JNEUROSCI.4112-11.2012>

Takeuchi, T., Duszkievicz, A. J., & Morris, R. G. M. (2013). The synaptic plasticity and memory hypothesis: encoding, storage and persistence. *Philosophical Transactions of the Royal Society B: Biological Sciences*, 369(1633), 20130288–20130288. <https://doi.org/10.1098/rstb.2013.0288>

Tanaka, K. Z., Pevzner, A., Hamidi, A. B., Nakazawa, Y., Graham, J., & Wiltgen, B. J. (2014). Cortical Representations Are Reinstated by the Hippocampus during Memory Retrieval. *Neuron*, 84(2), 347–354. <https://doi.org/10.1016/j.neuron.2014.09.037>

Taylor, K. K., Tanaka, K. Z., Reijmers, L. G., & Wiltgen, B. J. (2013). Reactivation of Neural Ensembles during the Retrieval of Recent and Remote Memory. *Current Biology*, 23(2), 99–106. <https://doi.org/10.1016/j.cub.2012.11.019>

Tischmeyer, W., & Grimm, R. (1999) Activation of immediate early genes and memory formation. *Cell Mol Life Sci* 55:564–574.

Tonegawa, S., Liu, X., Ramirez, S., & Redondo, R. (2015). Memory Engram Cells Have Come of Age. *Neuron*, 87(5), 918–931. <https://doi.org/10.1016/j.neuron.2015.08.002>

Varga, A. G., & Wesson, D. W. (2013). Distributed auditory sensory input within the mouse olfactory cortex. *European Journal of Neuroscience*, 37(4), 564–571. <https://doi.org/10.1111/ejn.12063>

Vermetten E, Bremner JD. (2003). Olfaction as a traumatic reminder in posttraumatic stress disorder: case reports and review. *J Clin Psychiatry* 64:202–7.

Wang, M. E., Wann, E. G., Yuan, R. K., Ramos Alvarez, M. M., Stead, S. M., & Muzzio, I. A. (2012). Long-Term Stabilization of Place Cell Remapping Produced by a Fearful Experi-

ence. *Journal of Neuroscience*, 32(45), 15802–15814. <https://doi.org/10.1523/JNEUROSCI.0480-12.2012>

Weinberger, N. M. (1995). Dynamic Regulation of Receptive Fields and Maps in the Adult Sensory Cortex. *Annual Review of Neuroscience*, 18(1), 129–158. <https://doi.org/10.1146/annurev.ne.18.030195.001021>

Weinberger, N. M. (2004). Specific long-term memory traces in primary auditory cortex. *Nature Reviews Neuroscience*, 5(4), 279–290. <https://doi.org/10.1038/nrn1366>

Wilson, D. A., & Stevenson, R. J. (2003). The fundamental role of memory in olfactory perception. *Trends in Neurosciences*, 26(5), 243–247. [https://doi.org/10.1016/S0166-2236\(03\)00076-6](https://doi.org/10.1016/S0166-2236(03)00076-6)

Wilson, D. A. (2009). Pattern Separation and Completion in Olfaction. *Annals of the New York Academy of Sciences*, 1170(1), 306–312. <https://doi.org/10.1111/j.1749-6632.2009.04017.x>

Witter M. P., Groenewegen H. J., Lopes Da Silva F. H. & Lohman, A. H. M. (1989) Functional organization of the extrinsic and intrinsic circuitry of the parahippocampal region. *Prog. Neurobiol.* 33:161–253.

Wulff, P., & Arenkiel, B. R. (2012). Chemical genetics: receptor–ligand pairs for rapid manipulation of neuronal activity. *Current Opinion in Neurobiology*, 22(1), 54–60. <https://doi.org/10.1016/j.conb.2011.10.008>

Zhan, C., & Luo, M. (2010). Diverse Patterns of Odor Representation by Neurons in the Anterior Piriform Cortex of Awake Mice. *Journal of Neuroscience*, 30(49), 16662–16672. <https://doi.org/10.1523/JNEUROSCI.4400-10.2010>

Zhan, C., Zhou, J., Feng, Q., Zhang, J. -e., Lin, S., Bao, J., ... Luo, M. (2013). Acute and Long-Term Suppression of Feeding Behavior by POMC Neurons in the Brainstem and Hypothalamus, Respectively. *Journal of Neuroscience*, 33(8), 3624–3632. <https://doi.org/10.1523/JNEUROSCI.2742-12.2013>

Zhang, Z., Ferretti, V., Güntan, İ., Moro, A., Steinberg, E. A., Ye, Z., ... Franks, N. P. (2015). Neuronal ensembles sufficient for recovery sleep and the sedative actions of $\alpha 2$ adrenergic agonists. *Nature Neuroscience*, 18(4), 553–561. <https://doi.org/10.1038/nn.3957>

Ziv, Y., Burns, L. D., Cocker, E. D., Hamel, E. O., Ghosh, K. K., Kitch, L. J., ... Schnitzer, M. J. (2013). Long-term dynamics of CA1 hippocampal place codes. *Nature Neuroscience*, 16(3), 264–266. <https://doi.org/10.1038/nn.3329>

CHAPTER 7

- Birtoli., B. & Ulrich D. (2004) Firing Mode-Dependent Synaptic Plasticity in Rat Neocortical Pyramidal Neurons *Journal of Neuroscience* 26 May 2004, 24 (21) 4935-4940
- Brandalise, F., Carta, S., Helmchen, F., Lisman, J. & Gerber U. (2016) Dendritic NMDA spikes are necessary for timing-dependent associative LTP in CA3 pyramidal cells *Nat. Comm.* 7:13480
- Brandalise, F. & Gerber U.(2014) Mossy fiber-evoked subthreshold responses induce timing-dependent plasticity at hippocampal CA3 recurrent synapses *PNAS* 111(11) 4303-4308.
- Clopath, C. & Gerstner W. (2010), Voltage and spike timing interact in STDP – a unified model *Frontiers in Synaptic Neuroscience* 2(25), 1
- Clopath, C., Büsing, L., Vasilaki, E., & Gerstner, W. (2010). Connectivity reflects coding: a model of voltage based spike-timing-dependent plasticity with homeostasis. *Nat.Neurosci.* 13, 344-352.
- Gambino, F., Pages, S., Kehayas, V., Baptista D., Tatti, R., Carleton, A., & Holtmaat, A. (2014) Sensory-evoked LTP driven by dendritic plateau potentials in vivo *Nature*
- Hebb, D. O. (1949). *The Organisation of Behavior*. New York:Wiley
- Holthoff, K., Kovalchuk, Y., Yuste, R., & Konnerth, A. (2004). Single-shock LTD by local dendritic spikes in pyramidal neurons of mouse visual cortex: Dendritic spikes and LTD. *The Journal of Physiology*, 560(1), 27–36.
- Humeau, Y., & Lüthi, A. (2007). Dendritic calcium spikes induce bi-directional synaptic plasticity in the lateral amygdala. *Neuropharmacology*, 52(1), 234–243.
- Kampa B.M., Letzkus J.J. & Stuart G.J. (2007) Dendritic mechanisms controlling spike-timing-dependent synaptic plasticity *Trends in Neurosciences* 30(9), 456
- Kampa, B. & Stuart, G. (2006). Calcium spikes in basal dendrites of layer 5 pyramidal neurons during action potential bursts *The Journal of Neuroscience* 26(28):7424 -7432.
- Kampa, B., Letzkus, J. & Stuart, G. (2006). Requirement of dendritic calcium spikes for induction of spike-timing-dependent synaptic plasticity. *J. Physiol.* 574.1, 283-290.
- Letzkus, J., Kampa, B., & Stuart, G. (2006). Learning rules for spike timing-dependent plasticity depend on dendritic synapse location. *J. Neurosci.* 26, 10420-10429
- Lisman, J. & Spruston, N. (2005) Postsynaptic depolarization requirements for LTP and LTD: a critique of spike timing dependent plasticity *Nature Neuroscience* 8(7), 839
- Lisman, J. & Spruston, N. (2010) Questions about STDP as a general model of synaptic plasticity *Frontiers in Synaptic Neuroscience* 2(140), 1

Remy, S., & Spruston, N. (2007). Dendritic spikes induce single-burst long-term potentiation. *Proceedings of the National Academy of Sciences*, 104(43), 17192–17197.

Rubin, J.E., Gerkin, R.C., Bi, G. & Chow, C.C. (2005). Calcium Time Course as a Signal for Spike-Timing-Dependent Plasticity *J Neurophysiol* 93: 2600–2613

Sjöström, P.J., Turrigiano, G.G. & Nelson, S.B. (2001). Rate, timing and cooperativity jointly determine cortical synaptic plasticity. *Neuron* 32, 1149–1164.

Wang, H.-X., Gerkin, R., Nauen, D., & Wang, G.-Q. (2005). Coactivation and timing-dependent integration of synaptic potentiation and depression. *Nat. Neurosci.* 8, 187–193.

Xia, Z. & Storm, D. R. (2005) The role of calmodulin as a signal integrator for synaptic plasticity. *Nat.Reviews* 6, 267–276.



Francis Bernard